

**International
Journal of
Engineering
Technologies
(IJET)**

Printed ISSN: 2149-0104

e-ISSN: 2149-5262

Volume: 2

No: 3

September 2016

© Istanbul Gelisim University Press, 2016

Certificate Number: 23696

All rights reserved.

International Journal of Engineering Technologies is an international peer-reviewed journal and published quarterly. The opinions, thoughts, postulations or proposals within the articles are but reflections of the authors and do not, in any way, represent those of the Istanbul Gelisim University.

CORRESPONDENCE and COMMUNICATION:

Istanbul Gelisim University Faculty of Engineering and Architecture
Cihangir Mah. Şehit P. Onb. Murat Şengöz Sk. No: 8
34315 Avcilar / Istanbul / TURKEY
Phone: +90 212 4227020 Ext. 221
Fax: +90 212 4227401
e-Mail: ijet@gelisim.edu.tr
Web site: <http://ijet.gelisim.edu.tr>
<http://dergipark.ulakbim.gov.tr/ijet>
Twitter: @IJETJOURNAL


Printing and binding:

Anka Matbaa
Sertifika No: 12328
Tel: +90 212 5659033 - 4800571
e-Posta: ankamatbaa@gmail.com

International Journal of Engineering Technologies (IJET) is included in:



**International Journal of Engineering Technologies (IJET) is
harvested by the following service:**

Organization	URL	Starting Date	Feature
 The OpenAIRE2020 Project	https://www.openaire.eu/	2015	Open Access



INTERNATIONAL JOURNAL OF ENGINEERING TECHNOLOGIES (IJET)
International Peer-Reviewed Journal
Volume 2, No 3, September 2016, Printed ISSN: 2149-0104, e-ISSN: 2149-5262

Owner on Behalf of Istanbul Gelisim University
Rector Prof. Dr. Burhan AYKAÇ

Editor-in-Chief
Prof. Dr. İlhami ÇOLAK

Associate Editors
Dr. Selin ÖZÇİRA
Dr. Mehmet YEŞİLBUDAK

Layout Editor
Seda ERBAYRAK

Proofreader
Özlemnur ATAOL

Copyeditor
Mehmet Ali BARIŞKAN

Contributor
Ahmet Şenol ARMAĞAN

Cover Design
Tarık Kaan YAĞAN

Editorial Board

Professor İlhami COLAK, Istanbul Gelisim University, Turkey

Professor Dan IONEL, Regal Beloit Corp. and University of Wisconsin Milwaukee, United States

Professor Fujio KUROKAWA, Nagasaki University, Japan

Professor Marija MIROSEVIC, University of Dubrovnik, Croatia

Prof. Dr. Şeref SAĞIROĞLU, Gazi University, Graduate School of Natural and Applied Sciences, Turkey

Professor Adel NASIRI, University of Wisconsin-Milwaukee, United States

Professor Mamadou Lamina DOUMBIA, University of Québec at Trois-Rivières, Canada

Professor João MARTINS, University/Institution: FCT/UNL, Portugal

Professor Yoshito TANAKA, Nagasaki Institute of Applied Science, Japan

Dr. Youcef SOUFI, University of Tébessa, Algeria

Prof.Dr. Ramazan BAYINDIR, Gazi Üniversitesi, Turkey

Professor Goce ARSOV, SS Cyril and Methodius University, Macedonia

Professor Tamara NESTOROVIĆ, Ruhr-Universität Bochum, Germany

Professor Ahmed MASMOUDI, University of Sfax, Tunisia

Professor Tsuyoshi HIGUCHI, Nagasaki University, Japan

Professor Abdelghani AISSAOUI, University of Bechar, Algeria

Professor Miguel A. SANZ-BOBI, Comillas Pontifical University /Engineering School, Spain

Professor Mato MISKOVIĆ, HEP Group, Croatia

Professor Nilesh PATEL, Oakland University, United States

Assoc. Professor Juan Ignacio ARRIBAS, Universidad Valladolid, Spain

Professor Vladimir KATIC, University of Novi Sad, Serbia

Professor Takaharu TAKESHITA, Nagoya Institute of Technology, Japan

Professor Filote CONSTANTIN, Stefan cel Mare University, Romania

Assistant Professor Hulya OBDAN, Istanbul Yildiz Technical University, Turkey

Professor Luis M. San JOSE-REVUELTA, Universidad de Valladolid, Spain

Professor Tadashi SUETSUGU, Fukuoka University, Japan

Associate Professor Zehra YUMURTACI, Istanbul Yildiz Technical University, Turkey

Dr. Rafael CASTELLANOS-BUSTAMANTE, Instituto de Investigaciones Eléctricas, Mexico

Assoc. Prof. Dr. K. Nur BEKIROGLU, Yildiz Technical University, Turkey

Professor Gheorghe-Daniel ANDREESCU, Politehnica University of Timisoara, Romania

Dr. Jorge Guillermo CALDERÓN-GUIZAR, Instituto de Investigaciones Eléctricas, Mexico

Professor VICTOR FERNÃO PIRES, ESTSetúbal/Polytechnic Institute of Setúbal, Portugal

Dr. Hiroyuki OSUGA, Mitsubishi Electric Corporation, Japan

Professor Serkan TAPKIN, Istanbul Arel University, Turkey

Professor Luis COELHO, ESTSetúbal/Polytechnic Institute of Setúbal, Portugal

Professor Furkan DINCER, Mustafa Kemal University, Turkey

Professor Maria CARMEZIM, ESTSetúbal/Polytechnic Institute of Setúbal, Portugal

Associate Professor Lale T. ERGENE, Istanbul Technical University, Turkey

Dr. Hector ZELAYA, ABB Corporate Research, Sweden

Professor Isamu MORIGUCHI, Nagasaki University, Japan

Associate Professor Kiruba SIVASUBRAMANIAM HARAN, University of Illinois, United States

Associate Professor Leila PARSA, Rensselaer Polytechnic Institute, United States

Professor Salman KURTULAN, Istanbul Technical University, Turkey

Professor Dragan ŠEŠLIJA, University of Novi Sad, Serbia

Professor Birsen YAZICI, Rensselaer Polytechnic Institute, United States

Assistant Professor Hidenori MARUTA, Nagasaki University, Japan

Associate Professor Yilmaz SOZER, University of Akron, United States

Associate Professor Yuichiro SHIBATA, Nagasaki University, Japan

Professor Stanimir VALTCHEV, Universidade NOVA de Lisboa, (Portugal) + Burgas Free University, (Bulgaria)

Professor Branko SKORIC, University of Novi Sad, Serbia

Dr. Cristea MIRON, Politehnica University in Bucharest, Romania

Dr. Nobumasa MATSUI, Faculty of Engineering, Nagasaki Institute of Applied Science, Nagasaki, Japan

Professor Mohammad ZAMI, King Fahd University of Petroleum and Minerals, Saudi Arabia

Associate Professor Mohammad TAHA, Rafik Hariri University (RHU), Lebanon

Assistant Professor Kyungnam KO, Jeju National University, Republic of Korea

Dr. Guray GUVEN, Conductive Technologies Inc., United States

Dr. Tuncay KAMAŞ, Eskişehir Osmangazi University, Turkey

From the Editor

Dear Colleagues,

On behalf of the editorial board of International Journal of Engineering Technologies (IJET), I would like to share our happiness to publish the seventh issue of IJET. My special thanks are for members of editorial board, editorial team, referees, authors and other technical staff.

Please find the seventh issue of International Journal of Engineering Technologies at <http://dergipark.ulakbim.gov.tr/ijet>. We invite you to review the Table of Contents by visiting our web site and review articles and items of interest. IJET will continue to publish high level scientific research papers in the field of Engineering Technologies as an international peer-reviewed scientific and academic journal of Istanbul Gelisim University.

Thanks for your continuing interest in our work,

Professor ILHAMI COLAK
Istanbul Gelisim University
icolak@gelisim.edu.tr

<http://dergipark.ulakbim.gov.tr/ijet>

Printed ISSN: 2149-0104

e-ISSN: 2149-5262

International Journal of
Engineering Technologies
IJET

Table of Contents

	Page
<i>From the Editor</i>	<i>vii</i>
<i>Table of Contents</i>	<i>ix</i>
<u>Elastostatic Deformation Analysis of Thick Isotropic Beams by Using Different Beam Theories and a Meshless Method</u>	
<i>Armagan Karamanli</i>	83-93
<u>Development of a Lidar System Based on an Infrared RangeFinder Sensor and SlipRing Mechanism</u>	
<i>Gokhan Bayar, Alparslan Uludag</i>	94-99
<u>Calculation and Optimizing of Brake Thermal Efficiency of Diesel Engines Based on Theoretical Diesel Cycle Parameters</u>	
<i>Safak Yildizhan, Vedat Karaman, Mustafa Ozcanli, Hasan Serin</i>	100-104
<u>Analysis of Bending Deflections of Functionally Graded Beams by Using Different Beam Theories and Symmetric Smoothed Particle Hydrodynamics</u>	
<i>Armagan Karamanli</i>	105-117
<u>Fluorescent Lamp Modelling and Electronic Ballast Design by the Support of Root Placement</u>	
<i>Ibrahim Aliskan, Ridvan Keskin</i>	118-123
<u>Dynamic Spectrum Access: A New Paradigm of Converting Radio Spectrum Wastage to Wealth</u>	
<i>Jide J. Popoola, Oluwaseun A. Ogunlana, Ferdinad O. Ajie, Olaleye Olakunle, Olufemi A. Akiogbe, Saint M. Ani-Initi, Sunday K. Omotola</i>	124-131

International Journal of Engineering Technologies, IJET

e-Mail: ijet@gelisim.edu.tr
Web site: <http://ijet.gelisim.edu.tr>
<http://dergipark.ulakbim.gov.tr/ijet>
Twitter: @IJETJOURNAL

Elastostatic Deformation Analysis of Thick Isotropic Beams by Using Different Beam Theories and a Meshless Method

Armagan Karamanli*[‡]

*Department of Mechatronics Engineering, Faculty of Engineering and Architecture, Istanbul Gelisim University, 34215 Istanbul, Turkey.

(afkaramanli@gelisim.edu.tr)

[‡]Corresponding Author; Armagan Karamanli, Department of Mechatronics Engineering, Faculty of Engineering and Architecture, Istanbul Gelisim University, 34215 Istanbul, Turkey, Tel: +90 2124227020, armagan_k@yahoo.com

Received: 17.05.2016 Accepted: 27.07.2016

Abstract-The elastostatic deformations of thick isotropic beams subjected to various sets of boundary conditions are presented by using different beam theories and the Symmetric Smoothed Particle Hydrodynamics (SSPH) method. The analysis is based on the Euler-Bernoulli, Timoshenko and Reddy-Bickford beam theories. The performance of the SSPH method is investigated for the comparison of the different beam theories for the first time. For the numerical results, various numbers of nodes are used in the problem domain. Regarding to the computed results for RBT, various number of terms in the Taylor Series Expansions (TSEs) is employed. To validate the performance of the SSPH method, comparison studies in terms of transverse deflections are carried out with the analytical solutions. It is found that the SSPH method has provided satisfactory convergence rate and smaller L2 error.

Keywords Meshless Method, Element-Free, Beam, Euler-Bernoulli, Timoshenko, Reddy-Bickford.

1. Introduction

The kinematics of deformation of a beam can be represented by using various beam theories. Among them, the Euler Bernoulli Beam Theory (EBT), the Timoshenko Beam Theory (TBT) and the Reddy-Bickford Beam Theory (RBT) are commonly used. The effect of the transverse shear deformation neglected in the EBT is allowed in the latter two beam theories.

Euler Bernoulli Beam Theory is the simplest beam theory and assumes that the cross sections which are normal to the mid-plane before deformation remain plane/straight and normal to the mid-plane after deformation. Both transverse shear and transverse normal strains are neglected by using these assumptions. In the TBT, the normality assumption of the EBT is relaxed and the cross sections do not need to normal to the mid-plane but still remain plane. The TBT requires the shear correction factor (SCF) to compensate the error due to the assumption of the constant transverse shear strain and shear stress through the beam

thickness. The SCF depends on the geometric and material parameters of the beam but the loading and boundary conditions are also important to determine the SCF [1-2]. In the third order shear deformation theory which is named as the RBT, the transverse shear strain is quadratic through the thickness of the beam [3].

The need for the further extension of the EBT is raised for the engineering applications of the beam problems often characterized by high ratios, up to 40 for the composite structures, between the Young modulus and the shear modulus [4]. Various higher order beam theories are introduced in which the straightness assumption is removed and the vanishing of shear stress at the upper and lower surfaces are accommodated. For this purpose, higher order polynomials incorporating either one, or more, extra terms [5-11] or trigonometric functions [12-13] or exponential functions [14] are included in the expansion of the longitudinal point-wise displacement component through the thickness of the beam. The higher order theories introduce additional unknowns that make the governing equations

more complicated and provide the solutions much costly in terms of CPU time. The theories which are higher than the third order shear deformation beam theory are seldom used because the accuracy gained by these theories which require much effort to solve the governing equations is so little [4].

The beam theories are still the reference technique in many engineering applications. They continue to be advantageous in the analysis of slender bodies such as airplane wings, helicopter blades, bridges and frames where the cumbersome two-dimensional 2D (plate and shell theories) and three-dimensional 3D analysis require higher cost and computational effort because of their complexity.

Meshless methods are widely used in static and dynamic analyses of the engineering beam problems [15-20]. To obtain the approximate solution of the problem by a meshless method, the selection of the basis functions is almost the most important issue. The accuracy of the computed solution can be increased by employing different number of terms in TSE or increasing number of nodes in the problem domain or by increasing the degree of complete polynomials. Many meshless methods have been proposed by researchers to obtain the approximate solution of the problem. The Smoothed Particle Hydrodynamics (SPH) method is proposed by Lucy [21] to the testing of the fission hypothesis. However, this method has two important shortcomings, lack of accuracy on the boundaries and the tensile instability. To remove these shortcomings, many meshless methods have been proposed such as the Corrected Smoothed Particle Method [22,23], Reproducing Kernel Particle Method [24-26], Modified Smoothed Particle Hydrodynamics (MSPH) method [27-30], the Symmetric Smoothed Particle Hydrodynamics method [31-36] and the Strong Form Meshless Implementation of Taylor Series Method [37-38], Moving Kringing Interpolation Method [39-40], the meshless Shepard and Least Squares (MSLS) Method [42], Spectral Meshless Radial Point Interpolation (SMRPI) Method [42].

It is seen from the above literature survey regarding to the SSPH method, there is no reported work on the elastostatic deformations of the thick isotropic beams subjected to the different boundary conditions by employing the TBT and RBT.

Linear elastic problems including quasi-static crack propagation [31-33], crack propagation in an adhesively bonded joint [34], 2D Heat Transfer problems [35] and 1D 4th order nonhomogeneous variable coefficient boundary value problems [36] have been successfully solved by employing the SSPH method.

The SSPH method has an advantage over the MLS, RKPM, MSPH and the SMITSM methods because basis functions used to approximate the function and its derivatives are derived simultaneously and even a constant weight function can be employed to obtain the approximate solution [31-36]. The matrix to be inverted for finding kernel estimates of the trial solution and its derivatives is asymmetric in the MSPH. In SSPH method which made the matrix to be inverted symmetric, reduced the storage requirement and the CPU time.

In view of the above, the objectives of this paper mainly are to present the SSPH method formulation for the isotropic thick beams subjected to different boundary conditions within the framework of EBT, TBT and RBT, to perform numerical calculations to obtain the transverse deflections of the studied beam problems and finally to compare the results obtained by using the SSPH method with analytical solutions. It is believed that researchers will probably find the SSPH method helpful to solve their engineering problems.

In section 2, the formulation of the EBT, TBT and RBT is. In section 3, the formulation of the SSPH method is given for 1D problem. In Section 4, numerical results are given based on the two types of engineering beam problem which are a simply supported beam under uniformly distributed load and a cantilever beam under the uniformly distributed load. The performance of the SSPH method is compared with the analytical solutions.

2. Formulation of Beam Theories

To describe the EBT, TBT and RBT, the following coordinate system is introduced. The x-coordinate is taken along the axis of the beam and the z-coordinate is taken through the height (thickness) of the beam. In the general beam theory, all the loads and the displacements (u,w) along the coordinates (x,z) are only the functions of the x and z coordinates. [4] The formulation of the EBT, TBT and RBT are given below.

2.1. Euler Bernoulli Beam Theory

The following displacement field is given for the EBT,

$$\begin{aligned} u(x, z) &= -z \frac{dw}{dx} \\ w(x, z) &= w_0(x) \end{aligned} \quad (1)$$

where w_0 is the transverse deflection of the point (x,0) which is on the mid-plane ($z=0$) of the beam. By using the assumption of the smallness of strains and rotations, the only the axial strain which is nonzero is given by,

$$\varepsilon_{xx} = \frac{du}{dx} = -z \frac{d^2w_0}{dx^2} \quad (2)$$

The virtual strain energy of the beam in terms of the axial stress and the axial strain can be expressed by

$$\delta U = \int_0^L \int_A \sigma_{xx} \delta \varepsilon_{xx} dA dx \quad (3)$$

where δ is the variational operator, A is the cross sectional area, L is the length of the beam, σ_{xx} is the axial stress. The bending moment of the EBT is given by,

$$M_{xx} = \int_A z \sigma_{xx} dA \quad (4)$$

By using equation (2) and equation (4), equation (3) can be rewritten as,

$$\delta U = - \int_0^L M_{xx} z \frac{d^2 \delta w_0}{dx^2} \quad (5)$$

The virtual potential energy of the load $q(x)$ which acts at the central axis of the beam is given by

$$\delta V = - \int_0^L q(x) \delta w_0 dx \quad (6)$$

If a body is in equilibrium, $\delta W = \delta U + \delta V$, the total virtual work (δW) done equals zero. Then one can obtain,

$$\delta W = - \int_0^L \left(M_{xx} z \frac{d^2 \delta w_0}{dx^2} + q(x) \delta w_0 \right) dx = 0 \quad (7)$$

After performing integration for the first term in equation (7) twice and since δw_0 is arbitrary in $(0 < x < L)$, one can obtain the following equilibrium equation,

$$- \frac{d^2 M_{xx}}{dx^2} = q(x) \text{ for } 0 < x < L \quad (8)$$

By introducing the shear force Q_x and rewrite equation (8) in the following form

$$- \frac{dM_{xx}}{dx} + Q_x = 0, \quad - \frac{dQ_x}{dx} = q(x) \quad (9)$$

By using Hooke's law, one can obtain

$$\sigma_{xx} = E \varepsilon_{xx} = -Ez \frac{d^2 w_0}{dx^2} \quad (10)$$

where E is the modulus of elasticity. If the equation (10) is put into equation (4), it is obtained,

$$M_{xx} = - \int_A E z^2 \frac{d^2 w_0}{dx^2} dA = -D_x \frac{d^2 w_0}{dx^2} \quad (11)$$

where $D_{xx} = EI_y$ is the flexural rigidity of the beam and $I_y = \int_A z^2 dA$ the second moment of area about the y -axis. The substitution of equation (11) into equation (9) yields the EBT governing equation

$$\frac{d^2}{dx^2} (D_{xx} \frac{d^2 w_0}{dx^2}) = q(x) \text{ for } 0 < x < L \quad (12)$$

2.2. Timoshenko Beam Theory

The following displacement field is given for the TBT,

$$\begin{aligned} u(x, z) &= z\phi(x) \\ w(x, z) &= w_0(x) \end{aligned} \quad (13)$$

where $\phi(x)$ is the rotation of the cross section. By using equation (13), the strain-displacement relations are given by

$$\begin{aligned} \varepsilon_{xx} &= \frac{du}{dx} = -z \frac{d\phi}{dx} \\ \gamma_{xz} &= \frac{du}{dz} + \frac{dw}{dx} = \phi + \frac{dw_0}{dx} \end{aligned} \quad (14)$$

The virtual strain energy of the beam including the virtual energy associated with the shearing strain can be written as,

$$\delta U = \int_0^L \int_A (\sigma_{xx} \delta \varepsilon_{xx} + \sigma_{xz} \delta \gamma_{xz}) dA dx \quad (15)$$

where σ_{xz} is the transverse shear stress and γ_{xz} is the shear strain. The bending moment and the shear force can be written respectively,

$$M_{xx} = \int_A z \sigma_{xx} dA, \quad Q_x = \int_A \sigma_{xz} dA \quad (16)$$

By using equation (14) and equation (16), one can rewrite equation (15) as,

$$\delta U = \int_0^L \left[M_{xx} \frac{d\delta\phi}{dx} + Q_x \left(\delta\phi + \frac{d\delta w_0}{dx} \right) \right] dx \quad (17)$$

The virtual potential energy of the load $q(x)$ which acts at the central axis of the Timoshenko beam is given by

$$\delta V = - \int_0^L q(x) \delta w_0 dx \quad (18)$$

Since the total virtual work done equals zero and the coefficients of $\delta\phi$ and δw_0 in $0 < x < L$ are zero, one can obtain the following equations,

$$- \frac{dM_{xx}}{dx} + Q_x = 0, \quad - \frac{dQ_x}{dx} = q(x) \quad (19)$$

The bending moment and shear force can be expressed in terms of generalized displacement (w_0, ϕ) by using the constitutive equations $\sigma_{xx} = E \varepsilon_{xx}$ and $\sigma_{xz} = G \gamma_{xz}$,

$$M_{xx} = \int_A z \sigma_{xx} dA = D_x \frac{d\phi}{dx} \quad (20)$$

$$Q_x = \kappa_s \int_A \sigma_{xz} dA = \kappa_s A_{xz} \left(\phi + \frac{dw_0}{dx} \right) \quad (21)$$

Where κ_s is the shear correction factor, G is the shear modulus, $D_{xx} = EI_y$ is the flexural rigidity of the beam and $A_{xz} = GA$ is the shear rigidity. The SCF is used to compensate the error caused by the assumption of a constant transverse shear stress distribution along the beam thickness. The governing equations of the TBT is obtained in terms of generalized displacements by substituting equation (20) and equation (21) into equation (19),

$$- \frac{d}{dx} \left(D_{xx} \frac{d\phi}{dx} \right) + \kappa_s A_{xz} \left(\phi + \frac{dw_0}{dx} \right) = 0 \quad (22)$$

$$- \frac{d}{dx} \left[\kappa_s A_{xz} \left(\phi + \frac{dw_0}{dx} \right) \right] = q(x) \quad (23)$$

2.3. Reddy-Bickford Beam Theory

The following displacement field is given for the RBT,

$$\begin{aligned} u(x, z) &= z\phi(x) - \alpha z^3 \left(\phi(x) + \frac{dw(x)}{dx} \right) \\ w(x, z) &= w_0(x) \end{aligned} \quad (24)$$

where $\alpha = 4/(3h^2)$. By using equation (24), the strain-displacement relations of the RBT are given by

$$\begin{aligned} \varepsilon_{xx} &= \frac{du}{dx} = z \frac{d\phi}{dx} - \alpha z^3 \left(\frac{d\phi}{dx} + \frac{d^2 w_0}{dx^2} \right) \\ \gamma_{xz} &= \frac{du}{dz} + \frac{dw}{dx} = \phi + \frac{dw_0}{dx} - \beta z^2 \left(\phi + \frac{dw_0}{dx} \right) \end{aligned} \quad (25)$$

where $\beta = 3\alpha = 4/(h^2)$.

The virtual strain energy of the beam can be written as,

$$\delta U = \int_0^L \int_A (\sigma_{xx} \delta \varepsilon_{xx} + \sigma_{xz} \delta \gamma_{xz}) dA dx \quad (26)$$

The usual bending moment and the shear force are,

$$M_{xx} = \int_A z \sigma_{xx} dA, \quad Q_x = \int_A \sigma_{xz} dA \quad (27)$$

and P_{xx} and R_x are the higher order stress resultants can be written respectively,

$$P_{xx} = \int_A z^3 \sigma_{xx} dA, \quad R_x = \int_A z^2 \sigma_{xz} dA \quad (28)$$

By using equation (25), equation (27) and equation (2.28), one can rewrite the equation (26) as,

$$\delta U = \int_0^L \left[(M_{xx} - \alpha P_{xx}) \frac{d\delta\phi}{dx} - \alpha P_{xx} \frac{d^2\delta w_0}{dx^2} + (Q_x - \beta R_x) \left(\delta\phi + \frac{d\delta w_0}{dx} \right) \right] dx \quad (29)$$

In the RBT there is no need to use a SCF unlike the TBT. The virtual potential energy of the transverse load $q(x)$ is given by

$$\delta V = - \int_0^L q(x) \delta w_0 dx \quad (30)$$

The virtual displacements principle is applied and the coefficients of $\delta\phi$ and δw_0 in $0 < x < L$ are set to zero, the governing equations of the RBT are obtained in terms of displacements ϕ and w_0 as follows,

$$\begin{aligned} -\frac{d}{dx} \left(\bar{D}_{xx} \frac{d\phi}{dx} - \alpha \hat{F}_{xx} \frac{d^2 w_0}{dx^2} \right) + \bar{A}_{xz} \left(\phi + \frac{dw_0}{dx} \right) &= 0 \\ -\alpha \frac{d^2}{dx^2} \left(\hat{F}_{xx} \frac{d\phi}{dx} - \alpha H_{xx} \frac{d^2 w_0}{dx^2} \right) - \frac{d}{dx} \left[\bar{A}_{xz} \left(\phi + \frac{dw_0}{dx} \right) \right] &= q(x) \end{aligned} \quad (31)$$

where

$$\begin{aligned} \bar{A}_{xz} &= \hat{A}_{xz} - \beta \hat{D}_{xz}, \quad \bar{D}_{xx} = \hat{D}_{xx} - \alpha \hat{F}_{xx} \\ \hat{D}_{xx} &= D_{xx} - \alpha F_{xx}, \quad \hat{F}_{xx} = F_{xx} - \alpha H_{xx} \\ \hat{A}_{xz} &= A_{xz} - \beta D_{xz}, \quad \hat{D}_{xz} = D_{xz} - \beta F_{xz} \\ (D_{xx}, F_{xx}, H_{xx}) &= \int_A (z^2, z^4, z^6) E dA \\ (A_{xz}, D_{xz}, F_{xz}) &= \int_A (1, z^2, z^4) G dA \end{aligned} \quad (32)$$

3. Formulation of Symmetric Smoothed Particle Hydrodynamics

Taylor Series Expansion (TSE) of a scalar function can be given by

$$f(\xi_1) = \sum_{m=0}^n \frac{1}{m!} \left[(\xi_1 - x_1) \frac{d}{dx_1} \right]^m f(x_1) \quad (33)$$

where $f(\xi_1)$ is the value of the function at $\xi = (\xi_1)$ located in near of $x = (x_1)$. If the zeroth to sixth order terms are employed and the higher order terms are neglected, the equation (33) can be written as follows,

$$f(\xi) = P(\xi, x) Q(x) \quad (34)$$

where

$$Q(x) = \left[f(x), \frac{df(x)}{dx_1}, \frac{1}{2!} \frac{d^2 f(x)}{dx_1^2}, \dots, \frac{1}{6!} \frac{d^6 f(x)}{dx_1^6} \right]^T \quad (35)$$

$$P(\xi, x) = [1, (\xi_1 - x_1), (\xi_1 - x_1)^2, \dots, (\xi_1 - x_1)^6] \quad (36)$$

To determine the unknown variables given in the $Q(x)$, both sides of equation (34) are multiplied with $W(\xi, x)P(\xi, x)^T$ and evaluated for every node in the CSD. The following equation is obtained where $N(x)$ is the number nodes in the compact support domain (CSD) of the $W(\xi, x)$ as shown in Fig. 1.

$$\begin{aligned} \sum_{j=1}^{N(x)} f(\xi^{r(j)}) W(\xi^{r(j)}, x) P(\xi^{r(j)}, x)^T \\ = \sum_{j=1}^{N(x)} \left[P(\xi^{r(j)}, x)^T W(\xi^{r(j)}, x) P(\xi^{r(j)}, x) \right] Q(x) \end{aligned} \quad (37)$$

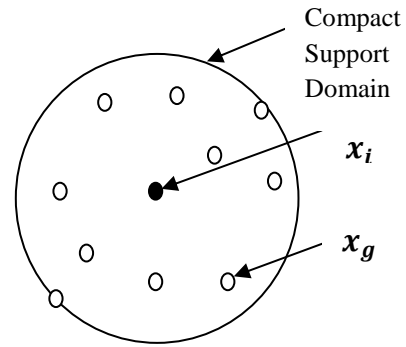


Fig. 1. Compact support of the weight function $W(\xi, x)$ for the node located at $x = (x_i, y_i)$

Then, equation (37) can be given by

$$C(\xi, x) Q(x) = D(\xi, x) F^{(x)}(\xi, x) \quad (38)$$

where $C(\xi, x) = P(\xi, x)^T W(\xi, x) P(\xi, x)$ and $D(\xi, x) = P(\xi, x)^T W(\xi, x)$.

The solution of equation (38) is given by

$$Q(x) = K(\xi, x) F(\xi) \quad (39)$$

where $K^{(x)}(\xi, x) = C(\xi, x)^{-1} D(\xi, x)$. Equation (39) can be also written as follows

$$Q_I(x) = \sum_{j=1}^M K_{Ij} F_j, \quad I = 1, 2, \dots, 6 \quad (40)$$

Where M is the number of nodes and $F_j = f(\xi^j)$. Seven components of equation (40) for 1D case are can be written as

$$\begin{aligned} f(x) &= Q_1(x) = \sum_{j=1}^M K_{1j} F_j \\ \frac{df(x)}{dx_1} &= Q_2(x) = \sum_{j=1}^M K_{2j} F_j \\ \frac{d^2 f(x)}{dx_1^2} &= 2! Q_3(x) = \sum_{j=1}^M K_{3j} F_j \\ \frac{d^3 f(x)}{dx_1^3} &= 3! Q_4(x) = \sum_{j=1}^M K_{4j} F_j \\ \frac{d^4 f(x)}{dx_1^4} &= 4! Q_5(x) = \sum_{j=1}^M K_{5j} F_j \\ \frac{d^5 f(x)}{dx_1^5} &= 5! Q_6(x) = \sum_{j=1}^M K_{6j} F_j \\ \frac{d^6 f(x)}{dx_1^6} &= 6! Q_7(x) = \sum_{j=1}^M K_{7j} F_j \end{aligned} \quad (41)$$

4. Numerical Results

The pure bending of two engineering beam problems by using the formulation of the EBT, TBT and RBT are solved by using the SSPH method. Different loading and boundary conditions are applied with different node distributions in the problem domain. For the numerical solutions obtained by the RBT are evaluated with different node distributions in the

problem domain and varying number of terms in the TSEs. The numerical results obtained by the SSPH method regarding to different beam theories are compared with the analytical solution of problem.

4.1. Simply Supported Beam

Static transverse deflections of a simply supported beam under uniformly distributed load of intensity q_0 as shown in Fig.2. is studied.

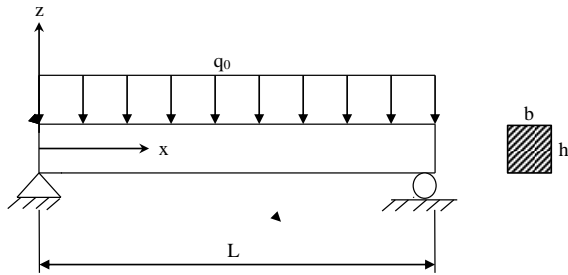


Fig. 2. Simply supported beam with uniformly distributed load

The physical parameters of the beam are given as $L=2m$, $h=0.2m$, $b=0.02m$. Modulus of elasticity E is 210 GPa, shear modulus G is 80.8 GPa and the distributed load q_0 is set to 150000 N/m.

Based on the EBT, the governing equation of the problem can be given by,

$$\frac{d^2}{dx^2} (D_{xx} \frac{d^2 w_0}{dx^2}) = q_0 \quad \text{for } 0 < x < L \quad (42)$$

where $D_{xx} = EI_y$ is the flexural rigidity of the beam and $I_y = bh^3/12$ the second moment of area about the y-axis. The boundary conditions regarding to the EBT are given as follows

$$x = 0, \quad \frac{d^2 w_0}{dx^2} = 0 \text{ and } w_0 = 0 \text{ m}$$

$$x = L, \quad \frac{d^2 w_0}{dx^2} = 0 \text{ and } w_0 = 0 \text{ m}$$

The analytical solution of this boundary value problem based on the EBT is given by

$$w_0^E(x) = \frac{q_0 L^4}{24 D_{xx}} \left(\frac{x}{L} - \frac{2x^3}{L^3} + \frac{x^4}{L^4} \right) \quad (43)$$

where the superscript E denotes the quantities in the EBT.

The governing equations of the problem can be written by using TBT as follows,

$$-\frac{d}{dx} \left(D_{xx} \frac{d\phi}{dx} \right) + \kappa_s A_{xz} \left(\phi + \frac{dw_0}{dx} \right) = 0 \quad (44)$$

$$-\frac{d}{dx} \left[\kappa_s A_{xz} \left(\phi + \frac{dw_0}{dx} \right) \right] = q_0 \quad (45)$$

where $D_{xx} = EI_y$ is the flexural rigidity of the beam, $I_y = bh^3/12$ is the second moment of area about the y-axis, $A_{xz} = GA = Gbh$ is the shear rigidity and the SCF is assumed to be constant $\kappa_s = 5/6$ for the rectangular cross section.

The boundary conditions regarding to the TBT are given as follows;

$$x = 0, \quad \frac{d\phi}{dx} = 0 \text{ and } w_0 = 0 \text{ m}$$

$$x = L, \quad \frac{d\phi}{dx} = 0 \text{ and } w_0 = 0 \text{ m}$$

The analytical solution of this boundary value problem based on the TBT is given by

$$w_0^T(x) = \frac{q_0 L^4}{24 D_{xx}} \left(\frac{x}{L} - \frac{2x^3}{L^3} + \frac{x^4}{L^4} \right) + \frac{q_0 L^2}{2 \kappa_s A_{xz}} \left(\frac{x}{L} - \frac{x^2}{L^2} \right) \quad (46)$$

where the superscript T denotes the quantities in the TBT.

The governing equations of the problem can be written by using RBT as follows,

$$-\frac{d}{dx} \left(\bar{D}_{xx} \frac{d\phi}{dx} - \alpha \hat{F}_{xx} \frac{d^2 w_0}{dx^2} \right) + \bar{A}_{xz} \left(\phi + \frac{dw_0}{dx} \right) = 0 \quad (47)$$

$$-\alpha \frac{d^2}{dx^2} \left(\hat{F}_{xx} \frac{d\phi}{dx} - \alpha H_{xx} \frac{d^2 w_0}{dx^2} \right) - \frac{d}{dx} \left[\bar{A}_{xz} \left(\phi + \frac{dw_0}{dx} \right) \right] = q \quad (48)$$

where $D_{xx} = EI_y$ is the flexural rigidity of the beam, $I_y = bh^3/12$ is the second moment of area about the y-axis, $A_{xz} = GA = Gbh$ is the shear rigidity, $\alpha = 4/(3h^2)$ and $\beta = 4/(h^2)$. \bar{D}_{xx} , \bar{A}_{xz} , \hat{F}_{xx} , H_{xx} are calculated according to the equations given in equation (32).

The boundary conditions regarding to the TBT are given as follows

$$x = 0, \quad \hat{D}_{xx} \frac{d\phi}{dx} - \alpha F_{xx} \frac{d^2 w_0}{dx^2} = 0, \text{ and } w_0 = 0 \text{ m}$$

$$x = L, \quad \hat{D}_{xx} \frac{d\phi}{dx} - \alpha F_{xx} \frac{d^2 w_0}{dx^2} = 0, \text{ and } w_0 = 0 \text{ m}$$

The analytical solution of this boundary value problem based on the RBT is given by

$$w_0^T(x) = \frac{q_0 L^4}{24 D_{xx}} \left(\frac{x}{L} - \frac{2x^3}{L^3} + \frac{x^4}{L^4} \right) + \left(\frac{q_0 \mu}{\lambda^4} \right) \left(\frac{\hat{D}_{xx}}{\hat{A}_{xz} D_{xx}} \right) \left[-\tanh \left(\frac{\lambda L}{2} \right) \sinh \lambda x + \cosh \lambda x + \frac{\lambda^2}{2} x(L-x) - 1 \right] \quad (49)$$

where

$$\lambda^2 = \frac{\bar{A}_{xz} D_{xx}}{\alpha (F_{xx} D_{xx} - F_{xx} D_{xx})}, \quad \mu = \frac{\hat{A}_{xz} \hat{D}_{xz}}{\alpha (F_{xx} \hat{D}_{xz} - F_{xx} D_{xx})}$$

The above boundary value problems are solved by using the SSPH method for the node distributions of 21, 41 and 161 equally spaced nodes in the domain $x \in [0, 2]$. As the weight function, the Revised Super Gauss Function (RSGF) which gives the least L_2 error norms in numerical solutions in [31] is used.

$$W(x, \xi) = \frac{G}{(h\sqrt{\pi})^\lambda} \begin{cases} (36 - d^2)e^{-d^2} & 0 \leq d \leq 6 \\ 0 & d > 6 \end{cases}$$

$$d = |x - \xi|/h \quad (50)$$

where d is the radius of the CSD, h is the smoothing length. G and λ are the parameters which are eliminated by the formulation of the SSPH method.

The numerical solutions are performed according to the following meshless parameters; the radius of the support

domain (d) is chosen as 6 and the smoothing length (h) equals to 1.1Δ where Δ is the minimum distance between two adjacent nodes. The meshless parameters, d and h, are selected to obtain the lowest error.

For the numerical solutions based on the formulation of the RBT, it is also investigated the effect of the different numbers of terms employed in the TSE when the number of nodes in the problem domain increases. Computed results obtained by using the SSPH method are compared with the analytical solutions, and their accuracy and convergence properties are investigated by employing the global L₂ error norm which is given in equation (51).

$$\|Error\|_2 = \frac{[\sum_{j=1}^m (v_{num}^j - v_{exact}^j)^2]^{1/2}}{[\sum_{j=1}^m (v_{exact}^j)^2]^{1/2}} \quad (51)$$

The L₂ error norms of the numerical solutions based on the EBT are given in Table 1. For the numerical analysis different numbers of nodes are considered in the problem domain with 5 terms in TSEs expansion. It is observed in Table 1 that the accuracy of the SSPH method is not improved by increasing of the number of nodes in the problem domain. At least for the problem studied here, it is impossible to evaluate the convergence rate of the SSPH method because of the level of the numerical errors which are too small obtained for different number of nodes in the problem domain.

It is observed in Fig. 3 that the SSPH method agrees very well with the analytical solution. The transverse deflection of the beam computed by the SSPH method is virtually indistinguishable from that for the analytical solution.

Table 1. L₂ error norm for different number of nodes based on EBT

Meshless Method	Number of Nodes		
	21 Nodes	41 Nodes	161 Nodes
SSPH	3.8563x10 ⁻⁹	9.0440x10 ⁻⁸	3.6898x10 ⁻⁷

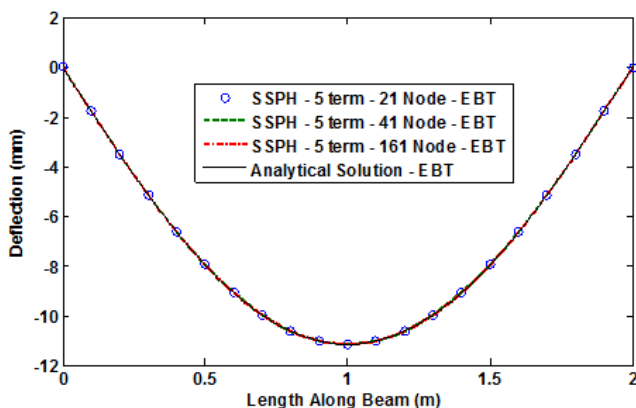


Fig. 3. Deflections of the beam computed based on the EBT and the analytical solution

The global L₂ error norms of the solutions based on the TBT are given in Table 2 where different numbers of nodes are considered with 5 terms in TSEs expansion. The results in Table 2 are obtained for the meshless parameters d and h which give the best accuracy for each method. It is observed

in Table 2 that the SSPH method almost gives the exact solution of the problem. The SSPH method gives accurate values of the displacement even for 21 nodes in the problem domain. It is observed in Fig. 4 that the SSPH method agrees very well with the analytical solution.

Table 2. L₂ error norm for different number of nodes based on TBT

Meshless Method	Number of Nodes		
	21 Nodes	41 Nodes	161 Nodes
SSPH	4.3044x10 ⁻¹⁰	3.7090x10 ⁻⁹	3.5981x10 ⁻⁹

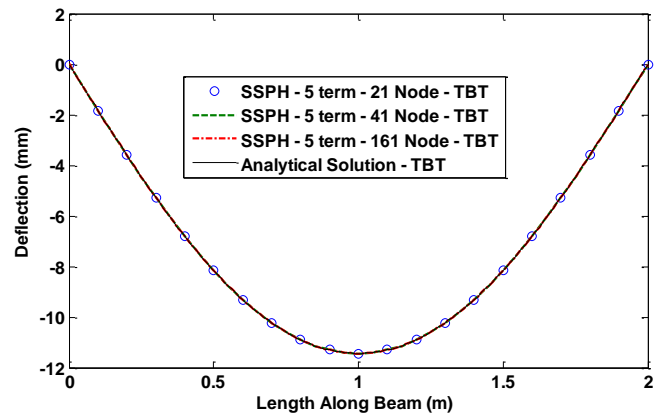


Fig. 4. Deflections of the beam computed based on the TBT and the analytical solution

The global L₂ error norms of the solutions based on the RBT are given in Table 3 where different numbers of nodes are considered with varying number of terms in TSEs expansion. The results in Table 3 are obtained for the meshless parameters d and h which gives the best accuracy for each method. Different numbers of terms in TSEs, 5 to 7, are employed to evaluate the performance of the SSPH method. It is found that the convergence rate of the computed solution increases by increasing the degree of complete polynomials. The rate of convergence for the SSPH method increases by increasing the number of nodes in the problem domain. It is clear that numerical solutions obtained by the SSPH method agree very well with the analytical solution given in Fig. 5 to Fig. 7.

Table 3. L₂ error norm for different number of nodes with varying number of terms in the TSEs

Nodes	Terms in the TSEs		
	5 Term	6 Term	7 Term
21	2.0631	2.0475	2.0014
41	2.0631	2.0317	1.6977
161	2.0631	1.9371	0.5556

Comparison of the analytical solutions in terms of transverse deflections obtained by the EBT, TBT and RBT are given in Fig. 8. It is observed that the analytical solution obtained by the EBT is similar to the analytical solution obtained by the RBT than the TBT. It is clear that the RBT is a higher order shear deformation theory that yields more accurate results than the other theories which are studied in this paper.

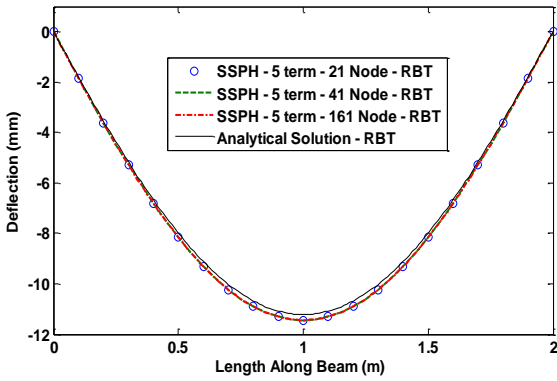


Fig. 5. Deflections of the beam computed based on the RBT and the analytical solution – 5 term

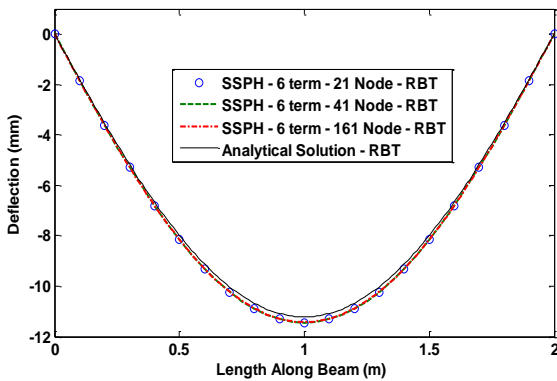


Fig. 6. Deflections of the beam computed based on the RBT and the analytical solution – 6 term

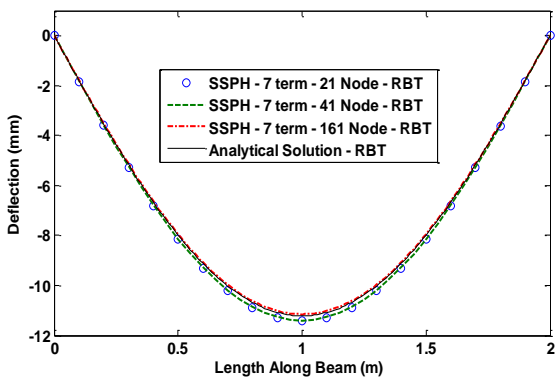


Fig. 7. Deflections of the beam computed based on the RBT and the analytical solution – 7 term

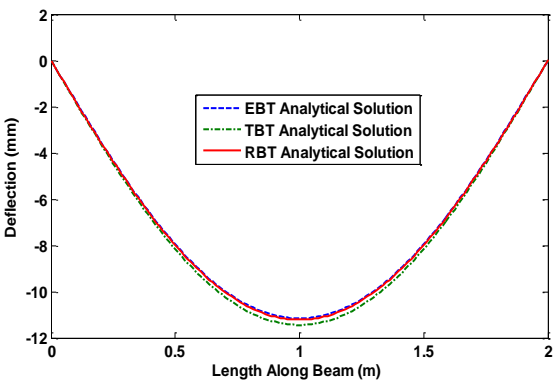


Fig. 8. Comparison of the analytical solutions in terms of deflections obtained by the EBT, TBT and RBT

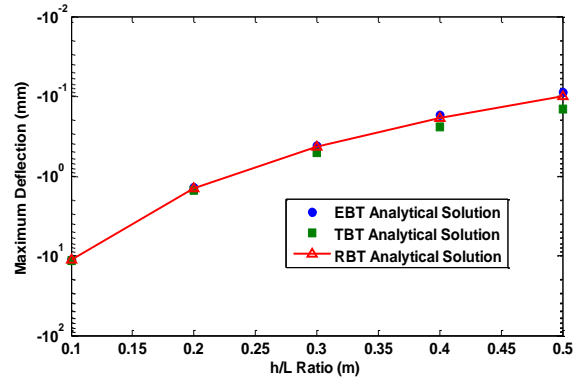


Fig. 9. Comparison of the analytical solutions in terms of maximum deflections obtained with varying h/L ratio

For the future studies, the effect of the h/L ratio can be investigated to evaluate the accuracy of the TBT in terms of transverse deflection. In Fig. 8, the h/L ratio is 0.1. It is observed in Fig. 9 that when the h/L ratio increases the accuracy of the TBT decreases in terms of transverse deflection.

4.2. Cantilever Beam

For a cantilever beam the static transverse deflections under uniformly distributed load of intensity q_0 as shown in Figure 10 is studied.

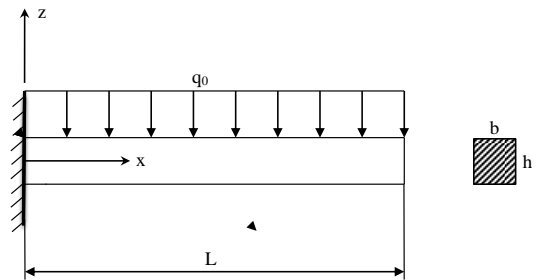


Fig. 10. Simply supported beam with uniformly distributed load

The physical parameters are given as $L=2\text{m}$, $h=0.2\text{m}$, $b=0.02\text{m}$. Modulus of elasticity E is 210 GPa, shear modulus G is 80.8 GPa and the uniformly distributed load q_0 is set to 50000 N/m.

Based on the EBT, the governing equation of the problem is as given in equation (42). The boundary conditions are given by;

$$x = 0, \quad \frac{dw_0}{dx} = 0 \text{ and } w_0 = 0 \text{ m}$$

$$x = L, \quad \frac{d^2w_0}{dx^2} = 0 \text{ and } \frac{d^3w_0}{dx^3} = 0$$

The analytical solution of this boundary value problem based on the EBT is given by

$$w_0^E(x) = \frac{q_0 L^4}{24D_{xx}} \left(6 \frac{x^2}{L^2} - 4 \frac{x^3}{L^3} + \frac{x^4}{L^4} \right) \quad (52)$$

Based on the TBT, the governing equations of the problem are given in equation (44) and equation (45). The

boundary conditions regarding to the TBT are given as follows

$$x = 0, \quad \phi = 0 \text{ and } w_0 = 0 \text{ m}$$

$$x = L, \quad \frac{d\phi}{dx} = 0 \text{ and } \phi + \frac{dw_0}{dx} = 0$$

The analytical solution of this boundary value problem based on the TBT is given by

$$w_0^T(x) = \frac{q_0 L^4}{24 D_{xx}} \left(6 \frac{x^2}{L^2} - 4 \frac{x^3}{L^3} + \frac{x^4}{L^4} \right) + \frac{q_0 L^2}{2 \kappa_5 A_{xz}} \left(2 \frac{x}{L} - \frac{x^2}{L^2} \right) \quad (53)$$

Based on the RBT, the governing equations of the problem are given in equation (47) and equation (48). The boundary conditions regarding to the RBT are given as follows

$$x = 0, \quad \phi = 0 \text{ and } w_0 = 0 \text{ m}$$

$$x = L, \quad \hat{D}_{xx} \frac{d\phi}{dx} - \alpha F_{xx} \frac{d^2 w_0}{dx^2} = 0, \text{ and } \phi + \frac{dw_0}{dx} = 0$$

The analytical solution of this boundary value problem based on the TBT is given by

$$w_0^R(x) = w_0^E(x) + \left(\frac{q_0 \mu}{2 \lambda^2} \right) \left(\frac{\hat{D}_{xx}}{\hat{A}_{xz} D_{xx}} \right) (2 L x - x^2) + \left(\frac{q_0 \mu}{\lambda^4 \cosh \lambda L} \right) \left(\frac{\hat{D}_{xx}}{\hat{A}_{xz} D_{xx}} \right) \left[\cosh \lambda x + \lambda L \sinh \lambda (L - x) - \left(\frac{q_0 \mu}{\lambda^4} \right) \left(\frac{\hat{D}_{xx}}{\hat{A}_{xz} D_{xx}} \right) \left(\frac{1 + \lambda L \sinh \lambda L}{\cosh \lambda L} \right) \right] \quad (54)$$

The above boundary value problems are solved by using the SSPH method for different node distributions of 21, 41 and 161 equally spaced nodes in the domain $x \in [0, 2]$. The Revised Super Gauss Function given in equation (50) is used as the weight function.

For the numerical solutions, the radius of the support domain (d) is chosen as 5 and the smoothing length (h) is chosen as 1.3Δ . Also, for the numerical solutions based on the RBT, it is investigated the effect of the various numbers of terms employed in the TSEs when the number of nodes in the problem domain increases. The meshless parameters, d and h, are selected to obtain the best accuracy. Computed results by the SSPH method are compared with the analytical solutions, and their rate of convergence and accuracy properties are investigated by using the global L2 error norm given in equation (51). In Table 4 the global L2 error norms of the solutions based on the EBT are given for different numbers of nodes in the problem domain with 5 terms in TSEs expansion. The similar case observed in the previous problem is also found in this problem.

The accuracy of the SSPH method is not improved by increasing of the number of nodes in the problem domain. At least for the problem studied here, it is impossible to evaluate the convergence of the SSPH method because of the level of the numerical errors which are too small obtained for different number of nodes in the problem domain. The computed transverse deflection of the beam is virtually indistinguishable from that for the analytical solution as seen from Fig. 12.

Table 4. L₂ error norm for different number of nodes based on EBT

Meshless Method	Number of Nodes		
	21 Nodes	41 Nodes	161 Nodes
SSPH	9.3439×10^{-8}	5.7719×10^{-6}	7.8041×10^{-6}

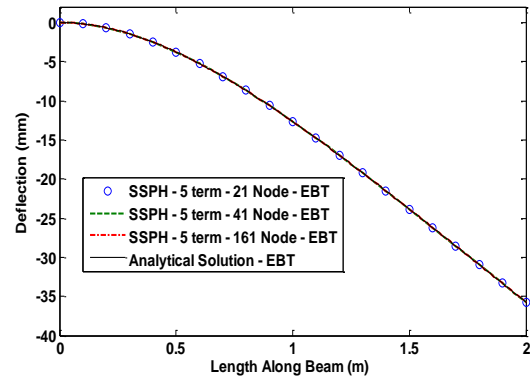


Fig. 12. Deflections of the beam computed based on the EBT and the analytical solution

By using different numbers of nodes in the problem domain with 5 terms in TSEs expansion, the global L₂ error norms of the solutions obtained for the TBT are given in Table 5. It is clear in Table 5 that the SSPH method provides satisfactory numerical results and rate of convergence. It is observed in Fig. 13 that the SSPH method agrees very well with the analytical solution.

Table 5. Global L₂ error norm for different number of nodes based on TBT

Meshless Method	Number of Nodes		
	21 Nodes	41 Nodes	161 Nodes
SSPH	1.1353×10^{-8}	3.2478×10^{-7}	7.2764×10^{-8}

The global L₂ error norms of the solutions based on the RBT are given in Table 6 where different numbers of nodes are considered with varying number of terms in TSEs expansion. It is observed that the convergence rate of the computed solution increases by increasing the degree of complete polynomials for 161 nodes in the problem domain.

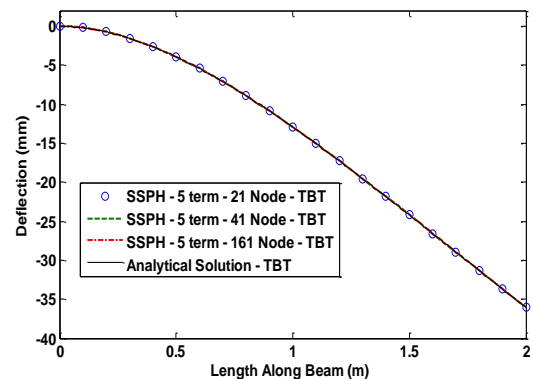


Fig. 13. Deflections of the beam computed based on the TBT and the analytical solution.

Table 6. L_2 error norm for different number of nodes with varying number of terms in the TSEs

Number of Nodes	Number of Terms in the TSEs		
	5 Term	6 Term	7 Term
21	1.7608	1.7608	1.7479
41	1.7783	1.7784	1.8504
161	1.7920	1.7919	1.5278

The convergence rate of the SSPH method is increasing as the number of nodes is increased in the problem domain even by using same number of terms in the TSEs. It is clear that the transverse displacement computed with the SSPH method closer to the analytical solution of the problem given in Fig. 14 to Fig. 16.

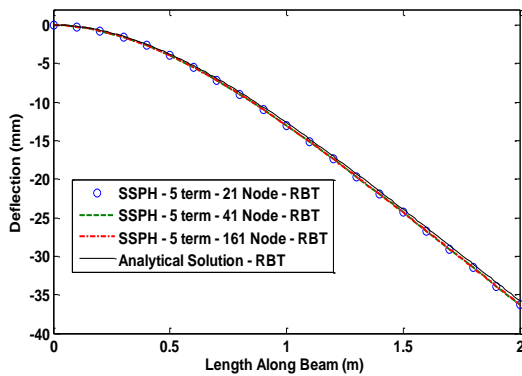


Fig. 14. Deflections of the beam based on the RBT along the x-axis computed by the SSPH method using different number of nodes and the analytical solution – 5 term

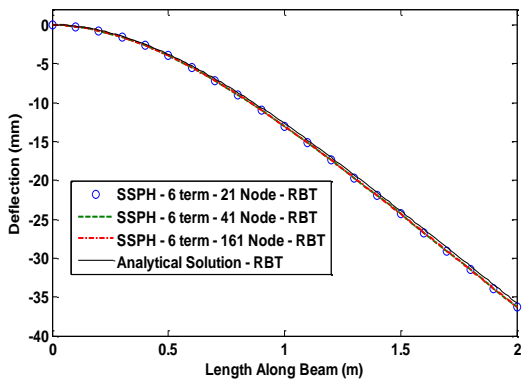


Fig. 15. Deflections of the beam based on the RBT along the x-axis computed by the SSPH method using different number of nodes and the analytical solution – 6 term

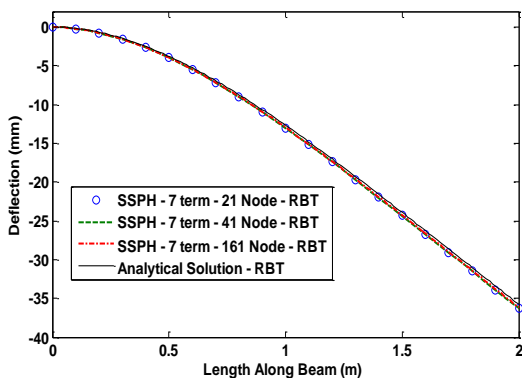


Fig. 16. Deflections of the beam based on the RBT along the x-axis computed by the SSPH method using different number of nodes and the analytical solution – 7 term

The analytical solutions of the EBT, TBT and RBT are compared in Fig. 17. It is clear that the analytical solution obtained by the EBT is more close to the analytical solution obtained by the RBT than the TBT. At least for the problem studied here, the EBT yields more accurate results in terms of transverse deflection than the TBT.

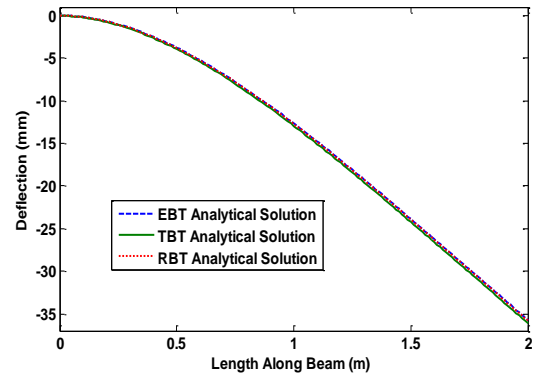


Fig. 17. Comparison of the analytical solutions in terms of deflections obtained by the EBT, TBT and RBT ($h/L=0.1$)

It is observed that the accuracy of the numerical results in terms of transverse deflection for TBT decrease with increasing h/L ratio. The h/L ratio is 0.1 in Fig. 17. It is found that increasing of the h/L ratio is decreasing the accuracy of the TBT in terms of transverse deflection as shown in Fig. 18.

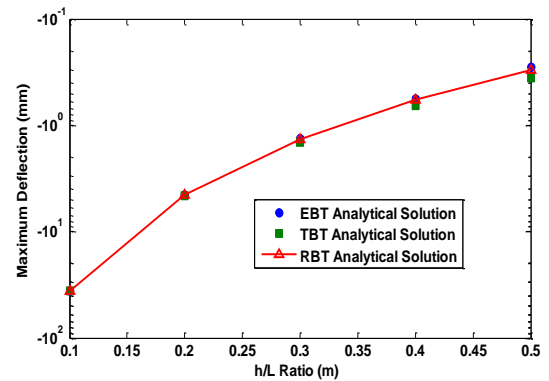


Fig. 18. Comparison of the analytical solutions in terms of maximum deflections obtained with varying h/L ratio

5. Conclusion

The SSPH basis functions are employed to numerically solve the transverse deflections of the thick isotropic beams subjected to different sets of boundary conditions and uniformly distributed load by using strong formulation of the problem. The numerical calculations are performed by using different number of nodes uniformly distributed in the problem domain and by employing different beam theories which are the EBT, TBT and RBT. The performance of the SSPH method is investigated for the solution of the beam problems with the TBT and RBT for the first time. It is found that the SSPH method provides satisfactory results and

convergence rate for the studied problems here. It is observed that the computed results of transverse deflections agree very well with the analytical solutions.

For the problems studied, it is found that the accuracy of the computed results based on the TBT is deteriorated by the aspect ratio (h/L). The accuracy of the transverse deflections computed by using analytical solution based on the TBT decreases with an increase in the aspect ratio of the beam.

It is observed that when the EBT formulation employed for the solution of the problems by using the SSPH method, the computed results in terms of the displacement are virtually indistinguishable from that for analytical solution and the solution obtained by the RBT formulation.

Based on the results of two numerical examples it is recommended that the SSPH method can be applied for solving linear beam problems by employing different shear deformation theories.

Acknowledgements

Author thanks to anonymous reviewers.

References

- [1] Love, A.E.H., A Treatise on the Mathematical Theory of Elasticity, fourth ed. Dover Publications, New York, 1927.
- [2] Timoshenko, S.P., Goodier, J.C., Theory of Elasticity, McGraw-Hill Co. Inc., New York, 1970.
- [3] Wang, C.M., Reddy, J.N., Lee, K.H., Shear Deformable Beams and Plates Relations with Classical Solutions, Elsevier Science Ltd., Oxford 2000.
- [4] Polizzotto, C., From the Euler-Bernoulli beam to the Timoshenko one through a sequence of Reddy-type shear deformable beam models of increasing order, European Journal of Mechanics A/Solids, 53, 62-74, 2015.
- [5] Levinson, M., A new rectangular beam theory, Journal of Sound and Vibration, 74, 81-87, 1981.
- [6] Bickford, W.B., A consistent higher order beam theory, Theor. Appl. Mech. 11, 137-150, 1982.
- [7] Heyliger, P.R., Reddy, J.N., A higher order beam finite element for bending and vibration problems, Journal of Sound and Vibration, 126 (2), 309-326, 1988.
- [8] Subramanian, P., Dynamic analysis of laminated composite beams using higher order theories and finite elements, Composite Structures, 73, 342-353, 2006.
- [9] Reddy, J.N., Nonlocal theories for bending, buckling and vibration of beams, Int. J. Eng. Sci. 45, 288-307, 2007.
- [10] Carrera, E., Giunta, G., Refined beam theories based on a unified formulation, Int. J. Appl. Mech. 2 (1), 117-143, 2010.
- [11] Giunta, G., Biscani, F., Bellouettar, S., Ferreira, A.J.M., Carrera, E., Free vibration analysis of composite beams via refined theories, Composites Part B, 44, 540-552, 2013.
- [12] Arya, H., A new zig-zag model for laminated composite beams: free vibration analysis, Journal of Sound and Vibration, 264, 485-490, 2003.
- [13] Jun, L., Hongxing, H., Dynamic stiffness analysis of laminated composite beams using trigonometric shear deformation theory, Composite Structures, 89, 433-442, 2009.
- [14] Kurama, M., Afaq, K.S., Mistou, S., Mechanical behavior of laminated composite beams by the new multi-layered laminated composite structures model with trigonometric shear stress continuity, Int. J. Solids Struct, 40, 1525-1546, 2003.
- [15] Donning, B.M., Liu, W.K., Meshless methods for shear-deformable beams and plates, Computer Methods in Applied Mechanics and Engineering, 152, 47-71, 1998.
- [16] Gu, Y.T., Liu, G.R., A local point interpolation method for static and dynamic analysis of thin beams, Computer Methods in Applied Mechanics and Engineering, 190, 42, 5515-5528, 2001.
- [17] Ferreira, A.J.M., Roque, C.M.C., Martins, P.A.L.S., Radial basis functions and higher-order shear deformation theories in the analysis of laminated composite beams and plates, Composite Structures, 66, 287-293, 2004.
- [18] Ferreira, A.J.M., Fasshauer, G.E., Computation of natural frequencies of shear deformable beams and plates by an RBF-pseudospectral method, Computer Methods in Applied Mechanics and Engineering, 196, 134-146, 2006.
- [19] Moosavi, M.R., Delfanian, F., Khelil, A., The orthogonal meshless finite volume method for solving Euler-Bernoulli beam and thin plate problems, Thin-Walled Structures, 49, 923-932, 2011.
- [20] Roque, C.M.C., Figaldo, D.S., Ferreira, A.J.M., Reddy, J.N., A study of a microstructure-dependent composite laminated Timoshenko beam using a modified couple stress theory and a meshless method, Composite Structures, 96, 532-537, 2013.
- [21] Lucy LB, A numerical approach to the testing of the fission hypothesis, Astronomical Journal, 82, 1013-1024, 1977.
- [22] Chen JK, Beraun JE, Jin CJ, An improvement for tensile instability in smoothed particle hydrodynamics, Computational Mechanics, 23, 279-287, 1999.
- [23] Chen JK, Beraun JE, Jin CJ, Completeness of corrective smoothed particle method for linear elastodynamics, Computational Mechanics, 24, 273-285, 1999.

- [24] Liu WK, Jun S, Zhang YF, Reproducing kernel particle methods, *International Journal for Numerical Methods in Fluids*, 20, 1081–1106, 1995.
- [25] Liu WK, Jun S, Li S, Adee J, Belytschko T, Reproducing kernel particle methods for structural dynamics, *International Journal for Numerical Methods in Engineering*, 38, 1655–1679, 1995.
- [26] Chen JS, Pan C, Wu CT, Liu WK, Reproducing kernel particle methods for large deformation analysis of nonlinear structures, *Computer Methods in Applied Mechanics and Engineering*, 139, 195–227, 1996.
- [27] Zhang GM, Batra RC, Modified smoothed particle hydrodynamics method and its application to transient problems, *Computational Mechanics*, 34, 137–146, 2004.
- [28] Batra RC, Zhang GM, Analysis of adiabatic shear bands in elasto-thermo- viscoplastic materials by modified smoothed particle hydrodynamics (MSPH) method, *Journal of Computational Physics*, 201, 172–190, 2004.
- [29] Zhang GM, Batra RC, Wave propagation in functionally graded materials by modified smoothed particle hydrodynamics (MSPH) method, *Journal of Computational Physics*, 222, 374–390, 2007.
- [30] Batra RC, Zhang GM, Search algorithm, and simulation of elastodynamic crack propagation by modified smoothed particle hydrodynamics (MSPH) method, *Computational Mechanics*, 40, 531–546, 2007.
- [31] Zhang GM, Batra RC, Symmetric smoothed particle hydrodynamics (SSPH) method and its application to elastic problems, *Computational Mechanics*, 43, 321–340, 2009.
- [32] Batra RC, Zhang GM, SSPH basis functions for meshless methods, and comparison of solutions with strong and weak formulations, *Computational Mechanics*, 41, 527–545, 2008.
- [33] Tsai CL, Guan YL, Batra RC, Ohanehi DC, Dillard JG, Nicoli E, Dillard DA, Comparison of the performance of SSPH and MLS basis functions for two-dimensional linear elastostatics problems including quasistatic crack propagation, *Computational Mechanics*, 51, 19–34, 2013.
- [34] Tsai CL, Guan YL, Ohanehi DC, Dillard JG, Dillard DA, Batra RC, Analysis of cohesive failure in adhesively bonded joints with the SSPH meshless method, *International Journal of Adhesion & Adhesives*, 51, 67–80, 2014.
- [35] Karamanli A, Mugan A, Solutions of two-dimensional heat transfer problems by using symmetric smoothed particle hydrodynamics method, *Journal of Applied and Computational Mathematics* 1, 1–6, 2012.
- [36] Karamanli A, Bending Deflection Analysis of a Semi-Trailer Chassis by Using Symmetric Smoothed Particle Hydrodynamics, *International Journal of Engineering Technologies*, 1, 4, 134–140, 2015.
- [37] Karamanli A, Mugan A, Strong form meshless implementation of Taylor series method, *Applied Mathematics and Computation*, 219, 9069–9080, 2013 .
- [38] Karamanli A, Different Implementation Approaches of the Strong Form Meshless Implementation of Taylor Series Method, *International Journal of Engineering Technologies*, Vol. 1, No:3, 2015.
- [39] Kaewumpai, S., Luadsong, A., Two-field-variable meshless method based on moving kriging interpolation for solving simply supported thin plates under various loads. *Journal of King Saud University - Science*, 1018–3647, 2014.
- [40] Yimnak, K., Luadsong, A., A local integral equation formulation based on moving kriging interpolation for solving coupled nonlinear reaction–diffusion equations. *Advances in Mathematical Physics*, 2014.
- [41] Zhuang, X., Zhu, H., Augarde, C., The meshless Shepard and least squares (MSLS) method, *Computational Mechanics*, 53, 343–357, 2014.
- [42] Fatahi, H., Nadjafi, JS, Shivanian, E, New spectral meshless radial point interpolation (SMRPI) method for the two-dimensional Fredholm integral equations on general domains with error analysis, *Journal of Computational and Applied Mathematics*, 264, 196–209, 2016.

Development of a Lidar System Based on an Infrared RangeFinder Sensor and SlipRing Mechanism

Gokhan Bayar*[‡], Alparslan Uludag*

*Department of Mechanical Engineering, Faculty of Engineering, Bulent Ecevit University, 67100 Zonguldak, Turkey.

(bayar@beun.edu.tr, alpdras@gmail.com)

[‡]Corresponding Author; Gokhan Bayar, Department of Mechanical Engineering, Faculty of Engineering, Bulent Ecevit University, 67100 Zonguldak, Turkey, Tel: +90 3722574010/1224, Fax: +90 3722574023, email: bayar@beun.edu.tr

Received: 06.06.2016 Accepted: 03.08.2016

Abstract-Lidar systems are one of the most important sensor infrastructures in autonomous vehicles and mobile robots. They are used for achieving indoor and outdoor mapping purposes. In the scope of this study, a new perspective to develop a lidar system is proposed. The system developed is constructed based on a low-cost infrared rangefinder sensor, low-cost slipping mechanism designed and manufactured, dc motor and microprocessor. The rangefinder sensor is mounted to a head-structure actuated by a dc motor that continuously rotates with a desired rotational velocity. The data coming from the rangefinder sensor flows through the microprocessor via the slipping. The design concept of the slipping mechanism gives an advantage that the data of the infrared rangefinder sensor can be taken while the sensor continuously rotates. The required power for the sensor can also be supplied by the slipping during motion. The decoding process of the data coming from the rangefinder sensor and motor control task are accomplished using an ATmega based microprocessor. A user interface is also created to communicate with the system and evaluate the performance of the whole structure developed. After conducting many experiments, successful results are obtained. The design steps of the system proposed and the experimental results are presented in this paper.

Keywords Lidar, infrared sensor, slipping, laser scanner, range finder.

1. Introduction

Autonomous vehicles and mobile robots require recognizing their surroundings. They are generally programmed to track a predefined trajectory / path in order to perform an autonomous task. While they effort to track a reference trajectory, a lidar system provides them the surrounding information (in order words lidar system behaves like their eyes). By this way, they can be able to recognize the obstacles, people, other vehicles, etc. The use of information coming from a lidar system can provide the opportunities to the autonomous systems to take some pre-actions so that any unexpected events could be prevented. In addition to recognizing the working environment of the autonomous vehicles, lidar systems are also used as a feedback sensor for the control systems. Desired trajectory tracking tasks including position, orientation and velocity control routines can be supported by the feedback information acquired from a lidar system.

In the autonomous vehicle applications, path planning is one of the most critical issues that should be carefully designed. To achieve a successful path tracking control, reference path should be constructed by taking into account the working environment structure, capabilities and capacities of the vehicle and sensors. Lidar systems are one of the solutions for developing real-time maps of the working area and planning the desired paths. They can be adapted into the path planning algorithms as a powerful feedback option. The feedback information can also be used for the localization issues. An autonomous vehicle application, in which the location of the vehicle during the motion should be known, requires real-time position and orientation information. This can also be achieved by the use of a lidar system. An autonomous orchard application may be a good example for such a task (as presented in Fig. 1). In this figure, an orchard environment including trees and rows of trees and a four-wheeled vehicle is shown. In this scenario, the vehicle should drive itself autonomously inside the orchard. A lidar is mounted at the

front-mid-center of the vehicle for recognizing the surroundings. Its responsibilities are to provide the required data which is used for both detecting trees and estimating rows of trees. The lidar data is also necessary for localizing the vehicle inside the orchard. Suppose that point (X_0, Y_0) is the starting position. The scanning radius of the lidar is shown by R . In order to create a safe drive, let's say this is an objective in this scenario, the vehicle should move on the center line that is exactly the middle of two neighboring rows. When there is a positioning error, indicated by y_e in Fig. 1, the lidar system should warn the control system to take the required actions for steering the vehicle through the desired path. This action is also depicted in Fig. 1.

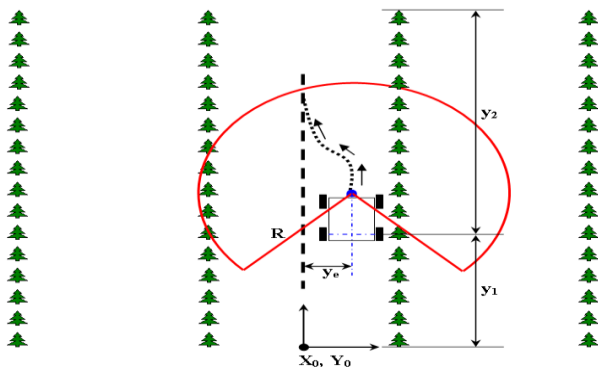


Fig. 1. The use of lidar in an autonomous orchard application

The importance of the use of lidar systems in autonomous applications is shown by a couple of examples presented above. Development of new lidar systems, approaches and models is still being continued. Parallel to the enhancements in the lidar research area, a new methodology for developing a lidar system is focused in this study. The new methodology involves the adaptation of a low-cost infrared rangefinder and a low-cost and easy-to-use slipping mechanism. The rangefinder sensor, which continuously rotates by the help of a head structure designed, is used to scan the 360° surrounding of the lidar system developed. This rotating mechanism enables that the working environment of the sensor can be sensed. Furthermore, when the sensor is surrounded by an object, the 2D shape of the object can be detected. The rotational motion is provided using a dc motor. The slipping mechanism is plugged to the system for achieving data flow from the rangefinder sensor to the microprocessor. ATmega based microprocessor is also used to achieve computation and communication purposes.

This paper is organized as follows: the next section presents the literature studies reviewed. Section 3 presents the lidar systems and their working principles. Section 4 introduces the lidar system proposed in this study. Prior to the concluding remarks, experimental results are given in Section 5.

2. Literature Studies

The studies related to lidar systems can be reviewed into two main topics. The first topic is about proposing

new approaches to develop lidar systems. The other topic focuses on implementing the lidar systems into the robotic applications.

In [1], a lidar application for agricultural tasks was proposed. The data coming from a lidar was the only sensor source that provides feedback information to the mathematical model developed. In the scope of this study, a lidar canopy height model was developed using a semi-automated pit filling algorithm. In [2], the accuracy enhancement of large scale canopy heights was focused. A new approach based on lidar output was. The system introduced was tested by the help of different scenarios. In [3], lidar system was used in city modeling and building recognition tasks. The use of methodology introduced for building footprints was presented. Classification of the roof structures of the buildings was also evaluated using algorithm created based on the lidar sensor data. In [4], lidar sensor was used for a planetary application. A system based on the lidar sensor data was constructed for achieving autonomous safe landing on planetary bodies. In [5], a lidar system was developed for forestry applications. The methodology was constructed based on laser induced fluorescence imaging technique. The system developed was tested to observe the performance of the proposed structure. Working characteristics of the system was also produced. In [6], a lidar was used to estimate individual tree heights in forestry applications. The data coming form lidar was accompanied with the aerial photography. In [7], a new approach for detecting stone monuments was proposed. The method was constructed based on data coming from a lidar. In [8], a lidar system was developed for observing the atmospheric events and the particle density inside in it. In [9], a crop monitoring system was proposed. The system was constructed based on a lidar and 3D stereoscopic vision system. The system developed was tested for autonomous agricultural applications. In [10], a lidar was placed on a mobile platform and the data was logged. The developed methodology used the data logged for extracting highway light poles and towers. In [11], an automatic classification of urban pavements system based on lidar was built. In [12], a lidar based intelligent system was developed for recognizing the ancient city walls. The modeling strategy was also used for doing digital documentation. In [13], a road detection system was constructed using lidar point clouds. The system was modeled in a way that could have the capability for adapting itself according to the data intensity. In [14], a lidar based system was built for detecting open water surfaces in an Arctic delta. The system was modeled by following the principles of decision tree classification technique.

As seen in the literature studies, lidar systems are commonly used in different applications ranging from defense to industrial robotics, agriculture to automation, unmanned ground vehicles to submarines, civil engineering to architecture. In the market, there are already some lidar systems [15, 16, 17, 18] that are ready-to-use for the researchers and engineers. However, they may not be affordable for small-scale projects, small-scale research companies, student works, startup formations, etc. Due to

their high-prices, many lidar development research studies have been continuing. Their common goal is to build low-price and easy-to-implement lidar systems. In parallel with the recent developments in the lidar research, this study aims to make a contribution to the continued investigations about developing lidar systems and to create a new perspective for this field.

3. Lidar Systems

Lidar systems are commonly used in different research studies and industrial applications. They are adapted into the real-time running unmanned aerial and autonomous ground vehicles. Path planning, mapping and control issues are supported by the data coming from lidar systems. They are also used for terrestrial scanning. Topography map creation, mining reconstruction, architecture, archaeology, building researches and city reconstruction require environmental data supplied by a lidar. Lidar systems are also intensively used for observation of agricultural and forestry areas, urban sites, industrial and power plants. Real-time mapping of such regions can be created using the information provided by the lidar systems. The moving platforms like industrial forklifts, public transportation vehicles, trains, boats, off-road and unmanned vehicles are also suited with the lidar systems so as to ensure safe drive. In addition to providing fast drive and safe product handling, such systems are also utilized for increasing the reliability and performance in manufacturing systems. They are also implemented to the tools and systems manufactured by the defense industries. The other usage area of the lidar systems is the marine industry. Lidar systems can be plugged into any marine platforms to increase safe drive capabilities and working performance. Creating autonomy in marine products needs to be used lidar system as well.

A 2D lidar, laser scanning, system is depicted in Fig. 2. The system consists of a light source, transmitter, receiver and mirror. The light hitting the object and returning back is sensed by the receiver and the distance between the light source and the object is obtained. If an actuator is coupled to this system, a rotating lidar system would be built.

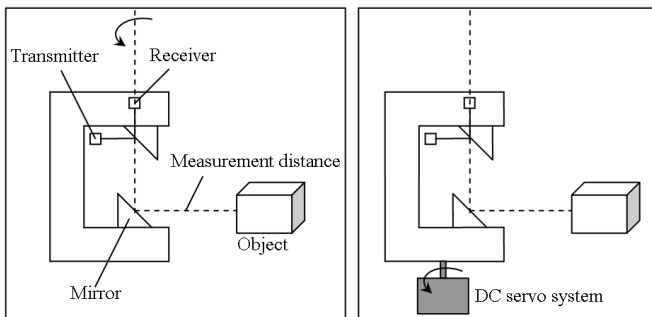


Fig. 2. Working principle of a lidar (laser scanning) system (left). Using an actuator to develop a rotating-lidar system (right)

4. Lidar System Developed in This Study

In this study, a design strategy to develop a lidar system is formed to meet the following criteria that the end product should be low-cost and accessible, easy-to-use and efficient. Following these design criteria, the lidar system consisting of three main subsections is taken into consideration. A low-cost infrared rangefinder sensor (Sharp GP2Y0A21YK) that can be easily found in the market is used. The Lidar system developed is able to detect the objects that are closer than 80 cm. To trigger the sensor, 5V DC voltage is required. It gives analog voltage as the output which should be decoded using a microprocessor. The block diagram of the system is shown in Fig. 3. In this figure, the reference input and outputs, data flows from sensors through the microprocessor and computer are shown. The control system constructed to control the dc actuator is also presented in this block diagram.

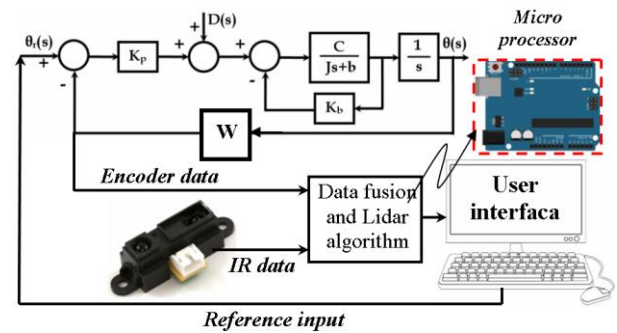


Fig. 3. Block diagram of the system developed

The infrared rangefinder sensor is mounted to a designed head-structure that continuously rotates (Fig. 4). The rotation is provided using a 6V DC motor driven by a L298 H-bridge (motor motion control unit). The torque regulation is accomplished via a gear-head attached to the DC motor. An ATmega based microprocessor, called computing unit, is used for decoding, computing and communication purposes (Fig. 4). It needs 5V DC supply voltage and is connected through the computer via USB.

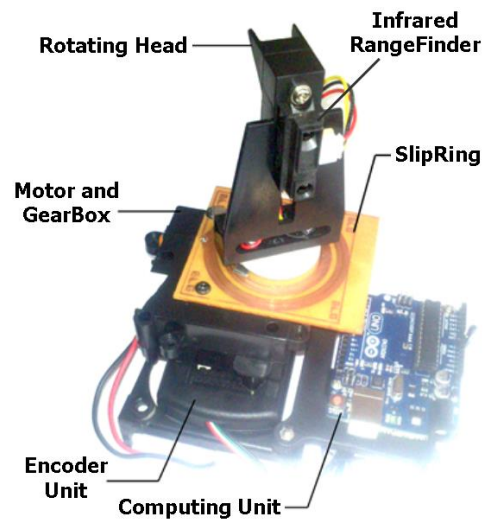


Fig. 4. General view of the lidar system developed in this study. Computing unit consists of an ATmega based microprocessor

To get the rotation information, a simple encoder unit presented in Fig. 5 is also built. This unit consists of an encoder disc and Omron photomicrosensor [19]. The resolution of the encoder unit is 36 pulses per revolution. The counting of the pulses is also achieved using the ATmega based computing unit.



Fig. 5. Encoder unit including an encoder disc and photomicrosensor

In order to achieve data flow from the infrared rangefinder sensor, which continuously rotates during operation, to the computing unit, a new design perspective for slipping mechanism is considered. The top and side views of the developed system are shown in Fig. 6. The infrared rangefinder sensor needs three cable connections; one is for data flow and the other two is for power supply. The simple slipping mechanism, presented in Fig. 6, is constructed to make these connections. The data flow is achieved using the inner circle and the power is supplied via the middle and the outer circles (Fig. 6-left).

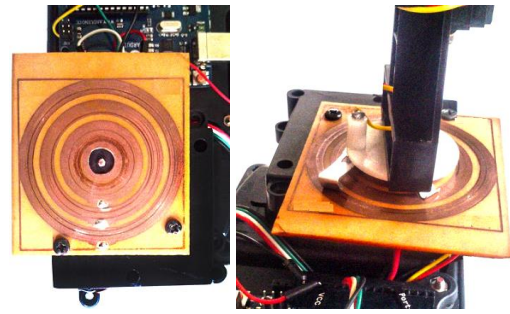


Fig. 6. Slipping mechanism developed. Top view (left) and side view (right) are shown.

5. Experimental Studies

In order to see the performance and accuracy of the lidar system proposed, the sensor structure introduced above is experimentally tested. It is placed at the center of a box which has the dimensions of 30 cm x 21 cm. The first experiment is performed for only 1 complete revolution. The resolution of the lidar system developed is 10 degrees therefore 36 distance measurements are obtained for one revolution. The results for this scenario are presented in Fig. 7 (top-left). To see the performance and accuracy enhancement while the number of turns is increased, experiments are performed from one to ten complete revolutions. The results obtained for “i” revolution(s), (i = 1, 2, ...,9), are shown in Fig. 7.

The experiment results including 10 full revolutions are given in Fig. 8. The results are presented in polar plots. The left polar plot shows all the measurements of the 10 turns whereas the right polar plot presents the average values of each measurement.

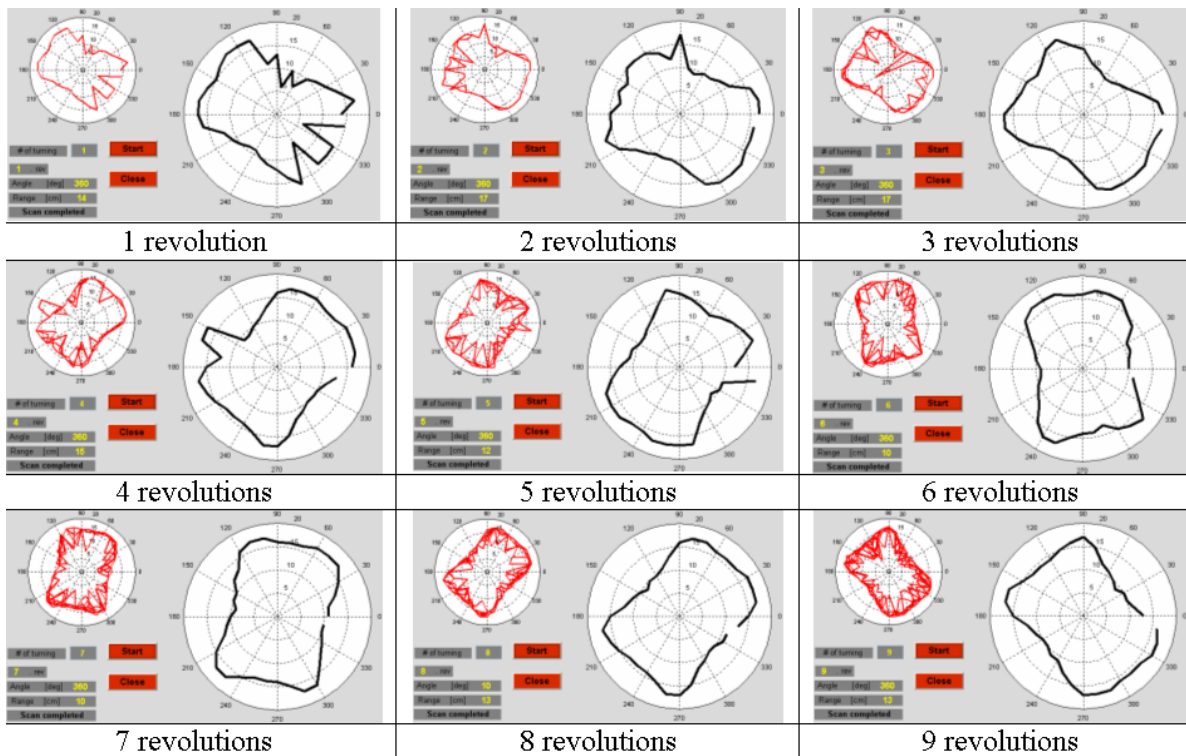


Fig. 7. Experiments performed using the lidar system. The results including 1 to 9 complete revolutions are presented

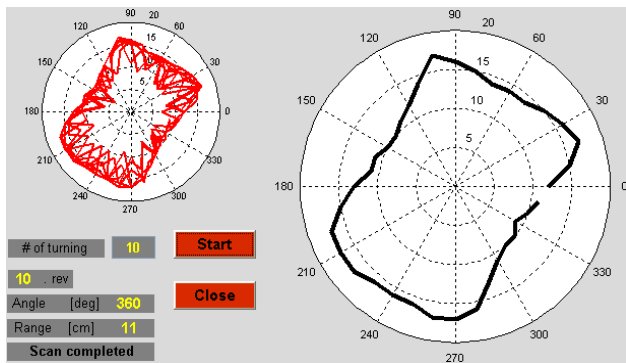


Fig. 8. Experiment results including 10 full revolutions. The left polar plot shows the measurement for all turns. The right polar plot indicates the average values of the measurements

The results given in Fig. 8 and 9 show that increasing the number of scans increases the accuracy and performance. The box's shape can be poorly estimated if only 1 revolution is performed (Fig. 9-a) whereas the shape obtained by the 10 complete revolutions is able to give almost the actual shape of the box (Fig. 9-b). These results emphasize that a lidar system developed using a low-cost infrared rangefinder sensor, a rotating head-structure and a simple slipping mechanism can be successfully used for scanning and recognizing purposes.

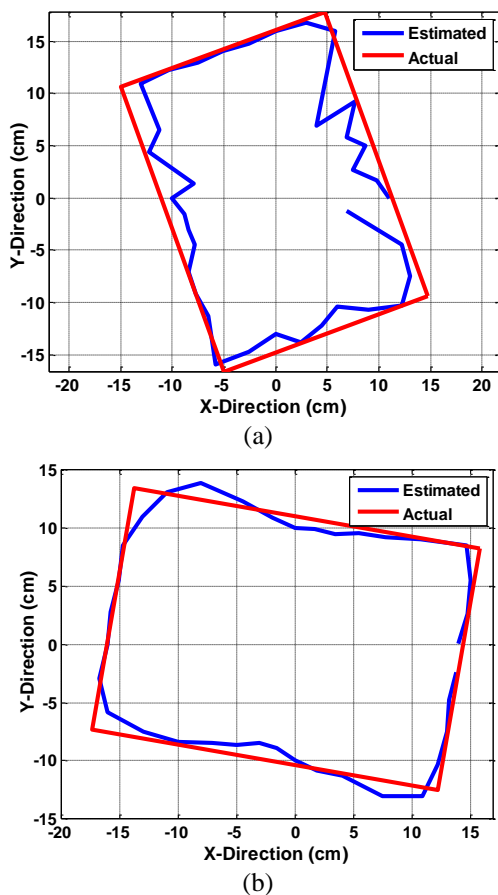


Fig. 9. The measurements of 1 revolution (a) and 10 revolutions (b). The red-colored-lines indicate the actual box's shape that has the dimensions of 30 cm x 21 cm. The blue-colored-lines indicate the experimental results

6. Analysis and Conclusion

In indoor and outdoor mapping applications used for autonomous drives and automations, one of the important sensorial systems is the lidar. They are adapted into the control systems for providing feedback information. Lidar systems are able to scan the surrounding from 0 to 360 degrees in variety of distances. The distances may range from 0 to a few kilometers. In the market, there are already some lidar systems that are used for autonomous research and applications. However, these products may not be accessible by the small companies, small research groups and students because of their high-cost. In the scope of this study, it is objected to develop a low-cost, easy-to-use and easy-to-implement lidar system. The system proposed is built using a low-cost infrared rangefinder sensor and a slipping mechanism designed. The end product is able to rotate continuously and give distance data in every 10 degrees. The rotation is provided via a dc motor and the rotation information is obtained using an encoder. An ATmega based microprocessor is also used as the computational unit of the lidar system. In order to see the accuracy and the performance of the system proposed, a user interface is created in the computer side. Many experiments are performed and successful results are obtained. The results obtained in this study emphasize that the design strategy introduced provides a new perspective for developing lidar systems and can be used for the further researches.

References

- [1] J. R. Ben-Arie, G. J. Hay, R. P. Powers, G. Castilla, B. St-Onge, Development of a pit filling algorithm for LiDAR canopy height models, *Computers & Geosciences*, Vol. 35, pp. 1940–1949, 2009.
- [2] M. Hollaus, W. Wagner, C. Eberhöfer, W. Karel, Accuracy of large-scale canopy heights derived from LiDAR data under operational constraints in a complex alpine environment, *ISPRS Journal of Photogrammetry & Remote Sensing*, Vol. 60, pp. 323–338, 2006.
- [3] C. Alexander, S. Smith-Voysey, C. Jarvis, Kevin Tansey, Integrating building footprints and LiDAR elevation data to classify roof structures and visualise buildings, *Computers, Environment and Urban Systems*, Vol. 33, pp. 285–292, 2009.
- [4] F. Amzajerdian, D. Pierrottet, L. Petway, M. Vanek, Development of lidar sensor systems for autonomous safe landing on planetary bodies, *International Conference on Space Optics*, Rhodes Island, Greece, 2010
- [5] Y. Saito, R. Saito, T. D. Kawahara, A. Nomura, S. Takeda, Development and performance characteristics of laser-induced fluorescence imaging lidar for forestry applications, *Forest Ecology and Management*, Vol. 128, pp. 129–137, 2000.

- [6] J. C. Suarez, C. Ontiveros, S. Smith, S. Snape, Use of airborne LiDAR and aerial photography in the estimation of individual tree heights in forestry, *Computers & Geosciences*, Vol. 31, pp. 253–262, 2005.
- [7] G. Cecchi, L. Pantani, V. Raimondi, L. Tomaselli, G. Lamenti, P. Tiano, R. Chiari, Fluorescence lidar technique for the remote sensing of stone monuments, *Journal of Cultural Heritage*, Vol. 1, pp. 29–36, 2000.
- [8] J. Bregeon, M. Compin, S. Rivoire, M. Sanguillon, G. Vasileiadis, An elastic lidar system for the H.E.S.S. Experiment, *Nuclear Instruments and Methods in Physics Research A*, Vol. 819, pp. 60–66, 2016.
- [9] M. Bietresato, G. Carabin, R. Vidoni, A. Gasparetto, F. Mazzetto, Evaluation of a LiDAR-based 3D-stereoscopic vision system for crop-monitoring applications, *Computers and Electronics in Agriculture*, Vol. 124, pp. 1–13, 2016.
- [10] W. Y. Yan, S. Morsy, A. Shaker, M. Tulloch, Automatic extraction of highway light poles and towers from mobile LiDAR data, *Optics & Laser Technology*, Vol. 77, pp. 62–168, 2016.
- [11] L. D. Vilariño, H. G. Jorge, M. Bueno, P. Arias, I. Puente, Automatic classification of urban pavements using mobile LiDAR data and roughness descriptors, *Construction and Building Materials*, Vol. 102, pp. 208–215, 2016.
- [12] L. Cheng, Y. Wang, Y. Chen, M. Li, Using LiDAR for digital documentation of ancient city walls, *Journal of Cultural Heritage*, Vol. 17, pp. 188–193, 2016.
- [13] Y. Li, B. Yong, H. Wu, R. An, H. Xu, Road detection from airborne LiDAR point clouds adaptive for variability of intensity data, *Optik*, Vol. 126, 4292–4298, 2015.
- [14] N. Crasto, C. Hopkinson, D. L. Forbes, L. Lesack, P. Marsh, I. Spooner, J. J. V. D. Sanden, A LiDAR-based decision-tree classification of open water surfaces in an Arctic delta, *Remote Sensing of Environment*, Vol. 164, pp. 90–102, 2015.
- [15] <http://www.rieglusa.com/lidar-scanners-and-sensors-systems.html>, Last accessed, June 05, 2016.
- [16] <http://www.phoenix-aerial.com/products/lidar-systems>, Last accessed, June 05, 2016.
- [17] <http://velodynelidar.com>, Last accessed, June 05, 2016.
- [18] <http://www.teledyneoptech.com/index.php/products/airborne-survey/lidar-systems>, Last accessed, June 05, 2016.
- [19] <https://www.omron.com/ecb/products/photo/#photo-micro>, Last accessed, June 05, 2016.

Calculation and Optimizing of Brake Thermal Efficiency of Diesel Engines Based on Theoretical Diesel Cycle Parameters

Safak Yildizhan^{*}, Vedat Karaman^{**‡}, Mustafa Ozcanli^{*}, Hasan Serin^{*}

^{*}Department of Automotive Engineering, Cukurova University, 01330 Adana, Turkey.

^{**}Department of Mechanical Engineering, Istanbul Gelisim University, 34315 Istanbul, Turkey.

(yildizhans@cu.edu.tr, vkaraman@gelisim.edu.tr, ozcanli@cu.edu.tr, hserin@cu.edu.tr)

[‡] Corresponding Author: Vedat Karaman, Department of Mechanical Engineering, Istanbul Gelisim University, 34315 Istanbul, Turkey, Tel:+90 212 422700, Fax: +90 2124227401, vkaraman@gelisim.edu.tr

Received: 25.07.2016 Accepted: 02.09.2016

Abstract-In this study, a theoretical study has been evaluated in order to calculate and optimize diesel engine brake thermal efficiency values. In the study three main parameters which are compression ratio, ratio of specific heat and cut-off ratio, based on ideal diesel cycle were evaluated. Compression ratio, ratio of specific heats and cut-off ratios were chosen between the interval of; 12:1-24:1, 1,2-1,4 and 1,5-3,0, respectively. Theoretical study showed that compression ratio significantly affects the engine characteristics that calculated in this study. Experiments revealed that the higher compression ratio results with higher brake thermal efficiency (BTHE) and thus lower specific fuel consumption (SFC). The calculation study showed that increasing cut-off ratio caused to decrease of brake thermal efficiency. Also, study revealed that increment of ratio of specific heats improved brake thermal efficiency.

Keywords Thermal efficiency, performance, compression ratio, specific heats, cut-off ratio, optimization.

1. Introduction

A large part of the energy consumed in the world is derived from fossil fuels such as petroleum, coal and natural gas. But, these petroleum based non-renewable resources will come to an end in the short run. Therefore, the investigations for renewable and sustainable alternative energy sources which can provide the necessary energy demand of the world has gained attention all over the world due to hazard of depletion of fuels, high price of petroleum and environmental concerns such as air pollution and global warming [1]. In the last decades, research interests on the internal combustion engines (ICE) have been explored in the area of alternate fuels, which are renewable, locally available, environment friendly [2]. Beside these fuel researches the operating conditions of engines have gained very importance by researchers and manufacturers. Improvement internal combustion engines by optimizing the all operating conditions have been one of the primary study subjects through researchers. To be able to increase the efficiency of an engine all effects of engine parameters should be known. Thus, many researchers have investigated

the effects of these parameters mostly using variable compression engine (VCR) [2-8].

The diesel engines are very fuel efficient and thus provide fuel economy. The operational simplicity of diesel engines makes diesel engines more preferable in the transportation sector and agricultural and forestry machinery. The extinction risk of fossil fuel and high cost of the petroleum causes to increase of effort in the means of alternative fuel development. [9].

After the oil crisis of the 1970s, investigation efforts on the field of the internal combustion engines have been extended in the area of alternative fuels, which are available locally, biodegradable, less toxic, environment friendly renewable, compared to fossil fuels [10]. Also, beside fuel researches many scientists have been working on engine parameters such as compression ratio and injection timing. These main parameters of engines effect directly performance and emission characteristics of ICE. Thus, many researchers have investigated the effects of these parameters mostly using variable compression engine (VCR).

Jindal et al. [3] reported a study which investigates the effects of the engine design parameters such as compression ratio (CR) and fuel injection pressure on the performance of the engine. The author studied the subject with some critical performance criterias such as brake thermal efficiency, specific fuel consumption, and emissions of carbon monoxide, carbon dioxide, hydrocarbons, nitrogen oxides and smoke opacity with Jatropa methyl ester as fuel. Depnath et al. [11] presented a study that investigates the variable compression ratio diesel engine when the engine is fueled with palm oil methyl ester thermodynamically. The effect of compression ratio (CR) and injection timing (IT) on energy and energy potential of a palm oil methyl ester (POME) was found by them. The test were performed in a single cylinder, direct injection, water cooled variable compression ratio diesel engine at a constant speed of 1500 rpm under a full load. Amarnath and Prabhakaran [10] reported a study which is related with the thermal performance and emissions of a variable compression ratio diesel engine fueled with karanja biodiesel and optimized the parameters based on experimental datas. Al Dawody and Bhatti[12] investigated the emission, performance and the combustion, characteristics of a diesel engine fueled with soybean biodiesel-diesel blends experimentally and computationally.

In this study, a theoretical calculation were evaluated based on ideal diesel cycle by using parameters of compression ratio, ratio of specific heats, and cut-off ratio in order to optimize the operational conditions of a diesel engine. Theoretical calculations in this study shows the effects of engine operating parameters which is important to have guess before performing time consuming and costly experiments.

2. Material Method

2.1. Calculation Method

The most crucial characteristic of diesel engine is its fuel economy, which can excel up to 40% in vehicle applications and even up to 50% in two-stroke units of marine exciting or generators. As a consequence, vehicles running with compression ignition engines have lower specific fuel consumption and reduced carbon dioxide emissions comparing to its counterpart spark ignition engines. Moreover, diesel engines are less sensitive in terms of air-fuel ratio variations, in peak cylinder pressures and temperatures absence of throttling, high torque and high tolerability make diesel engines more preferred.

Compression ignition engines are assumed to operate with the principle of ideal cycle. Actual working cycle of diesel cycle is significantly different from ideal cycles. Yet, to be able to study parametrically actual cycles are idealized with some assumptions.

Ideal Diesel Cycle

➤ In compression-ignition engines, air is compressed to above the auto ignition temperature of the fuel. After the injection of fuel spray the combustion occurs with a delay time (ignition delay, a few crank angles). Diesel

(compression ignition) engines are mostly used for heavy-duty vehicles, trucks, buses, etc. which require a very high amount of torque.

- Intake stroke: The piston starts to move downward from the top dead center to bottom dead center, the intake valve opens, and this movement lets the introducing the air charge inside the cylinder.
- Compression stroke: The piston moves back to top dead center from bottom dead center and compresses the air inside the cylinder and the temperature inside cylinder rises over the auto-ignition temperature of the fuel.
- Combustion stroke (power stroke) : At the end of the compression stroke (before the piston reaches the top dead center) the injectors start to inject fuel inside to cylinder. After the ignition delay period the fuel is spontaneously auto-ignites. The fuel-air mixture combust produce a pressure on the cylinder head and pushes the cylinder downward which is the main object of the engine.
- Exhaust stroke: After the piston hits the bottom of cylinder (bottom dead center) ,the piston start to move upward and the exhaust valve opens because between the cylinder and exhaust manifold pressure is different, and the sweep effect of the piston make the exhaust gases leave the cylinder to go out through the tail pipe.

The four steps of ideal diesel combustion ;

- 1-2 isentropic compression
- 2-3 constant pressure heat addition
- 3-4 isentropic expansion
- 4-1 constant volume heat rejection

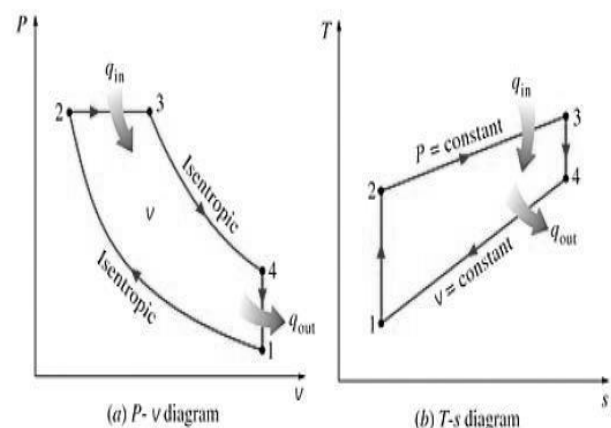


Fig 1.a.b P-V and T-S diagrams of idealized diesel cycle

Underlining that the ideal diesel cycle is operated in a closed system, and air-standard assumptions were made for working fluid (air). Variations of potential and kinetic energies are insignificant. During the two isentropic processes no heat transfer is involved. The energy balances processes are:

$$-w_{12} = u_2 - u_1 \tag{1}$$

$$-w_{34} = u_4 - u_3 \tag{2}$$

w_{12} is negative because of the compression and w_{34} is positive because of the expansion process which air does the work. Constant pressure heat addition process,

$$w_{23} = P_2(v_3 - v_2) \quad (3)$$

The energy balances:

$$q_{23} = u_3 - u_2 + w_{23} = h_3 - h_2 \quad (3.1)$$

Since there is no change in the volume there is no work in the heat rejection process. The energy balance;

$$q_{41} = u_1 - u_4 \quad (4)$$

Since the heat is added to the system q_{23} is positive and since the heat is rejected during the process q_{41} is negative.

For the full cycle,

$$q_{23} + q_{41} - w_{12} - w_{34} = 0 \quad (5)$$

Brake thermal efficiency (η_{th}): A gauge of overall engine efficiency is given by the brake thermal efficiency. Brake thermal efficiency is the ratio of energy in the brake power to the fuel energy. Figure A shows the entropy (S), pressure (P) and volume (V) diagrams of idealized diesel cycle. Thermodynamically;

$$W_{cycle} = \oint PdV = \oint Tds \quad (6)$$

$$Q_{2-3} = \int_{T_2}^{T_3} c_p dT \quad Q_{4-1} = - \int_{T_4}^{T_1} c_v dT$$

$$Q_{2-3} = c_p(T_3 - T_2) \quad Q_{4-1} = -c_v(T_1 - T_4) = c_v(T_4 - T_1)$$

$$\eta_{th} = \frac{Q_{2-3} - Q_{4-1}}{Q_{2-3}} \quad \eta_{th} = 1 - \frac{Q_{4-1}}{Q_{2-3}} \quad \gamma = \frac{c_p}{c_v} \quad (6.1)$$

$$\eta_{th} = 1 - \frac{c_v(T_4 - T_1)}{c_p(T_3 - T_2)} \quad \eta_{th} = 1 - \frac{(T_4 - T_1)}{\gamma(T_3 - T_2)}$$

$$\alpha = \frac{V_3}{V_2}$$

Since 1-2 adiabatic

$$T_2 = T_1 r^{\gamma-1} \quad (6.2)$$

Since 2-3 constant pressure

$$P_2 V_2 = mRT_2 \quad P_3 V_3 = mRT_3 \quad T_3 = T_2 \frac{V_3}{V_2}$$

$$T_3 = T_2 \alpha \quad T_3 = T_1 \alpha r^{\gamma-1}$$

$$P_4 V_4^\gamma = P_3 V_3^\gamma \quad P_4 V_4 V_4^{\gamma-1} = P_3 V_3 V_3^{\gamma-1} \quad (6.3)$$

$$P_4 V_4 = mRT_4 \quad P_3 V_3 = mRT_3$$

$$\frac{T_4}{T_3} = \left(\frac{V_3}{V_4}\right)^{\gamma-1}$$

$$\frac{T_4}{T_3} = \left(\frac{V_3}{V_4}\right)^{\gamma-1} = \left(\frac{V_3}{V_2}\right)^{\gamma-1} \left(\frac{V_2}{V_4}\right)^{\gamma-1}$$

$$\eta_{th} = 1 - \frac{1}{r^{\gamma-1}} \left(\frac{\alpha^\gamma - 1}{\gamma(\alpha - 1)}\right) \quad (6.4)$$

$$(\eta_{th}) = \text{BrakePower}/\text{Fuel Energy} \quad (6.5)$$

$$\eta_{th}(\%) = \frac{\text{BrakePower (kW)} \times 3600}{\text{FuelFlow} \left(\frac{\text{kg}}{\text{hr}}\right) \times \text{CalorificValue} \left(\frac{\text{kJ}}{\text{kg}}\right)} \times 100 \quad (6.6)$$

Where;

η_{th} is thermal efficiency,

α is the cut-off ratio (ratio between the end and start volume for the combustion phase),

c_p is specific heat at constant pressure,

c_v is specific heat at constant volume,

γ is ratio of specific heats (c_p/c_v),

r is the compression ratio.

Theoretical equation shows that thermal efficiency of the diesel cycle depends on three parameter which are; compression ratio (r), ratio of specific heats (γ) and cut-off ratio of the cycle (α).

3. Results and Discussion

In this study, a theoretical calculation of brake thermal efficiency (BTHE) was evaluated analytically. Three main parameters that effect the thermal efficiency calculation of ideal diesel cycle were studied. Compression ratio which is the main parameter that determines the theoretical BTHE value was varied between the range of 12:1 and 24:1. Ratio of specific heats (γ) and cut-off ratios (α) were chosen between the range of 1,2-1,4 and 1,5-3,00, respectively.

Figures (1-5) shows the BTHE values of for different compression ratios, cut-off ratios and specific heat ratios. The analyses revealed that, CR increment significantly increases BTHE values. For all cut-off ratios and specific heat ratios maximum BTHE values were obtained with 24:1 compression ratio value. Increasing specific heats (γ) values further increased BTHE values. But, increasing cut-off ratio (α) values caused a significant decrement in the means of BTHE values. According to calculation results, the best efficiency of thermal study was obtained with 1,4 specific heat ratio, 1,5 cut-off ratio and 24:1 CR.

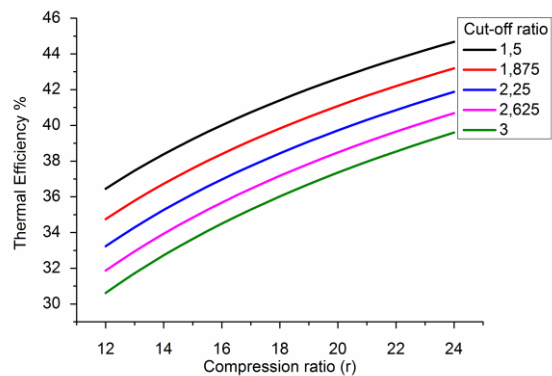


Fig. 1. The change in thermal efficiency according to different compression and cut off ratio in cases where ratio of specific heats (γ) is 1.2 constant

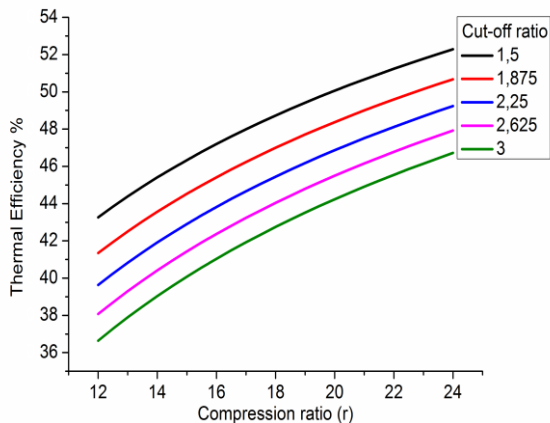


Fig. 2. The change in thermal efficiency according to different compression and cut off ratio in cases where ratio of specific heats (γ) is 1.25 constant

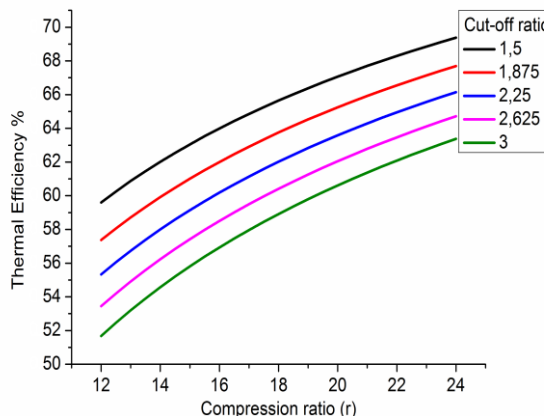


Fig. 5. The change in thermal efficiency according to different compression and cut off ratio in cases where ratio of specific heat (γ) is 1.4 constant

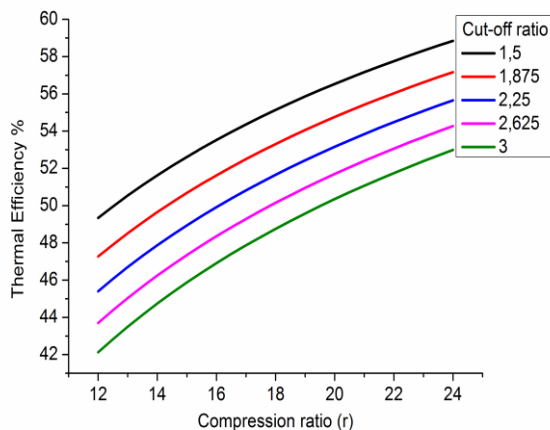


Fig. 3. The change in thermal efficiency according to different compression and cut off ratio in cases where ratio of specific heats (γ) is 1.3 constant

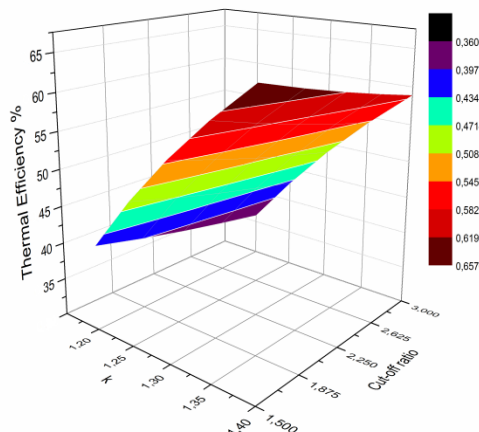


Fig. 6. The change in thermal efficiency according to different specific heats ratio and cut off ratio in cases where compression ratio is 18 constant

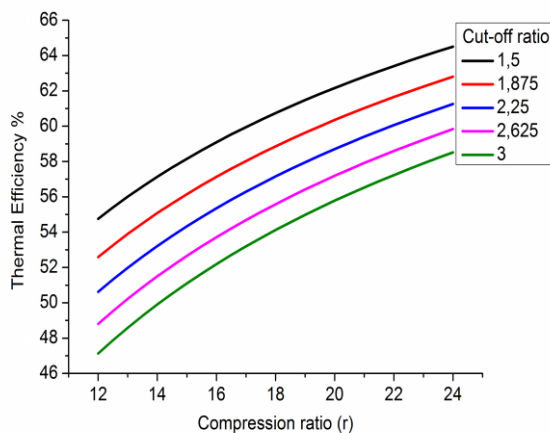


Fig. 4. The change in thermal efficiency according to different compression and cut off ratio in cases where ratio of specific heats (γ) is 1.35 constant

The calculation study showed that BTHE values can be obtained as up to 68%. But this value is not realistic for actual applications since this study was evaluated with the formula of ideal diesel cycle. Idealization of actual diesel cycle includes many assumptions and thus there are tremendous differences between calculation datas and experimental datas. Hariram and Shangar published an article that researchs the effects of the compression ratio on combustion characteristics of a compression ignition engine [13]. The authors studied with three different compression ratios (16:1, 17:1, and 18:1). The authors reported that increasing CR resulted with higher BTHE values and thus lower brake specific fuel consumption. The author reported that increasing compression ratio from 16:1 to 18:1 improved BTHE value up to 13% at full load conditions which is coincidence with the calculation datas obtained in this study.

In another study V. Gnanamoorthi and G. Devaradjaneto found the maximum possible and optimum replacement of diesel fuel by ethanol and compare the performance of diesel engine fuel led with ethanol-diesel

blend for various compression ratios (17.5:11, 18.5:1, 19.5:1) and study the effect of compression ratio and using the best emulsified technique to achieve acceptable range of efficiency up to E40.[14]

As it is shown in the experimental studies, increasing the compression ratio improves the efficiency of the engine. [2-5] In this study it was found a similar results that obtained in the previous studies.

3. Conclusions

- A theoretical study was evaluated with three parameters that effect the brake thermal efficiency of ideal diesel cycle.
- The parametrical study showed that increasing compression ratio significantly improves the brake thermal efficiency.
- The analyses revealed that, increasing ratio of specific heat further improves the brake thermal efficiency. But, increasing cut-off ratio resulted with lower brake thermal efficiency.
- Although, the calculation results were significantly different from the actual values, the trend of brake thermal efficiency with different parameters was compatible with actual processes.
- The calculations showed the effects of different operating parameters of the diesel engine based on ideal diesel cycle which can be used to optimize the operating conditions of a diesel engine.

References

- [1] Demirbas A. "Biodiesel production from vegetable oils via catalytic and non-catalytic supercritical methanol transesterification methods." *Progress in Energy and Combustion Science* vol.31,pp.466–87,2005
- [2] Amarnath, H.K., Prabhakaran, P., "A Study on the Thermal Performance and Emissions of a Variable Compression Ratio Diesel Engine Fuelled with Karanja Biodiesel and the Optimization of Parameters Based on Experimental Data." *International Journal of Green Energy*, vol.9:8, pp.841-863,2012.
- [3] Jindal S, Nandwana B.P., Rathore N.S., Vashistha V., "Experimental investigation of the effect of compression ratio and injection pressure in a direct injection diesel engine running on Jatropha methyl ester." *Applied Thermal Engineering*, vol.30,pp. 442-8, 2010.
- [4] Mohanraj, T., Murugu Mohan Kumar, K., "Operating Characteristics Of A Variable Compression Ratio Engine Using Esterified Tamanu Oil." *International Journal of Green Energy*, vol.10:3,pp. 285-301, 2013.
- [5] Muralidharan,K., Vasudevan, D., "Performance, emission and combustion characteristics of a variable compression ratio engine using methyl esters of waste cooking oil and diesel blends." *Applied Energy*, vol.88, pp. 3959-68, 2011.

[6] Hoeltgebaum, T., Simoni, R., Martins, D., "Reconfigurability of engines: A kinematic approach to variable compression ratio engine." *Mechanism and Machine Theory*, vol.96, pp. 308-22, 2016.

[7] Serin H., M. Ozcanli, M.K. Gokce., G. Tuccar "Biodiesel Production From Tea Seed (Camellia Sinensis) Oil and its Blends With Diesel Fuel." *International Journal of Green Energy*, vol.10:4, pp.370-7., 2013.

[8] Yildizhan, S., Yasar, A., "Performance and Emission Characteristics of Diesel Engine Operating on Biodiesel and Biodiesel Blended with Methanol and Propanol." *International Journal of Scientific and Technological Research*, Vol 1, No.1, pp.270-8 2015.

[9] Ramadhas A.S., Muraleedharan C., and Jayaraj, S., "Performance and Emission Evaluation of a Diesel Engine Fueled with Methyl Esters of Rubber Seed Oil", *Renewable Energy* vol. 30,pp. 1789-1800,2005.

[10] Amarnath, H.K., and Prabhakaran P., "A Study on the Thermal Performance and Emissions of a Variable Compression Ratio Diesel Engine Fuelled with Karanja Biodiesel and the Optimization of Parameters Based on Experimental Data." *International Journal of Green Energy*, vol.9:8, pp.841-863, 2012.

[11] Depnath, B.K., Sahoo, N., and Saha, U.K., "Thermodynamic analysis of a variable compression ratio diesel engine running with palm oil methyl ester." *Energy Conversion and Management* vol.65, pp.147-154. 2012.

[12] Al Dawody, M.F., and Bhatti, S.K., "Experimental and computational investigations for combustion, performance and emission parameters of a diesel engine fueled with soybean biodiesel-diesel blends." *Energy Procedia, biodiesel-diesel blends*. vol.52,pp. 421-430,2014.

[13] Hariram, V., and Shangar, R.V., "Influence of compression ratio on combustion and performance characteristics of direct injection compression ignition engine." *Alexandria Engineering Journal*, vol.54:4, pp.807-81,2015.

[14] V. Gnanamoorthi , G. Devaradjane "Effect of compression ratio on the performance, combustion and emission of DI diesel engine fueled with ethanol e Diesel blend." *Journal of the Energy Institute*,vol.88,pp.19-26,2015.

Analysis of Bending Deflections of Functionally Graded Beams by Using Different Beam Theories and Symmetric Smoothed Particle Hydrodynamics

Armagan Karamanli*

*Department of Mechatronics Engineering, Faculty of Engineering and Architecture, Istanbul Gelisim University, 34215 Istanbul, Turkey.

(afkaramanli@gelisim.edu.tr)

‡Corresponding Author; Armagan Karamanli, Department of Mechatronics Engineering, Faculty of Engineering and Architecture, Istanbul Gelisim University, 34215 Istanbul, Turkey, Tel: +90 2124227020, armagan_k@yahoo.com

Received: 28.07.2016 Accepted: 02.09.2016

Abstract-The elastostatic deformations of functionally graded beams under various boundary conditions are investigated by using different beam theories and the Symmetric Smoothed Particle Hydrodynamics (SSPH) method. The numerical calculations are performed based on the Euler-Bernoulli, Timoshenko and Reddy-Bickford beam theories. The performance of the SSPH method is investigated for the comparison of the different beam theories where the beams are composed of two different materials for the first time. For the numerical results various numbers of nodes are used in the problem domain. Regarding to the computed results for Reddy-Bickford beam theory various numbers of terms in the Taylor Series Expansions (TSEs) are employed to improve the accuracy. To validate the performance of the SSPH method, comparison studies in terms of transverse deflections are carried out with the analytical solutions by using the global L_2 error norm.

Keywords Meshless method, functionally graded beam, bending deflection, SSPH method, shear deformation theories.

1. Introduction

One of the biggest problems that the engineers face with during the new product development process is the selecting of the proper material to be used for the engineering applications. There are many factors to be considered for the optimization of the selection process such as the cost of raw material and production, fabrication techniques, logistics, material properties, requirements of customers with severe operating conditions for instance; the material should be hard but also ductile or the material can withstand very high surface temperature of 2000K and a temperature gradient of 1000K across a 10 mm thickness and so on. In 1984, a group of Japanese scientists working on a space shuttle project requiring a thermal barrier with high performance properties introduced a novel material called Functionally Graded Material (FGM). FGMs can be classified as advanced materials which are inhomogeneous and made up of two (or more) different materials combined in solid states with varying properties as the dimension changes.

The engineering applications where the FGMs may be used are the aerospace, biomedical, defence, energy, optoelectronics, automotive (engine components), turbine blade, reactor components (nuclear energy) and etc. FGMs may be used in different application areas with the development of new fabrication technologies, the reduction in cost of production, improvement in the properties of FGMs.

The advantages of the FGMs over the conventional and classical composite materials are basically due to varying material properties over a changing dimension which allows enhancing the bond strength through the layer interfaces, high resistance to temperature shocks, lower transverse shear stresses, etc. Researchers have been devoted a considerable number of studies to predict and to understand the mechanics of the FGM structures.

An elasticity solution of a FGM beam subjected to transverse loads based on the Euler Bernoulli Beam Theory (EBT) is given in [1]. By using the semi inverse method, a closed form 2D plane elasticity solution of a cantilever beam

with different loading conditions and gradation laws can be found in [2]. In [3], the analytical solution of a 2D plane stress problem for a Functionally Graded Beam (FGB) subjected to normal and shear tractions of arbitrary form on the top and bottom surfaces and under various end boundary conditions is presented. The bending solutions of the generally anisotropic beams with elastic compliance parameters being arbitrary functions of the thickness coordinate are investigated in [4]. The static behaviour of FGBs under ambient temperature by using the higher order beam theory is studied extensively in [5] for the transverse displacements, axial stress and transverse shear stress distribution. The static and dynamic behaviours of functionally graded Timoshenko and Euler–Bernoulli beams are investigated by introducing a new function which helps to decouple the governing equations and allows representing the transverse deflection and rotational angle only in the terms of this new function [6]. The static response of functionally graded material short beam is studied in [7] using the parabolic shear deformation theory and sinusoidal shear deformation theory to show the ability of higher order theories to enhance predictions provided by classical beam theories. The flexional bending of a simply supported FGB is studied by using different higher order beam theories with varying gradation laws [8]. The refined beam theories are introduced for the static analysis of the FGBs whose properties are graded along one or two directions in [9]. The determination of the shear correction factor is investigated in [10] for various gradation laws. The static bending solutions of the FGM Timoshenko Beams are obtained analytically in terms of the homogeneous Euler Bernoulli beams by using mathematical similarity and load equivalence between the governing equations [11]. The static behaviour of the FGBs are also studied by using the quasi-3D theory to show the effects of shear deformation and thickness stretching on the displacement and stresses [12]. Several refined beam finite elements obtained by means of the Carrera Unified Formulation (CUF) are used to static analysis of the FGBs [13]. In 14, the combination of the Timoshenko Beam Theory (TBT) and the finite volume method is developed for the static and the free vibration of the FGBs. Due to the different implementation areas of the FGMs in engineering applications, free and forced vibration [15-26] and buckling behaviour [27-34] of the functionally graded structures have been extensively investigated by several researchers.

As it is seen from above discussions, the studies related to analytical and semi-analytical solutions of these initial and boundary value problems which have complex governing equations are very limited in the literature. Therefore, one may easily show that the numerical methods such as finite element methods (FEM), meshless methods, GDQM, etc. are widely used and have shown great progress for the analysis of these complex problems. However, for convenience and generality considerations at least to the best of the author's knowledge, there is no common agreement and also no reported work regarding to the meshless methods of which best fit in terms of accuracy, CPU time, flexibility for dealing with the complex geometries, extendibility to multi-dimensional problems and etc., for the static and dynamic analysis of the FGBs based on the different beam theories.

Meshless methods are the most promising and have attracted considerable attention for the analysis of engineering problems with intrinsic complexity. Meshless methods are widely used in static and dynamic analyses of the isotropic, laminated composite and FGM beam problems [35-41]. To obtain the approximate solution of the problem by a meshless method, the selection of the basis functions is almost the most important issue. The accuracy of the computed solution can be increased by employing different number of terms in TSE or increasing number of nodes in the problem domain or by increasing the degree of complete polynomials. Many meshless methods have been proposed by researchers to obtain the approximate solution of the problem. The Smoothed Particle Hydrodynamics (SPH) method is proposed by Lucy [42] to the testing of the fission hypothesis. However, this method has two important shortcomings, lack of accuracy on the boundaries and the tensile instability. To remove these shortcomings, many meshless methods have been proposed by several researchers [43-63].

The main scope of this work is to evaluate the performance of the SSPH method employing the strong formulation for the static transverse deflection analysis of the FGBs based on various beam theories such as EBT, TBT and the Reddy – Bickford Beam Theory (RBT). To provide a fair and comparable evaluation, two FGB problems of which analytical solutions are available in the literature will be used for the numerical calculations.

Based on the above discussions, the main novelty of this work is that there is no reported work on the bending deflections of the functionally graded beams subjected to the different boundary conditions by using the SSPH method. Since the basis functions and the derivatives of these functions are obtained simultaneously and the usage of a constant weight function is possible to obtain the approximate solution, the SSPH method has an advantage over the Moving Least Squares, Reproducing Kernel Particle Method, Modified Smoothed Particle Hydrodynamics and the Strong Form Meshless Implementation of Taylor Series Method [51-56].

In section 2, the formulation of the basis function of the SSPH method is given. In section 2, the homogenization of material properties of the FGB is presented. The formulation of the EBT, TBT and RBT based on the FGM and the SSPH method are given in Section 4. In Section 5, numerical results are given based on the two FGB problems which are a simply supported FGB under uniformly distributed load and a cantilever FGB under the uniformly distributed load. The performance of the SSPH method is evaluated by using the analytical solutions of studied problems.

2. Formulation of Symmetric Smoothed Particle Hydrodynamics

Taylor Series Expansion (TSE) of a scalar function for 1D case can be given by

$$f(\xi) = \sum_{m=0}^n \frac{1}{m!} \left[(\xi - x) \frac{d}{dx} \right]^m f(x) \quad (1)$$

where $f(\xi)$ is the value of the function at ξ located in near of x . If the zeroth to sixth order terms are employed and the higher order terms are neglected, the equation (1) can be written as follows,

$$f(\xi) = P(\xi, x)Q(x) \quad (2)$$

where

$$Q(x) = \left[f(x), \frac{df(x)}{dx_1}, \frac{1}{2!} \frac{d^2 f(x)}{dx_1^2}, \dots, \frac{1}{6!} \frac{d^6 f(x)}{dx_1^6} \right]^T \quad (3)$$

$$P(\xi, x) = [1, (\xi_1 - x_1), (\xi_1 - x_1)^2, \dots, (\xi_1 - x_1)^6] \quad (4)$$

To determine the unknown variables given in the $Q(x)$, both sides of equation (2) are multiplied with $W(\xi, x)P(\xi, x)^T$ and evaluated for every node in the CSD. In the global numbering system, let the particle number of the k th particle in the compact support of $W(\xi, x)$ be $r(k)$. The following equation is obtained

$$\sum_{k=1}^{N(x)} f(\xi^{r(k)}) W(\xi^{r(k)}, x) P(\xi^{r(k)}, x)^T = \sum_{k=1}^{N(x)} \left[P(\xi^{r(k)}, x)^T W(\xi^{r(k)}, x) P(\xi^{r(k)}, x) \right] Q(x) \quad (5)$$

where $N(x)$ is the number nodes in the compact support domain (CSD) of the $W(\xi, x)$ as shown in Fig.1.

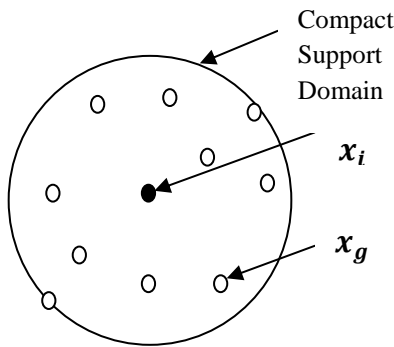


Fig. 1. Compact support of the weight function $W(\xi, x)$ for the node located at $x = (x_i, y_i)$

Then, equation (5) can be given by

$$C(\xi, x)Q(x) = D(\xi, x)F^{(x)}(\xi, x) \quad (6)$$

where $C(\xi, x) = P(\xi, x)^T W(\xi, x) P(\xi, x)$ and $D(\xi, x) = P(\xi, x)^T W(\xi, x)$.

The solution of equation (6) is given by

$$Q(x) = K(\xi, x)F(\xi) \quad (7)$$

where $K^{(x)}(\xi, x) = C(\xi, x)^{-1}D(\xi, x)$. Equation (7) can be also written as follows

$$Q_I(x) = \sum_{J=1}^M K_{IJ} F_J, \quad I = 1, 2, \dots, 6 \quad (8)$$

Where M is the number of nodes and $F_J = f(\xi^J)$. Seven components of equation (8) for 1D case are can be written as

$$f(x) = Q_1(x) = \sum_{J=1}^M K_{1J} F_J$$

$$\frac{df(x)}{dx} = Q_2(x) = \sum_{J=1}^M K_{2J} F_J$$

$$\frac{d^2 f(x)}{dx^2} = 2! Q_3(x) = \sum_{J=1}^M K_{3J} F_J$$

$$\frac{d^3 f(x)}{dx^3} = 3! Q_4(x) = \sum_{J=1}^M K_{4J} F_J$$

$$\frac{d^4 f(x)}{dx^4} = 4! Q_5(x) = \sum_{J=1}^M K_{5J} F_J$$

$$\frac{d^5 f(x)}{dx^5} = 5! Q_6(x) = \sum_{J=1}^M K_{6J} F_J$$

$$\frac{d^6 f(x)}{dx^6} = 6! Q_7(x) = \sum_{J=1}^M K_{7J} F_J \quad (9)$$

The formulation of the SSPH method can be found in [52-57].

3. Homogenization of Material Properties

We assume that the beam of length L , width b , thickness h is made of two randomly distributed different isotropic constituents. Further, the macroscopic response of the FGB is isotropic and the material parameters vary only in z direction as shown in Fig. 2. The rule of mixture is used to find the effective material properties at a point. According to the rule of mixtures, the effective material properties of the beam, Young's modulus E and shear modulus G can be given by

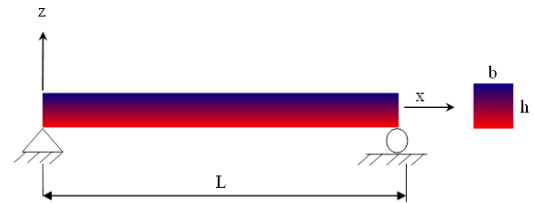


Fig. 2. Geometry of the FGB composed of two isotropic constituents

$$E(z) = E_1 V_1(z) + E_2 V_2(z)$$

$$G(z) = G_1 V_1(z) + G_2 V_2(z) \quad (10)$$

where E_1, E_2, G_1 and G_2 are the material properties of two constituents, V_1 and V_2 are volume fractions of the constituents. The relation of the volume fractions can be expressed as follows;

$$V_1(z) + V_2(z) = 1 \quad (11)$$

According to the power law form, the volume fraction of the constitute 1 can be given by

$$V_1(z) = \left(\frac{1}{2} + \frac{z}{h} \right)^p \quad (12)$$

where p is the gradation exponent which determines the material property through thickness of the beam. At the bottom surface of the beam, the volume fraction of the constitute 1 is zero, $V_1 = 0$. At the top surface it is found as $V_1 = 1$. The effective material properties can be found by using the equations (10), (11) and (12) as follows

$$E(z) = (E_1 - E_2) \left(\frac{1}{2} + \frac{z}{h} \right)^p + E_2$$

$$G(z) = (G_1 - G_2) \left(\frac{1}{2} + \frac{z}{h} \right)^p + G_2 \quad (13)$$

4. Formulation of Beam Theories

The kinematics of deformation of a beam can be represented by using various beam theories. Among them, the EBT, TBT and RBT are commonly used [64-67]. Various higher order beam theories are introduced in which the straightness assumption is removed and the vanishing of shear stress at the upper and lower surfaces is accommodated. For this purpose, higher order polynomials incorporating either one, or more, extra terms [68-74] or trigonometric functions [75,76] or exponential functions [77] are included in the expansion of the longitudinal point-wise displacement component through the thickness of the beam. The higher order theories introduce additional unknowns that make the governing equations more complicated and provide the solutions much costly in terms of CPU time. The theories which are higher than the third order shear deformation beam theory are seldom used because the accuracy gained by these theories which require much effort to solve the governing equations is so little [66].

4.1. Euler Bernoulli Beam Theory

The following displacement field is given for the EBT,

$$u(x, z) = -z \frac{dw}{dx}$$

$$w(x, z) = w_0(x) \quad (14)$$

where w_0 is the transverse deflection of the point $(x,0)$ which is on the mid-plane ($z=0$) of the beam. By using the assumption of the smallness of strains and rotations, the only the axial strain which is nonzero is given by,

$$\varepsilon_{xx} = \frac{du}{dx} = -z \frac{d^2w_0}{dx^2} \quad (15)$$

The virtual strain energy of the beam in terms of the axial stress and the axial strain can be expressed by

$$\delta U = \int_0^L \int_A \sigma_{xx} \delta \varepsilon_{xx} dA dx \quad (16)$$

where δ is the variation operator, A is the cross sectional area, L is the length of the beam, σ_{xx} is the axial stress. The bending moment of the EBT is given by,

$$M_{xx} = \int_A z \sigma_{xx} dA \quad (17)$$

By using equation (15) and equation (17), equation (16) can be rewritten as,

$$\delta U = - \int_0^L M_{xx} z \frac{d^2 \delta w_0}{dx^2} dx \quad (18)$$

The virtual potential energy of the load $q(x)$ which acts at the central axis of the beam is given by

$$\delta V = - \int_0^L q(x) \delta w_0 dx \quad (19)$$

If a body is in equilibrium, $\delta W = \delta U + \delta V$, the total virtual work (δW) done equals zero. Then one can obtain,

$$\delta W = - \int_0^L \left(M_{xx} z \frac{d^2 \delta w_0}{dx^2} + q(x) \delta w_0 \right) dx = 0 \quad (20)$$

After performing integration for the first term in equation (20) twice and since δw_0 is arbitrary in $(0 < x < L)$, one can obtain the following equilibrium equation,

$$- \frac{d^2 M_{xx}}{dx^2} = q(x) \text{ for } 0 < x < L \quad (21)$$

By introducing the shear force Q_x and rewrite equation (21) in the following form

$$- \frac{dM_{xx}}{dx} + Q_x = 0, \quad - \frac{dQ_x}{dx} = q(x) \quad (22)$$

By using Hooke's law, one can obtain

$$\sigma_{xx} = E(z) \varepsilon_{xx} = - \left[(E_1 - E_2) \left(\frac{1}{2} + \frac{z}{h} \right)^p + E_2 \right] z \frac{d^2 w_0}{dx^2} \quad (23)$$

If the equation (23) is put into equation (17), it is obtained,

$$M_{xx} = - \int_{-h/2}^{+h/2} \left[(E_1 - E_2) \left(\frac{1}{2} + \frac{z}{h} \right)^p + E_2 \right] z^2 \frac{d^2 w_0}{dx^2} dz = - D_{xx} \frac{d^2 w_0}{dx^2} \quad (24)$$

where

$$D_{xx} = \int_{-h/2}^{+h/2} \left[(E_1 - E_2) \left(\frac{1}{2} + \frac{z}{h} \right)^p + E_2 \right] z^2 dz \quad (25)$$

The substitution of equation (24) into equation (22) yields the EBT governing equation for a FGB subjected to the distributed load

$$\frac{d^2}{dx^2} (D_{xx} \frac{d^2 w_0}{dx^2}) = q(x) \text{ for } 0 < x < L \quad (26)$$

4.2. Timoshenko Beam Theory

The following displacement field is given for the TBT,

$$u(x, z) = z \phi(x)$$

$$w(x, z) = w_0(x) \quad (27)$$

where $\phi(x)$ is the rotation of the cross section. By using equation (27), the strain-displacement relations are given by

$$\varepsilon_{xx} = \frac{du}{dx} = z \frac{d\phi}{dx}$$

$$\gamma_{xz} = \frac{dw}{dz} + \frac{dw}{dx} = \phi + \frac{dw_0}{dx} \quad (28)$$

The virtual strain energy of the beam including the virtual energy associated with the shearing strain can be written as,

$$\delta U = \int_0^L \int_A (\sigma_{xx} \delta \varepsilon_{xx} + \sigma_{xz} \delta \gamma_{xz}) dA dx \quad (29)$$

where σ_{xz} is the transverse shear stress and γ_{xz} is the shear strain. The bending moment and the shear force can be written respectively,

$$M_{xx} = \int_A z \sigma_{xx} dA, \quad Q_x = \int_A \sigma_{xz} dA \quad (30)$$

By using equation (28) and equation (30), one can rewrite equation (29) as,

$$\delta U = \int_0^L \left[M_{xx} \frac{d\delta\phi}{dx} + Q_x \left(\delta\phi + \frac{d\delta w_0}{dx} \right) \right] dx \quad (31)$$

The virtual potential energy of the load $q(x)$ which acts at the central axis of the Timoshenko beam is given by

$$\delta V = - \int_0^L q(x) \delta w_0 dx \quad (32)$$

Since the total virtual work done equals zero and the coefficients of $\delta\phi$ and δw_0 in $0 < x < L$ are zero, one can obtain the following equations,

$$-\frac{dM_{xx}}{dx} + Q_x = 0, \quad -\frac{dQ_x}{dx} = q(x) \quad (33)$$

The constitutive equations can be written as follows

$$\sigma_{xx} = E(z)\varepsilon_{xx} = \left[(E_1 - E_2) \left(\frac{1}{2} + \frac{z}{h} \right)^p + E_2 \right] z \frac{d\phi}{dx} \quad (34)$$

$$\sigma_{xz} = G(z)\gamma_{xz} = \left[(G_1 - G_2) \left(\frac{1}{2} + \frac{z}{h} \right)^p + G_2 \right] \left(\phi + \frac{dw_0}{dx} \right) \quad (35)$$

The bending moment and shear force can be expressed in terms of generalized displacement (w_0, ϕ) by using the constitutive equations given above

$$\begin{aligned} M_{xx} &= \int_{-h/2}^{+h/2} z \sigma_{xx} dz = \int_{-h/2}^{+h/2} \left[(E_1 - E_2) \left(\frac{1}{2} + \frac{z}{h} \right)^p + E_2 \right] z^2 \frac{d\phi}{dx} dz = D_{xx} \frac{d\phi}{dx} \\ Q_x &= \kappa_s \int_{-h/2}^{+h/2} \sigma_{xz} dz = \kappa_s \int_{-h/2}^{+h/2} \left[(G_1 - G_2) \left(\frac{1}{2} + \frac{z}{h} \right)^p + G_2 \right] \left(\phi + \frac{dw_0}{dx} \right) dz = \kappa_s A_{xz} \left(\phi + \frac{dw_0}{dx} \right) \end{aligned} \quad (36)$$

where

$$\begin{aligned} D_{xx} &= \int_{-h/2}^{+h/2} \left[(E_1 - E_2) \left(\frac{1}{2} + \frac{z}{h} \right)^p + E_2 \right] z^2 dz \\ A_{xz} &= \int_{-h/2}^{+h/2} \left[(G_1 - G_2) \left(\frac{1}{2} + \frac{z}{h} \right)^p + G_2 \right] dz \end{aligned} \quad (37)$$

Where κ_s is the shear correction factor which is used to compensate the error caused by the assumption of a constant transverse shear stress distribution along the beam thickness.

The governing equations of the TBT is obtained in terms of generalized displacements by using the equations (33) and (36) as follows

$$-\frac{d}{dx} \left(D_{xx} \frac{d\phi}{dx} \right) + \kappa_s A_{xz} \left(\phi + \frac{dw_0}{dx} \right) = 0 \quad (38)$$

$$-\frac{d}{dx} \left[\kappa_s A_{xz} \left(\phi + \frac{dw_0}{dx} \right) \right] = q(x) \quad (39)$$

4.3. Reddy-Bickford Beam Theory

The following displacement field is given for the RBT,

$$\begin{aligned} u(x, z) &= z\phi(x) - \alpha z^3 \left(\phi(x) + \frac{dw(x)}{dx} \right) \\ w(x, z) &= w_0(x) \end{aligned} \quad (40)$$

where $\alpha = 4/(3h^2)$. By using equation (41), the strain-displacement relations of the RBT are given by

$$\begin{aligned} \varepsilon_{xx} &= \frac{du}{dx} = z \frac{d\phi}{dx} - \alpha z^3 \left(\frac{d\phi}{dx} + \frac{d^2 w_0}{dx^2} \right) \\ \gamma_{xz} &= \frac{du}{dz} + \frac{dw}{dx} = \phi + \frac{dw_0}{dx} - \beta z^2 \left(\phi + \frac{dw_0}{dx} \right) \end{aligned} \quad (41)$$

where $\beta = 3\alpha = 4/(h^2)$.

The virtual strain energy of the beam can be written as,

$$\delta U = \int_0^L \int_A (\sigma_{xx} \delta \varepsilon_{xx} + \sigma_{xz} \delta \gamma_{xz}) dA dx \quad (42)$$

The usual bending moment and the shear force are,

$$M_{xx} = \int_A z \sigma_{xx} dA, \quad Q_x = \int_A \sigma_{xz} dA \quad (43)$$

and P_{xx} and R_x are the higher order stress resultants can be written respectively,

$$P_{xx} = \int_A z^3 \sigma_{xx} dA, \quad R_x = \int_A z^2 \sigma_{xz} dA \quad (44)$$

By using equation (41), equation (43) and equation (44), one can rewrite the equation (42) as,

$$\delta U = \int_0^L \left[(M_{xx} - \alpha P_{xx}) \frac{d\delta\phi}{dx} - \alpha P_{xx} \frac{d^2 \delta w_0}{dx^2} + (Q_x - \beta R_x) \left(\delta\phi + \frac{d\delta w_0}{dx} \right) \right] dx \quad (45)$$

In the RBT there is no need to use a SCF unlike the TBT. The virtual potential energy of the transverse load $q(x)$ is given by

$$\delta V = - \int_0^L q(x) \delta w_0 dx \quad (46)$$

The virtual displacements principle is applied and the coefficients of $\delta\phi$ and δw_0 in $0 < x < L$ are set to zero, the governing equations of the RBT are obtained in terms of displacements ϕ and w_0 as follows,

$$\begin{aligned} -\frac{d}{dx} \left(\bar{D}_{xx} \frac{d\phi}{dx} - \alpha \hat{F}_{xx} \frac{d^2 w_0}{dx^2} \right) + \bar{A}_{xz} \left(\phi + \frac{dw_0}{dx} \right) &= 0 \\ -\alpha \frac{d^2}{dx^2} \left(\hat{F}_{xx} \frac{d\phi}{dx} - \alpha H_{xx} \frac{d^2 w_0}{dx^2} \right) - \frac{d}{dx} \left[\bar{A}_{xz} \left(\phi + \frac{dw_0}{dx} \right) \right] &= q(x) \end{aligned} \quad (47)$$

where

$$\begin{aligned} \bar{A}_{xz} &= \hat{A}_{xz} - \beta \hat{D}_{xz}, \quad \bar{D}_{xx} = \hat{D}_{xx} - \alpha \hat{F}_{xx} \\ \hat{D}_{xx} &= D_{xx} - \alpha F_{xx}, \quad \hat{F}_{xx} = F_{xx} - \alpha H_{xx} \\ \hat{A}_{xz} &= A_{xz} - \beta D_{xz}, \quad \hat{D}_{xz} = D_{xz} - \beta F_{xz} \\ (D_{xx}, F_{xx}, H_{xx}) &= \int_{-h/2}^{+h/2} \left[(E_1 - E_2) \left(\frac{1}{2} + \frac{z}{h} \right)^p + E_2 \right] (z^2, z^4, z^6) dz \\ (A_{xz}, D_{xz}, F_{xz}) &= \int_{-h/2}^{+h/2} \left[(G_1 - G_2) \left(\frac{1}{2} + \frac{z}{h} \right)^p + G_2 \right] (1, z^2, z^4) dz \end{aligned} \quad (48)$$

5. Numerical Results

The bending deflections of two FGB problems are investigated by using the formulation of the EBT, TBT and RBT and the SSPH method. Different loading and boundary conditions are applied with different node distributions in the problem domain. By employing different aspect ratios and gradation exponents, the maximum transverse deflections are calculated. The numerical results obtained by the SSPH method regarding to different beam theories are compared with the analytical solution of problems.

5.1. Simply Supported Beam

Static transverse deflections of a simply supported FGB under uniformly distributed load of intensity q_0 as shown in Fig.3. is studied.

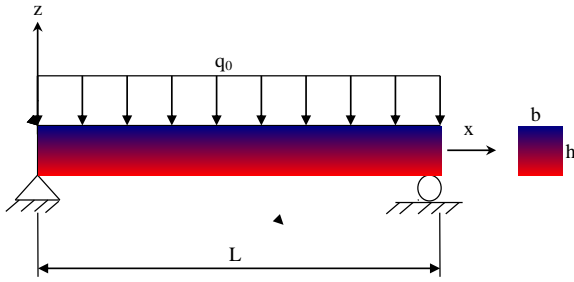


Fig. 2. Simply supported fgb with uniformly distributed load

The physical parameters of the beam are given as $L=1m$, $h=0.1m$, $b=0.1m$. The distributed load q_0 is set to 10000 N/m. The material properties of the two constitues are given as

$$E_1 = 70GPa, E_2 = 151GPa, G_1 = 27GPa, G_2 = 58GPa$$

Based on the EBT, the governing equation of the problem can be presented as algebraic equations by using the SSPH basis function given in equation (9) and replacing $f(x)$ with $w_0(x)$ as follows,

$$D_{xx} \sum_{j=1}^M 24K_{5j}W_j = q_0 \quad \text{for } 0 < x < L \quad (49)$$

The boundary conditions regarding to the EBT are given as follows;

$$x = 0, \quad \sum_{j=1}^M 2K_{3j}W_j = 0 \text{ and } \sum_{j=1}^M K_{1j}W_j = 0 m$$

$$x = L, \quad \sum_{j=1}^M 2K_{3j}W_j = 0 \text{ and } \sum_{j=1}^M K_{1j}W_j = 0 m$$

The analytical solution of this boundary value problem based on the EBT is given by

$$w_0^E(x) = \frac{q_0L^4}{24D_{xx}} \left(\frac{x}{L} - \frac{2x^3}{L^3} + \frac{x^4}{L^4} \right) \quad (50)$$

where the superscript E denotes the quantities in the EBT.

The governing equations of the problem can be written in a similar way by replacing $f(x)$ given in equation (9) with $w_0(x)$ and $\phi(x)$ and by using the SSPH basis functions as follows,

$$\sum_{j=1}^M \kappa_s A_{xz} K_{2j} W_j + \sum_{j=1}^M [\kappa_s A_{xz} K_{2j} - 2D_{xx} K_{3j}] \Phi_j = 0 \quad (51)$$

$$-\sum_{j=1}^M 2\kappa_s A_{xz} K_{3j} W_j - \sum_{j=1}^M \kappa_s A_{xz} K_{2j} \Phi_j = q_0 \quad (52)$$

The SCF is assumed to be constant as $\kappa_s = 5/6$ for the rectangular cross section,

The boundary conditions regarding to the TBT are given as follows;

$$x = 0, \quad \sum_{j=1}^M K_{2j} \Phi_j = 0 \text{ and } \sum_{j=1}^M K_{1j} W_j = 0 m$$

$$x = L, \quad \sum_{j=1}^M K_{2j} \Phi_j = 0 \text{ and } \sum_{j=1}^M K_{1j} W_j = 0 m$$

The analytical solution of this boundary value problem based on the TBT is given by

$$w_0^T(x) = \frac{q_0L^4}{24D_{xx}} \left(\frac{x}{L} - \frac{2x^3}{L^3} + \frac{x^4}{L^4} \right) + \frac{q_0L^2}{2\kappa_s A_{xz}} \left(\frac{x}{L} - \frac{x^2}{L^2} \right) \quad (53)$$

where the superscript T denotes the quantities in the TBT.

By using RBT and the SSPH basis functions the governing equations can be written by replacing $f(x)$ given in equation (9) with $w_0(x)$ and $\phi(x)$ as follows,

$$\sum_{j=1}^M [\bar{A}_{xz} K_{2j} + 6\alpha \hat{F}_{xx} K_{4j}] W_j + \sum_{j=1}^M [\bar{A}_{xz} K_{1j} - 2\bar{D}_{xx} K_{3j}] \Phi_j = 0 \quad (54)$$

$$\sum_{j=1}^M [-2\bar{A}_{xz} K_{3j} + 24\alpha^2 H_{xx} K_{4j}] W_j + \sum_{j=1}^M [-\bar{A}_{xz} K_{2j} - 6\alpha \hat{F}_{xx} K_{4j}] \Phi_j = q \quad (55)$$

The boundary conditions regarding to the TBT are given as follows;

$$x = 0, \quad \sum_{j=1}^M \bar{D}_{xx} K_{2j} \Phi_j - \sum_{j=1}^M 2\alpha F_{xx} K_{3j} W_j = 0, \text{ and } \sum_{j=1}^M K_{1j} W_j = 0 m$$

$$x = L, \quad \sum_{j=1}^M \bar{D}_{xx} K_{2j} \Phi_j - \sum_{j=1}^M 2\alpha F_{xx} K_{3j} W_j = 0, \text{ and } \sum_{j=1}^M K_{1j} W_j = 0 m$$

The analytical solution of this boundary value problem based on the RBT is given by

$$w_0^R(x) = \frac{q_0L^4}{24D_{xx}} \left(\frac{x}{L} - \frac{2x^3}{L^3} + \frac{x^4}{L^4} \right) + \left(\frac{q_0\mu}{\lambda^4} \right) \left(\frac{\bar{D}_{xx}}{\bar{A}_{xz}D_{xx}} \right) \left[-\tanh\left(\frac{\lambda L}{2}\right) \sinh \lambda x + \cosh \lambda x + \frac{\lambda^2}{2} x(L-x) - 1 \right] \quad (56)$$

where

$$\lambda^2 = \frac{\bar{A}_{xz}D_{xx}}{\alpha(F_{xx}\bar{D}_{xx} - \hat{F}_{xx}D_{xx})}, \quad \mu = \frac{\hat{A}_{xz}\bar{D}_{xx}}{\alpha(F_{xx}\bar{D}_{xx} - \hat{F}_{xx}D_{xx})}$$

For the numerical computations performed by the SSPH method uniformly distributed 21, 41 and 161 nodes are used in the domain $x \in [0, 1]$. The Revised Super Gauss Function (RSGF) which gives the least L_2 error norms in numerical solutions in [52] is used.

$$W(x, \xi) = \frac{G}{(h\sqrt{\pi})^\lambda} \begin{cases} (36 - d^2)e^{-d^2} & 0 \leq d \leq 6 \\ 0 & d > 6 \end{cases} \quad (57)$$

$$d = |x - \xi|/h$$

where d is the radius of the CSD, h is the smoothing length. G and λ are the parameters which are eliminated by the formulation of the SSPH method.

The numerical solutions are performed according to the following meshless parameters; the radius of the support domain (d) is chosen as 6 and the smoothing length (h) equals to 1.1Δ where Δ is the minimum distance between two adjacent nodes. The meshless parameters, d and h , are selected to obtain the lowest error.

Computed results obtained by using the SSPH method are compared with the analytical solutions, and their accuracy and convergence properties are investigated by employing the global L_2 error norm which is given by

$$L_2 = \frac{[\sum_{j=1}^m (v_{num}^j - v_{exact}^j)^2]^{1/2}}{[\sum_{j=1}^m (v_{exact}^j)^2]^{1/2}} \quad (58)$$

The computed L_2 error norms of the numerical solutions based on the EBT are given in Table 1. For the numerical

analysis different numbers of nodes are considered in the problem domain with 5 terms in TSEs expansion and varying gradation exponents. It is observed in Table 1 that the difference between the computed and analytical results is too small and the SSPH method almost gives the analytical solution of the problem. In Table 2, maximum deflection of the FGB is presented with varying aspect ratios and gradation exponent values.

Table 1. L_2 error norm for different number of nodes with varying gradation exponent (p) and aspect ratio $L/h=10$ - EBT

Gradation Exponent - p	Number of Nodes		
	21	41	161
0	$3.8621 \cdot 10^{-9}$	$9.0384 \cdot 10^{-8}$	$3.6786 \cdot 10^{-7}$
0.5	$3.8606 \cdot 10^{-9}$	$9.0484 \cdot 10^{-8}$	$3.7665 \cdot 10^{-7}$
1	$3.8636 \cdot 10^{-9}$	$9.0442 \cdot 10^{-8}$	$3.6774 \cdot 10^{-7}$
2	$3.8591 \cdot 10^{-9}$	$9.0416 \cdot 10^{-8}$	$3.7251 \cdot 10^{-7}$
5	$3.8635 \cdot 10^{-9}$	$9.0434 \cdot 10^{-8}$	$3.6998 \cdot 10^{-7}$

Table 2. Maximum deflection (mm) of the beam with varying gradation exponent and different aspect ratios for 41 nodes - EBT

Gradation Exponent (p)	Aspect Ratio (L/h)			
	5	10	20	50
0	-0.0279	-0.2232	-1.7857	-27.9018
0.5	-0.0195	-0.1561	-1.2489	-19.5145
1	-0.0176	-0.1414	-1.1312	-17.6753
2	-0.0164	-0.1317	-1.0539	-16.4681
5	-0.0152	-0.1221	-0.9776	-15.2758

Table 3. L_2 error norm for different number of nodes with varying gradation exponent (p) and aspect ratio $L/h=10$ - TBT

Gradation Exponent (p)	Number of Nodes		
	21	41	161
0	$4.1559 \cdot 10^{-10}$	$3.5002 \cdot 10^{-9}$	$5.9457 \cdot 10^{-9}$
0.5	$4.0629 \cdot 10^{-10}$	$3.5696 \cdot 10^{-9}$	$4.8358 \cdot 10^{-9}$
1	$3.8775 \cdot 10^{-10}$	$3.4994 \cdot 10^{-9}$	$5.6451 \cdot 10^{-9}$
2	$4.1133 \cdot 10^{-10}$	$3.5803 \cdot 10^{-9}$	$2.8734 \cdot 10^{-9}$
5	$3.9839 \cdot 10^{-10}$	$3.6220 \cdot 10^{-9}$	$4.3202 \cdot 10^{-9}$

In Fig. 3, the numerical results in terms of transverse deflections are compared with the analytical solutions with different number of nodes in the problem domain and varying gradation exponent values. The aspect ratio (L/h) is set as 50. It is observed in Fig. 4 that the SSPH method agrees very well with the analytical solution. The transverse deflection of the FGB computed by the SSPH method is virtually indistinguishable from that for the analytical solution.

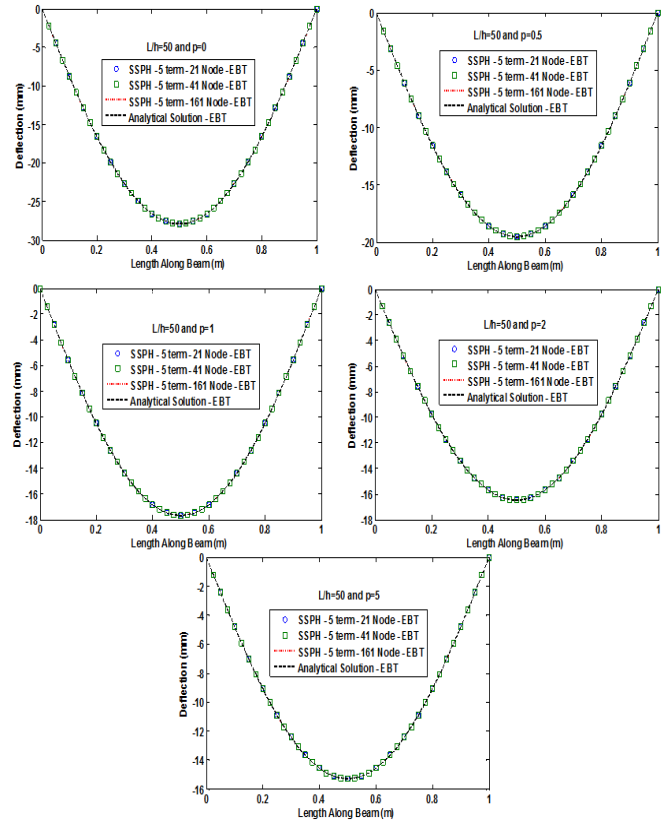


Fig. 3. Deflections of the beam computed based on the EBT with varying number of nodes and the analytical solution.

Table 4. Maximum deflection (mm) of the beam with varying gradation exponent and different aspect ratios for 41 nodes -TBT

Gradation Exponent (p)	Aspect Ratio (L/h)			
	5	10	20	50
0	-0.0306	-0.2287	-1.7968	-27.9295
0.5	-0.0215	-0.1601	-1.2569	-19.5346
1	-0.0194	-0.1449	-1.1383	-17.6929
2	-0.0180	-0.1349	-1.0603	-16.4839
5	-0.0166	-0.1250	-0.9833	-15.2900

The global L_2 error norms of the solutions based on the TBT with different numbers of nodes in the problem domain, 5 terms in TSEs expansion and varying gradation exponents are given in Table 3. One can easily notice that the computed results are very close to analytical values when global L_2 error norms are investigated. The results in Table 3 are obtained for the meshless parameters d and h which gives the best accuracy for each method. In Table 4, maximum deflection of the FGB is presented with varying aspect ratios and gradation exponent values. As expected, the deflection value increases either an increase or a decrease for the aspect ratio and the gradation exponent. It is clear that numerical solutions obtained by the SSPH method agree very well with the analytical solution given in Fig. 5.

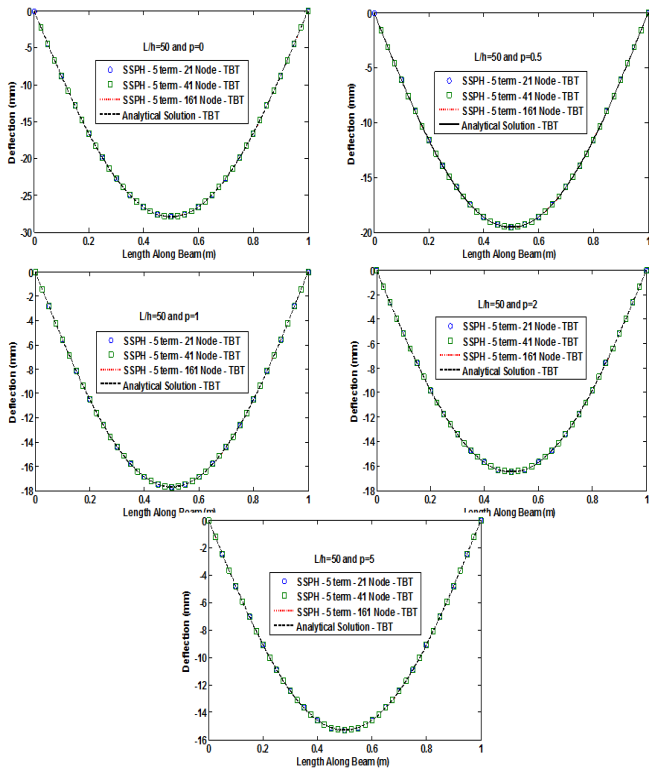


Fig. 4. Deflections of the beam computed based on the TBT and the analytical solution.

Table 5. L_2 error norm for different number of nodes with varying gradation exponent (p) and aspect ratio $L/h=10-5$ terms in TSEs -RBT

Gradation Exponent (p)	Number of Nodes		
	21	41	161
0	2.056779	2.056786	2.056786
0.5	2.167582	2.167589	2.167589
1	2.064060	2.064066	2.064067
2	1.924057	1.924063	1.924063
5	1.845563	1.845569	1.845569

Table 6. L_2 error norm for different number of nodes with varying gradation exponent (p) and aspect ratio $L/h=10-7$ terms in TSEs - RBT

Gradation Exponent (p)	Number of Nodes		
	21	41	161
0	1.7794	1.6913	0.5618
0.5	1.8838	1.7994	0.4541
1	1.7866	1.6986	0.5545
2	1.6544	1.5619	0.6909
5	1.5820	1.4860	0.7665

By setting the aspect ratio as 10, the global L_2 error norms of the solutions based on the RBT are computed for different number of nodes, varying gradation exponent and different number of terms in TSEs. By using 5 terms in TSEs, the accuracy of the SSPH method is not improved when the number of nodes increases in the problem domain.

However, the convergence of the SSPH method increases when 7 terms in TSEs are employed.

Table 7. Maximum deflection (mm) of the beam with varying gradation exponent and different aspect ratios for 161 nodes - RBT

Gradation Exponent (p)	Aspect Ratio (L/h)			
	5	10	20	50
0	-0.0271	-0.2231	-1.7524	-27.2619
0.5	-0.0189	-0.1562	-1.2259	-19.0676
1	-0.0172	-0.1413	-1.1101	-17.2700
2	-0.0160	-0.1315	-1.0340	-16.0899
5	-0.0149	-0.1218	-0.9591	-14.9247

It is observed that the numerical solutions obtained by employing 7 terms in TSEs and using 161 equally spaced nodes in the problem domain agree very well with the analytical solution given in Fig. 5.

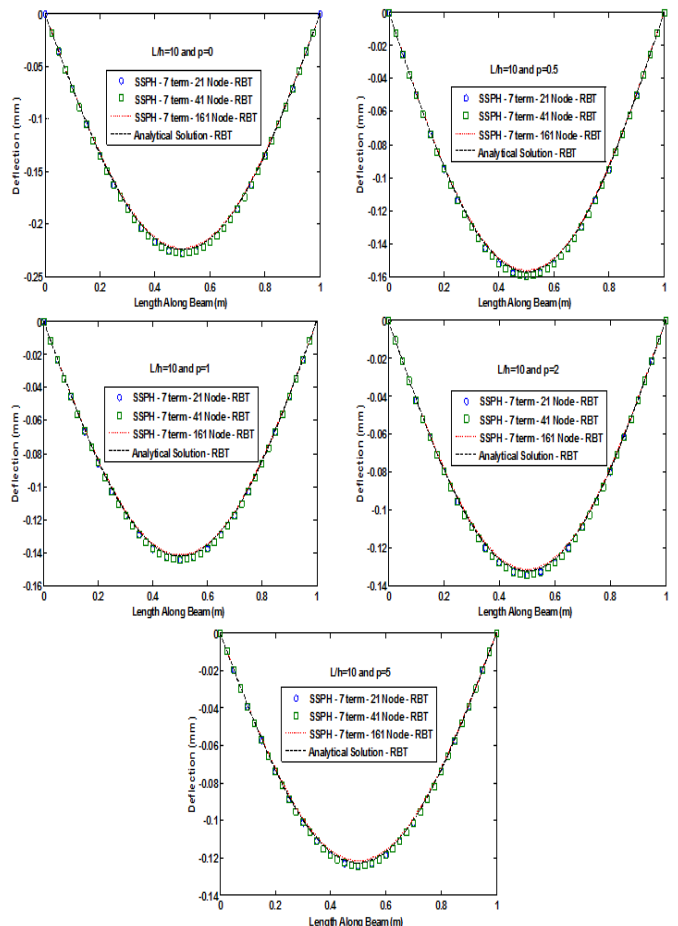


Fig. 5. Deflections of the beam computed based on the RBT and the analytical solution

5.2. Cantilever Beam

For a cantilever FGB the static transverse deflections under uniformly distributed load of intensity q_0 is studied as shown in Figure 6.

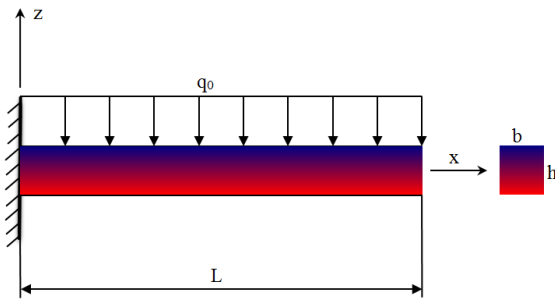


Fig. 6. Simply supported FGB with uniformly distributed load

As the physical parameters, the similar material geometry and properties are used. The uniformly distributed load q_0 is set to 10000 N/m.

The governing equation of the problem is given in equation (49). The boundary conditions are given by;

$$x = 0, \sum_{j=1}^M K_{2j} W_j = 0 \text{ and } \sum_{j=1}^M K_{1j} W_j = 0 \text{ m}$$

$$x = L, \sum_{j=1}^M 2K_{3j} W_j = 0 \text{ and } \sum_{j=1}^M 6K_{4j} W_j = 0$$

The analytical solution of this boundary value problem based on the EBT is given by

$$w_0^E(x) = \frac{q_0 L^4}{24D_{xx}} \left(6 \frac{x^2}{L^2} - 4 \frac{x^3}{L^3} + \frac{x^4}{L^4} \right) \quad (59)$$

The governing equations of the problem based on the TBT formulation are given in equation (51) and equation (52). The boundary conditions regarding to the TBT are given as follows;

$$x = 0, \sum_{j=1}^M K_{1j} \Phi_j = 0 \text{ and } \sum_{j=1}^M K_{1j} W_j = 0 \text{ m}$$

$$x = L, \sum_{j=1}^M K_{2j} \Phi_j = 0 \text{ and } \sum_{j=1}^M K_{1j} \Phi_j + \sum_{j=1}^M K_{2j} W_j = 0$$

The analytical solution of this boundary value problem based on the TBT is given by

$$w_0^T(x) = \frac{q_0 L^4}{24D_{xx}} \left(6 \frac{x^2}{L^2} - 4 \frac{x^3}{L^3} + \frac{x^4}{L^4} \right) + \frac{q_0 L^2}{2\kappa_s A_{xz}} \left(2 \frac{x}{L} - \frac{x^2}{L^2} \right) \quad (60)$$

Based on the RBT, the governing equations of the problem are given in equation (54) and equation (55). The boundary conditions regarding to the RBT are given as follows;

$$x = 0, \sum_{j=1}^M K_{1j} \Phi_j = 0 \text{ and } \sum_{j=1}^M K_{1j} W_j = 0 \text{ m}$$

$$x = L, \sum_{j=1}^M \hat{D}_{xx} K_{2j} \Phi_j - \sum_{j=1}^M 2\alpha F_{xx} K_{3j} W_j = 0, \text{ and } \sum_{j=1}^M K_{1j} \Phi_j + \sum_{j=1}^M K_{2j} W_j = 0$$

The analytical solution of this boundary value problem based on the TBT is given by

$$w_0^R(x) = w_0^E(x) + \left(\frac{q_0 \mu}{2\lambda^2} \right) \left(\frac{\hat{D}_{xx}}{\hat{A}_{xz} D_{xx}} \right) (2Lx - x^2) + \left(\frac{q_0 \mu}{\lambda^4 \cosh \lambda L} \right) \left(\frac{\hat{D}_{xx}}{\hat{A}_{xz} D_{xx}} \right) \left[\cosh \lambda x + \lambda L \sinh \lambda(L - x) - \left(\frac{q_0 \mu}{\lambda^4} \right) \left(\frac{\hat{D}_{xx}}{\hat{A}_{xz} D_{xx}} \right) \left(\frac{1 + \lambda L \sinh \lambda L}{\cosh \lambda L} \right) \right] \quad (61)$$

The above boundary value problems are solved by using the SSPH method for different node distributions of 21 and

161 equally spaced nodes in the domain $x \in [0, 1]$. The Revised Super Gauss Function given in equation (57) is used as the weight function.

For the numerical solutions, the radius of the support domain (d) is chosen as 5 and the smoothing length (h) is chosen as 1.3Δ . The meshless parameters, d and h , are selected to obtain the best accuracy. Computed results by the SSPH method are compared with the analytical solutions, and their rate of convergence and accuracy properties are investigated by using the global L_2 error norm given in equation (58).

In Table 8 the global L_2 error norms of the solutions based on the EBT are given for different numbers of nodes in the problem domain with varying gradation exponent and 5 terms in TSEs expansion. The aspect ratio is set to 10. The computed deflection values of the FGB are almost equal to analytical solution as seen Table 8 and Table 9. The computed transverse deflection of the beam is virtually indistinguishable from that for the analytical solution as seen from Fig. 7.

Table 8. L_2 error norm for different number of nodes with varying gradation exponent (p) and aspect ratio $L/h=10$ - EBT

Gradation Exponent (p)	Number of Nodes		
	21	41	161
0	$9.3464 \cdot 10^{-7}$	$5.7715 \cdot 10^{-6}$	$7.7978 \cdot 10^{-6}$
0.5	$9.3463 \cdot 10^{-7}$	$5.7716 \cdot 10^{-6}$	$7.8008 \cdot 10^{-6}$
1	$9.3462 \cdot 10^{-7}$	$5.7715 \cdot 10^{-6}$	$7.7981 \cdot 10^{-6}$
2	$9.3463 \cdot 10^{-7}$	$5.7716 \cdot 10^{-6}$	$7.7986 \cdot 10^{-6}$
5	$9.3462 \cdot 10^{-7}$	$5.7715 \cdot 10^{-6}$	$7.8015 \cdot 10^{-6}$

Table 9. Maximum deflection of the beam for different number of nodes with varying gradation exponent (p) and aspect ratio $L/h=10$ - EBT

Gradation Exponent (p)	Number of Nodes			Analytical Solution (mm)
	21	41	161	
0	-2.142857	-2.142857	-2.142856	-2.142857
0.5	-1.498715	-1.498715	-1.498715	-1.498715
1	-1.357466	-1.357465	-1.357465	-1.357466
2	-1.264755	-1.264755	-1.264755	-1.264755
5	1.1731843	1.1731842	1.1731842	-1.173184

By using different numbers of nodes in the problem domain with 5 terms in TSEs expansion, the global L_2 error norms of the solutions obtained for the TBT are given in Table 10. It is clear in Table 10 that the SSPH method provides satisfactory numerical results and rapid convergence to the analytical solution. In Table 11, maximum deflection values computed by using different number of nodes with varying gradation exponent are compared with the analytical solution. It is observed in Fig. 8 that the SSPH method agrees very well with the analytical solution.

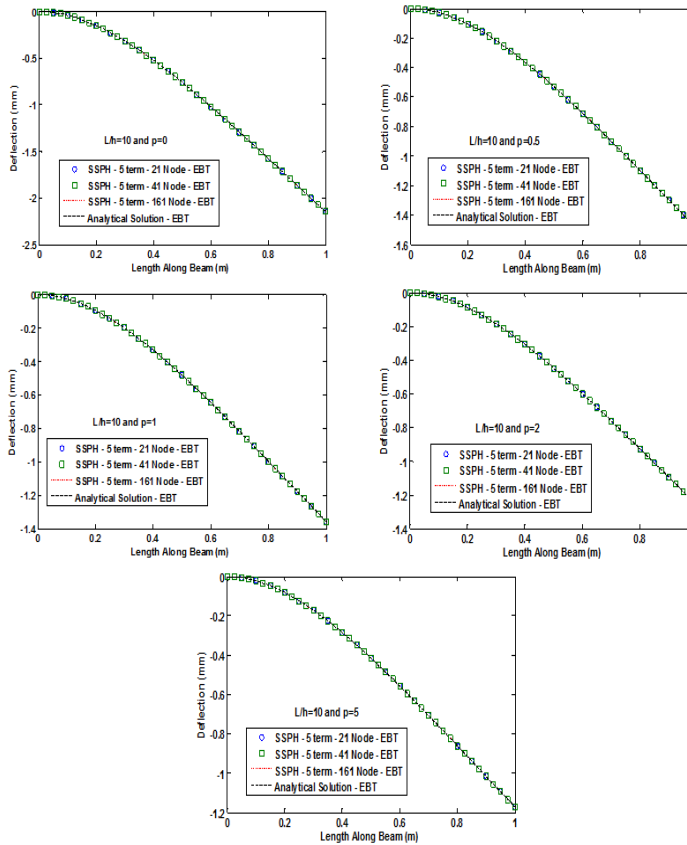


Fig. 7. Deflections of the beam computed based on the EBT and the analytical solution.

Table 10. L_2 error norm for different number of nodes with varying gradation exponent (p) and aspect ratio $L/h=10$ - TBT

Gradation Exponent (p)	Number of Nodes		
	21	41	161
0	$1.1737 \cdot 10^{-8}$	$3.2575 \cdot 10^{-7}$	$6.0033 \cdot 10^{-8}$
0.5	$1.0989 \cdot 10^{-8}$	$3.1489 \cdot 10^{-7}$	$5.3044 \cdot 10^{-8}$
1	$1.1602 \cdot 10^{-8}$	$3.2470 \cdot 10^{-7}$	$6.6439 \cdot 10^{-8}$
2	$1.1786 \cdot 10^{-8}$	$3.4013 \cdot 10^{-7}$	$5.8399 \cdot 10^{-8}$
5	$1.2413 \cdot 10^{-8}$	$3.4943 \cdot 10^{-7}$	$6.5123 \cdot 10^{-8}$

Table 11. Maximum deflection of the beam for different number of nodes with varying gradation exponent (p) and aspect ratio $L/h=10$ - TBT

Gradation Exponent (p)	Number of Nodes			Analytical Solution (mm)
	21	41	161	
0	-2.165079	-2.165079	-2.165079	-2.165079
0.5	-1.514786	-1.514786	-1.514786	-1.514786
1	-1.371583	-1.371583	-1.371583	-1.371583
2	-1.277342	-1.277342	-1.277342	-1.277342
5	-1.184540	-1.184540	-1.184540	-1.184540

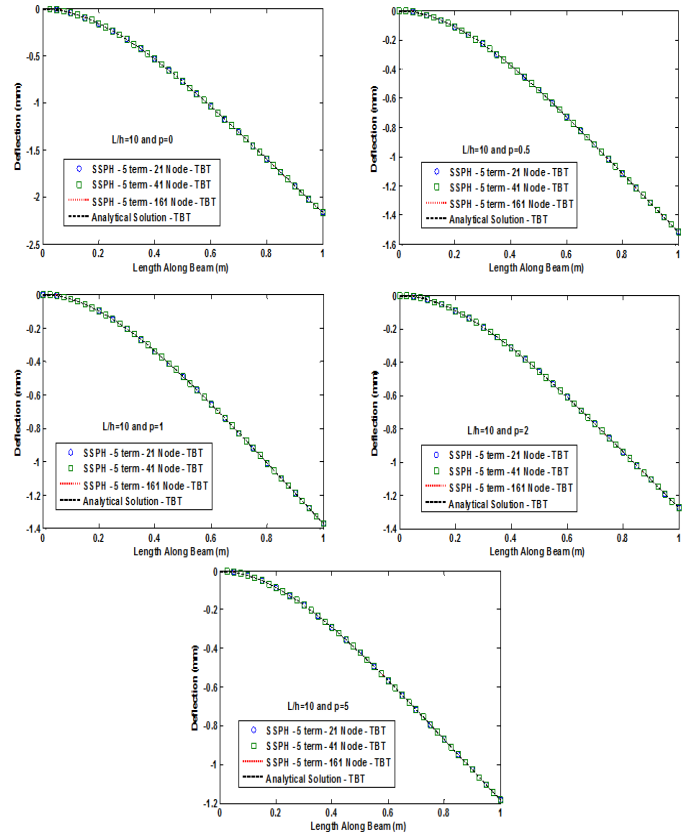


Fig. 8. Deflections of the beam computed based on the TBT and the analytical solution.

Table 12. L_2 error norm for different number of nodes with varying gradation exponent (p) and aspect ratio $L/h=10 - 5$ terms in TSEs - RBT

Gradation Exponent (p)	Number of Nodes		
	21	41	161
0	1.7557	1.7732	1.7868
0.5	1.8593	1.8778	1.8921
1	1.7615	1.7791	1.7927
2	1.6317	1.6481	1.6607
5	1.5523	1.5729	1.5850

Table 13. L_2 error norm for different number of nodes with varying gradation exponent (p) and aspect ratio $L/h=10 - 7$ terms in TSEs

Gradation Exponent (p)	Number of Nodes		
	21	41	161
0	1.7309	1.8455	1.5222
0.5	1.8357	1.9472	1.6351
1	1.7368	1.8512	1.5287
2	1.6054	1.7244	1.3857
5	1.5299	1.6518	1.3035

The global L_2 error norms of the solutions based on the RBT are given in Table 12 where different numbers of nodes and gradation exponents are considered with 5 terms in TSEs expansion. It is found that the number of terms in TSEs should be increased to obtain conventional convergence

properties. The results obtained by employing 7 terms in TSEs are better than the results given in Table 12 for 161 nodes in the problem domain. It is clear that the transverse displacement computed with the SSPH method closer to the analytical solution of the problem given in Fig. 9.

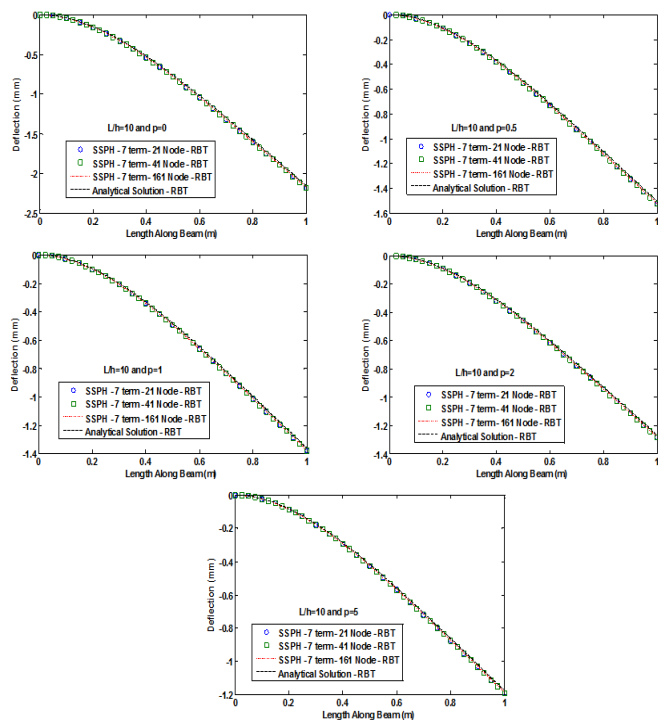


Fig. 9. Deflections of the beam computed based on the RBT and the analytical solution

6. Conclusion

The SSPH basis functions are employed to numerically solve the transverse deflections of the functionally graded beams subjected to different sets of boundary conditions and uniformly distributed load by using strong formulation of the problem. The numerical calculations are performed by using different number of nodes uniformly distributed in the problem domain and by employing different beam theories which are the EBT, TBT and RBT. The performance of the SSPH method is investigated for the solution of the functionally graded beam problems with the EBT, TBT and RBT for the first time. The performance of the SSPH method employing the strong formulation for the static transverse deflection analysis of the FGBs based on various beam theories are evaluated by comparing the analytical solutions which are available in the literature. It is found that the SSPH method provides satisfactory results and convergence rate for the studied problems here. It is observed that the computed values of transverse deflections agree very well with the analytical solutions. It is clear that when the EBT and TBT formulations are employed for the solution of the FGB problems by using the SSPH method, the computed results in terms of the transverse displacement are virtually indistinguishable from that for analytical solution. Based on the results of two numerical examples it is recommended that the SSPH method can be applied for solving linear functionally graded beam problems by employing different shear deformation theories.

References

- [1] Sankar, B.V., An elasticity solution for functionally graded beams, *Composites Science and Technology*, 2001, 61, 689-696.
- [2] Zhong, Z., Yu, T., Analytical solution of a cantilever functionally graded beam, *Composites Science and Technology*, 2007, 67, 481-488.
- [3] Nie, G.J., Zhong, Z., Chen, S., Analytical solution for a functionally graded beam with arbitrary graded material properties, *Composites Part B*, 2013, 44, 274-282.
- [4] Ding, H.J., Huang, D.J., Chen, W.Q., Elasticity solutions for plane anisotropic functionally graded beams, *International Journal of Solids and Structures*, 2007, 44, 176-196.
- [5] Kadoli, R., Akhtar, K., Ganesan, N., Static analysis of functionally graded beams using higher order shear deformation theory, *Applied Mathematical Modelling*, 2008, 32, 2509-2525.
- [6] Li, X.F., A unified approach for analyzing static and dynamic behaviors of functionally graded Timoshenko and Euler-Bernoulli beams, *Journal of Sound and Vibration*, 2008, 318, 1210-1229.
- [7] Benatta, M.A., Mechab, I., Tounsi, A., Abbas, A.B.E., Static analysis of functionally graded short beams including warping and shear deformation effects, *Computational Materials Science*, 2008, 44, 765-773.
- [8] Ben-Oumrane, S., Tounsi, A., Mechab, I., Mohamed, B.B., Mustapha, M., Abbas, A.B.E., theoretical analysis of flexional bending of Al/Al₂O₃ S-FGM thick beams, *Computational Materials Science*, 2009, 44, 1344-1350.
- [9] Giunta, G., Belouettar, S., Carrera, E., Analysis of FGM beams by means of classical and advanced theories, *Mechanics of Advanced Materials and Structures*, 2010, 17, 622-635.
- [10] Mena, R., Tounsi, A., Mouaici, F., Mechab, I., Zidi, M., Bedia, E.A.A., Analytical solutions for static shear correction factor of functionally graded rectangular beams, *Mechanics of Advanced Materials and Structures*, 2012, 19, 641-652.
- [11] Li, S.R., Cao, D.F., Wan, Z.Q., Bending solutions of FGM Timoshenko beams from those of the homogenous Euler-Bernoulli beams, *Applied Mathematical Modelling*, 2013, 37,7077-7085.
- [12] Vo, T.P., Thai, H.T., Nguyen, T.K., Inam, F., Lee, J., Static behaviour of functionally graded sandwich beams using a quasi-3D theory, *Composites Part B*, 2015, 68, 59-74.
- [13] Filippi, M., Carrera, E., Zenkour, A.M., Static analyses of FGM beams by various theories and finite elements, *Composites Part B*, 2015, 72, 1-9.
- [14] Jing, L.L., Ming, P.J., Zhang, W.P., Fu, L.R., Cao, Y.P., Static and free vibration analysis of functionally graded beams by combination Timoshenko theory and finite volume method, *Composite Structures*, 2016, 138, 192-213.
- [15] Aydogdu, M., Taskin, V., Free vibration analysis of functionally graded beams with simply supported edges, *Materials&Design*, 2007, 28:1651-6.

- [16] Sina S.A., Navazi H.M., Haddadpour H., An analytical method for free vibration analysis of functionally graded beams, *Materials&Design*, 2009, 30:741–7.
- [17] [17] Simsek, M., Fundamental frequency analysis of functionally graded beams by using different higher-order beam theories, *Nuclear Engineering and Design*, 2010, 240:697–705.
- [18] Simsek M., Kocaturk T., Free and forced vibration of a functionally graded beam subjected to a concentrated moving harmonic load, *Composite Structures*, 2009, 90:465–73.
- [19] Simsek, M., Vibration analysis of a functionally graded beam under a moving mass by using different beam theories, *Composite Structures*, 2010, 92:904–17.
- [20] Sanjay, A.K., Gupta, R.K., Ramachandran, P., Venkateswara, R.G., Free vibration analysis of functionally graded beams, *Defence Science Journal*, 2012, 62 (3):139–46.
- [21] Mahi, A., Adda Bedia E.A., Tounsi, A., Mechab, I., An analytical method for temperature-dependent free vibration analysis of functionally graded beams with general boundary conditions, *Composite Structures*, 2010, 92:1877–87.
- [22] Pradhan, K.K., Chakraverty, S., Free vibration of Euler and Timoshenko functionally graded beams by Rayleigh-Ritz method, *Composites Part B*, 2013, 51:175–84.
- [23] Pradhan, K.K., Chakraverty, S., Effects of different shear deformation theories on free vibration of functionally graded beams, *International Journal of Mechanical Sciences*, 2014, 82:149–60.
- [24] Nuttawit, W., Variddhi, U., Free vibration analysis of functionally graded beams with general elastically end constraints by DTM, *World Journal of Mechanics*, 2012, 2:297–310.
- [25] Su, H., Banerjee. J.R., Cheung, C.W., Dynamic stiffness formulation and free vibration analysis of functionally graded beams, *Composite Structures*, 2013, 106:854–62.
- [26] Li, S.R., Wan, Z.G., Zhang, J.H., Free vibration of functionally graded beams based on both classical and first-order shear deformation beam theories, *Applied Mathematics and Mechanics*, 2014, 35:591–606.
- [27] Aydogdu, M., Thermal buckling analysis of cross-ply laminated composite beams with general boundary conditions, *Composite Science and Technology*, 2007, 67:1096–104.
- [28] Aydogdu, M., Semi-inverse method for vibration and buckling of axially functionally graded beams, *Journal of Reinforced Plastics&Composites*, 2008, 27:683–91.
- [29] Kiani, Y., Eslami, M.R., Thermal buckling analysis of functionally graded material beams, *International Journal of Mechanics and Materials in Design*, 2010, 6:229–38.
- [30] Huang, Y., Li, X.F., Buckling analysis of nonuniform and axially graded columns with varying flexural rigidity, *Journal of Engineering Mechanics*, 2011, 137(1):73–81.
- [31] Shahba, A., Attarnejad, R., Marvi, M.T., Hajilar, S., Free vibration and stability analysis of axially functionally graded tapered Timoshenko beams with classical and non-classical boundary conditions, *Composites: Part B* 2011, 42:801–8.
- [32] Nateghi, A., Salamat-talab, M., Rezapour, J., Daneshian, B. Size dependent buckling analysis of functionally graded micro beams based on modified couple stress theory. *Applied Mathematical Modelling*, 2012, 36:4971–87.
- [33] [33] Akgöz B, Civalek Ö., Buckling analysis of functionally graded microbeams based on the strain gradient theory, *Acta Mechanica*, 2013; 224:2185–201.
- [34] Simsek M., Buckling of Timoshenko beams composed of two-dimensional functionally graded material (2D-FGM) having different boundary conditions, *Composite Structures*, 2016; 149: 304–314.
- [35] Donning, B.M., Liu, W.K., Meshless methods for shear-deformable beams and plates, *Computer Methods in Applied Mechanics and Engineering*, 1998, 152, 47-71.
- [36] Gu, Y.T., Liu, G.R., A local point interpolation method for static and dynamic analysis of thin beams, *Computer Methods in Applied Mechanics and Engineering*, 2001, 190,42, 5515-5528.
- [37] Ferreira, A.J.M., Roque, C.M.C., Martins, P.A.L.S., Radial basis functions and higher-order shear deformation theories in the analysis of laminated composite beams and plates, *Composite Structures*, 2004, 66, 287-293.
- [38] Ferreira, A.J.M., Fasshauer, G.E., Computation of natural frequencies of shear deformable beams and plates by an RBF-pseudospectral method, *Computer Methods in Applied Mechanics and Engineering*, 2006, 196, 134-146.
- [39] Moosavi, M.R., Delfanian, F., Khelil, A., The orthogonal meshless finite volume method for solving Euler–Bernoulli beam and thin plate problems, *Finite Elements in Analysis and Design*, 2011, 49, 923-932.
- [40] Wu, C.P., Yang, S.W., Wang, Y.M., Hu, H.T., A meshless collocation method for the plane problems of functionally graded material beams and plates using the DRK interpolation, *Mechanics Research Communications*, 2011, 38, 471-476.
- [41] Roque, C.M.C., Figaldo, D.S., Ferreira, A.J.M., Reddy, J.N., A study of a microstructure-dependent composite laminated Timoshenko beam using a modified couple stress theory and a meshless method, *Composite Structures*, 2013, 96, 532-537.
- [42] Lucy LB, A numerical approach to the testing of the fission hypothesis, *Astronomical Journal*, 1977, 82, 1013–1024.
- [43] Chen JK, Beraun JE, Jin CJ, An improvement for tensile instability in smoothed particle hydrodynamics, *Computational Mechanics*, 1999, 23, 279–287.
- [44] Chen JK, Beraun JE, Jin CJ, Completeness of corrective smoothed particle method for linear elastodynamics, *Computational Mechanics*, 1999, 24, 273–285.
- [45] Liu WK, Jun S, Zhang YF, Reproducing kernel particle methods, *International Journal for Numerical Methods in Fluids*, 1995, 20, 1081–1106.
- [46] Liu WK, Jun S, Li S, Adee J, Belytschko T, Reproducing kernel particle methods for structural dynamics, *International Journal for Numerical Methods in Engineering*, 1995, 38, 1655–1679.
- [47] Chen JS, Pan C, Wu CT, Liu WK, Reproducing kernel particle methods for large deformation analysis of non-linear structures, *Computer Methods in Applied Mechanics and Engineering*, 1996, 139, 195–227.

- [48] Zhang GM, Batra RC, Modified smoothed particle hydrodynamics method and its application to transient problems, *Computational Mechanics*, 2004, 34, 137–146.
- [49] Batra RC, Zhang GM, Analysis of adiabatic shear bands in elasto-thermo- viscoplastic materials by modified smoothed particle hydrodynamics (MSPH) method, *Journal of Computational Physics*, 2004, 201, 172–190.
- [50] Zhang GM, Batra RC, Wave propagation in functionally graded materials by modified smoothed particle hydrodynamics (MSPH) method, *Journal of Computational Physics*, 2007, 222, 374–390.
- [51] Batra RC, Zhang GM, Search algorithm, and simulation of elastodynamic crack propagation by modified smoothed particle hydrodynamics (MSPH) method, *Computational Mechanics*, 2007, 40, 531–546.
- [52] Zhang GM, Batra RC, Symmetric smoothed particle hydrodynamics (SSPH) method and its application to elastic problems, *Computational Mechanics*, 2009, 43, 321-340.
- [53] Batra RC, Zhang GM, SSPH basis functions for meshless methods, and comparison of solutions with strong and weak formulations, *Computational Mechanics*, 2008, 41, 527-545.
- [54] Tsai CL, Guan YL, Batra RC, Ohanehi DC, Dillard JG, Nicoli E, Dillard DA, Comparison of the performance of SSPH and MLS basis functions for two-dimensional linear elastostatics problems including quasistatic crack propagation, *Computational Mechanics*, 2013, 51, 19-34.
- [55] Tsai CL, Guan YL, Ohanehi DC, Dillard JG, Dillard DA, Batra RC, Analysis of cohesive failure in adhesively bonded joints with the SSPH meshless method, 2014, *International Journal of Adhesion & Adhesives*, 51, 67-80.
- [56] Karamanli A, Mugan A, Solutions of two-dimensional heat transfer problems by using symmetric smoothed particle hydrodynamics method, *Journal of Applied and Computational Mathematics*, 2012, 1, 1-6.
- [57] Karamanli A, Bending Deflection Analysis of a Semi-Trailer Chassis by Using Symmetric Smoothed Particle Hydrodynamics, *International Journal of Engineering Technologies*, 2015, Vol. 1, No:4, 134-140.
- [58] Karamanli A, Mugan A, Strong form meshless implementation of Taylor series method, *Applied Mathematics and Computation*, 2013, 219, 9069-9080.
- [59] Karamanli A, Different Implementation Approaches of the Strong Form Meshless Implementation of Taylor Series Method, *International Journal of Engineering Technologies*, 2015, Vol. 1, No:3, 95-105.
- [60] Kaewumpai, S., Luadsong, A., Two-field-variable meshless method based on moving kriging interpolation for solving simply supported thin plates under various loads. *Journal of King Saud University - Science*, 1018–3647, 2014.
- [61] Yimnak, K., Luadsong, A., A local integral equation formulation based on moving kriging interpolation for solving coupled nonlinear reaction–diffusion equations. *Advances in Mathematical Physics*, 2014,
- [62] Zhuang, X., Zhu, H., Augarde, C., The meshless Shepard and least squares (MSLS) method, *Computational Mechanics*, 53, 343-357, 2014.
- [63] Fatahi, H., Nadjafi, JS, Shivanian, E, New spectral meshless radial point interpolation (SMRPI) method for the two-dimensional Fredholm integral equations on general domains with error analysis, *Journal of Computational and Applied Mathematics*, 264, 196-209, 2016.
- [64] Love, A.E.H., 1927, *A Treatise on the Mathematical Theory of Elasticity*, fourth ed. Dover Publications, New York.
- [65] Timoshenko, S.P., Goodier, J.C., 1970, *Theory of Elasticity*, McGraw-Hill Co. Inc., New York.
- [66] Wang, C.M., Reddy, J.N., Lee, K.H., 2000, *Shear Deformable Beams and Plates Relations with Classical Solutions*, Elsevier Science Ltd., Oxford.
- [67] Polizzotto, C., 2015, From the Euler-Bernoulli beam to the Timoshenko one through a sequence of Reddy-type shear deformable beam models of increasing order, *European Journal of Mechanics A/Solids*, 53, 62-74.
- [68] Levinson, M., 1981. A new rectangular beam theory, *Journal of Sound and Vibration*, 74, 81-87.
- [69] Bickford, W.B., 1982. A consistent higher order beam theory, *Developments in Theoretical and Applied Mechanics*, 11, 137-150.
- [70] Heyliger, P.R., Reddy, J.N., 1988, A higher order beam finite element for bending and vibration problems, *Journal of Sound and Vibration*, 126 (2), 309-326.
- [71] Subramanian, P., 2006, Dynamic analysis of laminated composite beams using higher order theories and finite elements, *Composite Structures*, 73, 342-353.
- [72] Reddy, J.N., 2007, Nonlocal theories for bending, buckling and vibration of beams, *International Journal of Engineering Science*, 45, 288-307.
- [73] Carrera, E., Giunta, G., 2010, Refined beam theories based on a unified formulation, *International Journal of Applied Mechanics*, 2 (1), 117-143.
- [74] Giunta, G., Biscani, F., Bellouettar, S., Ferreira, A.J.M., Carrera, E., 2013, Free vibration analysis of composite beams via refined theories, *Composites Part B*, 44, 540-552.
- [75] Arya, H., 2003, A new zig-zag model for laminated composite beams: free vibration analysis, *Journal of Sound and Vibration*, 264, 485-490.
- [76] Jun, L., Hongxing, H., 2009, Dynamic stiffness analysis of laminated composite beams using trigonometric shear deformation theory, *Composite Structures*, 89, 433-442.
- [77] Kurama, M., Afaq, K.S., Mistou, S., 2003, Mechanical behavior of laminated composite beams by the new multi-layered laminated composite structures model with trigonometric shear stress continuity, *International Journal of Solids and Structures*, 40, 1525-1546.

Fluorescent Lamp Modelling and Electronic Ballast Design by the Support of Root Placement

Ibrahim Aliskan*[‡], Ridvan Keskin*

*Department of Electrical and Electronics Engineering, Faculty of Engineering, Bulent Ecevit University, 67100 Zonguldak, Turkey

(ialiskan@beun.edu.tr, ridvan.keskin@beun.edu.tr)

[‡]Corresponding Author: Ibrahim Aliskan, Department of Electrical and Electronics Engineering, Faculty of Engineering, Bulent Ecevit University, 67100 Zonguldak, Turkey, Tel: +090 3712911570, Fax: +90 3722574023, ialiskan@beun.edu.tr

Received: 28.07.2016 Accepted: 02.09.2016

Abstract-It is presented that high frequency electronic ballast for fluorescent lamps is designed with root placement method using natural frequency and damping ratio. Also, a fluorescent lamp is designed as to have dynamic resistant. The method proposes simple mathematical calculations instead of complex mathematical calculations and the approaches based one of the component of resonant tank, which arbitrary chosen value. Also it is capable to provide accurate values, which can be employed in new types to ballasts. Natural frequency and damping ratio, which are parameters of the method, are chosen switching frequency, 0.707, respectively. Transfer function of electronic ballast circuit is calculated by means of proposed method. After that, components of the circuit are find out. 220 V(rms) voltage was achieved at ignition and obtained 30 W lamp power in state space operation. Electronic ballast design and a fluorescent lamp are made of using Matlab/Simulink interface and the results are presented.

Keywords Electronic ballast, design parameters, switching frequency, fluorescent lamp.

1. Introduction

Humankind is always in the search of new energy sources and efficient use of current sources in view of the limited energy sources in earth. The economic crisis in the world in last years has shown that energy saving concerns has to consider to preserve natural resources. Many new developments have been applied to the traditional electrical equipment to improve the efficiency. Efficient usage of electricity, as a transformation phase of different energy types, has more importance. One of the most widely used fields of electricity is lighting. The most widely used light sources are incandescent and fluorescent lamps in lighting [1]. Even light bulbs are considered as the prior source of lighting, in 20th century, fluorescent lamps are developed to efficiently use energy. Usage of florescent bulbs in schools, offices and other places made the development of more efficient fluorescent lamps a necessity [2].

Fluorescent lamps or fluorescent tubes use electricity for heating mercury and vaporizing through filaments to produce light. Light is produced after many phases in fluorescent

lamps to be created after thermal radiation. When you turn on the electricity, it goes through the one electrode to another in the fluorescent lamp. When the initial voltage reached, mercury is vaporized and ultraviolet lights are emitted. By the help of phosphorus placed in tube, this ultraviolet light transforms to the emitted light to be seen by our eyes [3].

Fluorescent lamps have many advantages in comparison with regular bulbs. They are more expensive but have more than 10 times long life than regular bulbs. Because light is emitted from a larger source (not a single point like light bulbs) in florescent lamps, it emits more light. Blue light emitted by florescent bulbs are better for the eye comfort. An 18 W fluorescent lamp can emit light as much as a 75 W regular light bulb. It means that fluorescent lamps consume less energy and emit more light, which ends up in around 75% energy efficiency. In addition that, as the ballasts used in florescent lamps are developed, it is expected to increase their efficiency [4], [5], [6].

The ballast works as a part of a florescent lamp to reach starting voltage and to limits the current in the lamp terminals upon reached steady state. As the gas discharge starts, at

ignition, current continuously increases and lamp voltage decreases. If resistance of the lamp is formulized as $R_{lamp}=dV/dI$, it is seen that the resistant has a negative slope or the lamp has negative resistance character (NTC). This requires the current to be limited. In less powered lamps, to limit the current, serial resistances may be used. However, this causes to loss power. Therefore, using ballast is a better way to save energy. There are two main type ballasts as electromagnetic ballasts and electronic ballasts [3].

Inductive ballasts, which named as magnetic or electromagnetic, are made of core rounded with aluminium or copper. In a fluorecent lamp, network voltage of 220V is not enough to start lighting in the beginning. It requires around 300V for starting firing. Therefore, an auxiliary device is necessary to generate high breakdown voltage for start-up and to stabilize lamp current. This device is the “starter” as a switch and used in the lamps to start lighting in the beginning. It does not work during the regular working or steady state times of fluorecent lamps.

Electronic ballasts require higher frequency than magnetic ballasts ($f_e > 20 \text{ kHz}$). They do not require a starter to initiate start-up voltage. In other words, they can give the start-up voltage themselves. Electronic ballasts are 10-20% more efficient than the inductive ballasts [7]. When more lamps are used in a system, this efficiency becomes more important. The more efficient on lighting systems the less heat is emitted. It is listed below that advantages of electronic ballasts in compared with inductive ballast:

- Increases the effectiveness of the lamp and all lighting system.
- Prevents light vibration and stereoscopic events.
- Increases power factor and does not need compensation.
- Enables to use light current in any degree.
- With lower heat increase, heat loss is decreased too.
- Does not have noises.
- Two lamps can work through a ballast.
- Small size, less weight, high frequency [8] - [13].

In recent years, there has been quite works and researchers are studying about this topic. These works are about design to boosts efficiency and gain of electronic ballasts. As so the works based on lamp arc, it exists that based on one of the components of the circuit as well. These high-frequency fluorecent lamp models are used for optimization studies [3], [4], [5], [14], [15], [16], [17]. However, they are not enough finding components of the circuit and procuring optimum efficiency on account of the fact that it is not to calculate properly the components. In addition, Methods of them are based on one of the component of the resonant tank, which arbitrary chosen value, or to have complex resolutions.

In this study, circuit parameters and components of electronic ballast are calculated by using this method. The design is made with Matlab/Simulink interface. Natural

frequency and damping ratio, which is parameters of the method, is chosen as natural frequency is switching frequency and damping ratio is 0,707 with the purpose of optimum efficiency [18]. Also it is focused on the design of an optimum resonant tank by considering the lamp equivalent resistant R_{lamp} is variable at high frequency. Using this method increases the gain and efficiency of the circuit by means of calculate components of circuit exactly.

The paper divided into five sections. In section 2, the fluorecent lamp resistance is designed as dynamic resistance model. Instead of voltage and current parameters, power of the fluorecent lamp is considered as a parameter in this approach. In section 3, design of the electronic ballast is presented. In section 4, the simulation study is presented. In section 5, the results are shared.

2. Fluorecent Lamp Model With Dynamic Resistant

Circuit topology of a basic high frequency electronic ballast system is shown in Fig. 1. While it is supplied by dc power supply, there is no need for power factor corrector (PFC) circuits and the circuits to prevent total harmonic distortion (THD). The parallel resonant inverter behaves like a current source, which can be used to stabilize fluorecent lamp current [19].

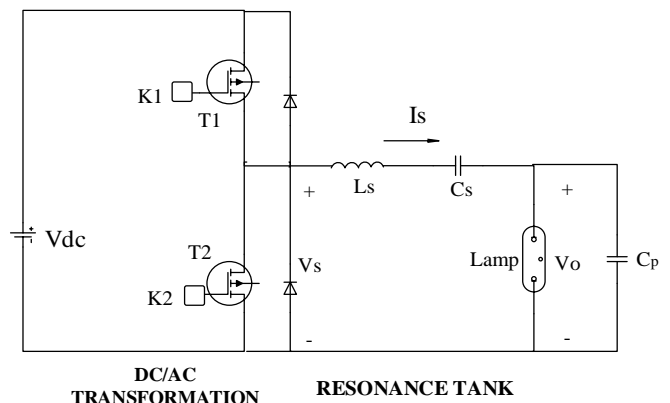


Fig. 1. Basic circuit configuration of an electronic ballast with half bridge series-resonant parallel-loaded inverter

While the circuit is supplying by dc battery, sinusoidal signal is obtained at desired high frequency level by use of T1 and T2 Mosfets, active power switches. This active power switches supplied with K1 and K2, square waves generators, are turned on and off alternately with a short dead time to drive the load resonant circuit at a high frequency. The parallel branch of resonant tank consists of a parallel capacitor, C_p , and a fluorecent lamp. Lamp Series branch of the circuit is formed by an inductor, L_s , and a capacitor, C_s . C_p is to provide a sufficiently high voltage across the lamp terminals during starting transient, afterwards a proper ac current at the steady state [20].

When lamp is off state, it behaves like an open circuit, resistant of lamp is almost equal to infinite value due to mercury mixture which is in fluorecent lamp tubes. However, the mixture is ionized and the resistant value decrease swiftly when the lamp is on state. Therefore, the

studies calculated resistant of lamp as a constant or with $R=V/I$ equation is not given proper calculation [4].

Various dynamic resistant approaches are developed to calculate resistant of fluorescent lamps [4]. The approaches based on voltage and current of the lamps are not given expected results due to the lamp resistant behaves as (NTC). That's why in this paper an approach based on lamp power to calculate resistant of the lamp is focused. A monotonic double exponential model is chosen to represent the electric characteristics of the lamp at high frequency optimally.

$$R_{lamp} = a.e^{(b.Plamp)} + c.e^{(d.Plamp)} \tag{1}$$

This equation is derived from a curve fitting to the experimental data of equivalent resistance versus average power [21]. A curve of equivalent resistance versus average power is presented in Fig.2 as a consequence of simulation made in Matlab/Simulink.

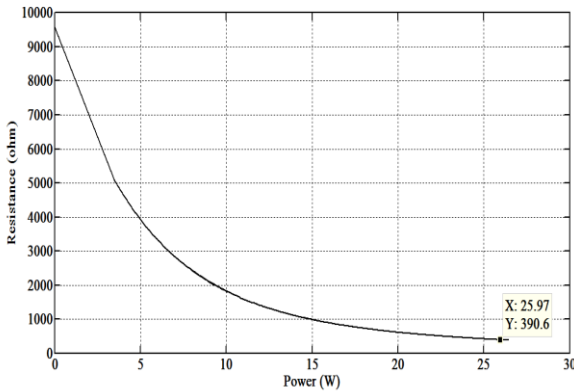


Fig. 2. Curve of Lamp resistant versus Average power in Simulink

3. Electronic Ballast Design

The purpose is to find values of the circuit parameters with mathematical calculation instead of based on one of circuit parameters or set value. By using this method, we find the parameter optimally. The control parameter used to vary the output power in all single stage topologies is switching frequency. These are variable frequency methods that higher frequency results in lower power delivered to the lamp [14]. First, damping ratio and switching frequency is chosen 0.707, 56.82 kHz, respectively. Then transfer function of circuit is find out. Poles and zeros of the function is calculated. System identification is evaluated by using transfer function of the circuit.

Table 1. Parameters of the circuits

ζ	Damping ratio	0.707
w_n	Natural frequency	358.14 k rad/s
s_1	A root of the transfer function	$(-2.53+2.53i).10^5$
s_2	A root of the transfer function	$(-2.53-2.53i).10^5$
s_3	A root of the transfer function	$-3.58.10^5$
L_s	Series inductor	1.31 mH
C_s	Series capacitor	14.4 nF
C_p	Parallel capacitor	2.97 nF

Transfer function of the circuit indicated in Fig.1 is find by following steps which is below and its poles are named as s_1, s_2, s_3 . After that, parameters of the circuit are calculated in consequence of committed calculations using natural frequency and damping ratio. As for gain of circuit, numerator of (3) must be maximize. Electronic ballast parameters are presented in table-1 in accordance with this foresight.

$$G(s) = V_o / V_s \tag{2}$$

$$i\omega L_s = X_{Ls} \tag{3}$$

$$1/(i\omega C_s) = X_{Cs} \tag{4}$$

$$1/(i\omega C_p) = X_{Cp} \tag{5}$$

$$V_o = i(s). \left(\frac{X_{Cp}.R_{lamp}}{(X_{Cp} + R_{lamp})} \right) \tag{6}$$

$$V_s = i(s). \left(X_{Ls} + X_{Cs} + \frac{X_{Cp}.R_{lamp}}{(X_{Cp} + R_{lamp})} \right). \tag{7}$$

Equation (6) is divided by equation (7) or from voltage-divide law,

$$\frac{V_o}{V_s} = \frac{R_{lamp} + \frac{1}{i\omega C_s}}{i\omega L_s + 1/(i\omega C_s) + (R_{lamp} + 1/(i\omega C_p))} \tag{8}$$

then transfer function of the circuit is found out as a third order function in s-domain.

$$G(s) = \frac{s}{C_p.L_s} \frac{1}{s^3 + \frac{s^2}{C_p.R_{lamp}} + \frac{(C_p + C_s).s}{C_p.C_s.L_s} + \frac{1}{C_p.C_s.L_s.R_{lamp}}} \tag{9}$$

The circuit is stable because all of poles are located left side of s-domain. As to the zero of transfer function, locates at origin owing to structure of circuit. These circumstances can be seen from the transfer function. However, the gain was interfered by way of coefficient of the zero.

Open representation of fluorescent lamps is shown in Fig.3. R_f resistance represents filaments of lamps situated at terminals of the lamps. The resistance value is chosen using experimental data [15].

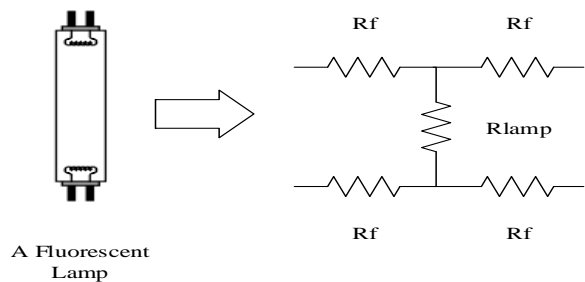


Fig. 3. Representation of a fluorescent lamp with filament resistances

4. Simulation Implementation of Fluorescent Lamp Model

The goal is to make simulation study ideally to comprehend behaviour of fluorescent lamp system shown in Fig.1. Matlab/Simulink interface is used as computer environment to implement the complex circuit easily.

Applied circuit is presented in Fig.4. It is supplied with battery to have 220-240 V. The mosfets are triggered with 0.5 fill rate by using a logical gate and a pulse generator. Also, they supply the resonance tank. Dynamic resistant model of the fluorescent lamp which is subsystem of Fig.4 is presented in Fig.5 clearly. Equation 1 is simulated using a function block parameter. A Controlled current source is used to execute dynamic resistant model. R_f represents a filament resistance of the fluorescent lamp shown in Table 2. In addition, other data used in Fig.4 and parameters of the monotonic double exponential function is shown in Table 2 as well.

Table 2. Monotonic double exponential function parameters and other values

Parameter	Explanation	Value
a	Value of variable	8147
b	Value of variable	-0.2113
c	Value of variable	1433
d	Value of variable	-0.5353
R_f	Resistance of filaments	$6\Omega \times 4$
V_{dc}	DC Voltage	236 V
f_s	Switching frequency	56.82 kHz
$ I_{in} $	Amplitude of the current (I_{in})	0.26 A
$ V_{in} $	Amplitude of input voltage (V_{in})	236 V
R_{lamp}	Equivalent resistance of the lamp	389Ω
P_{lamp}	Power of the lamp	26.1 W

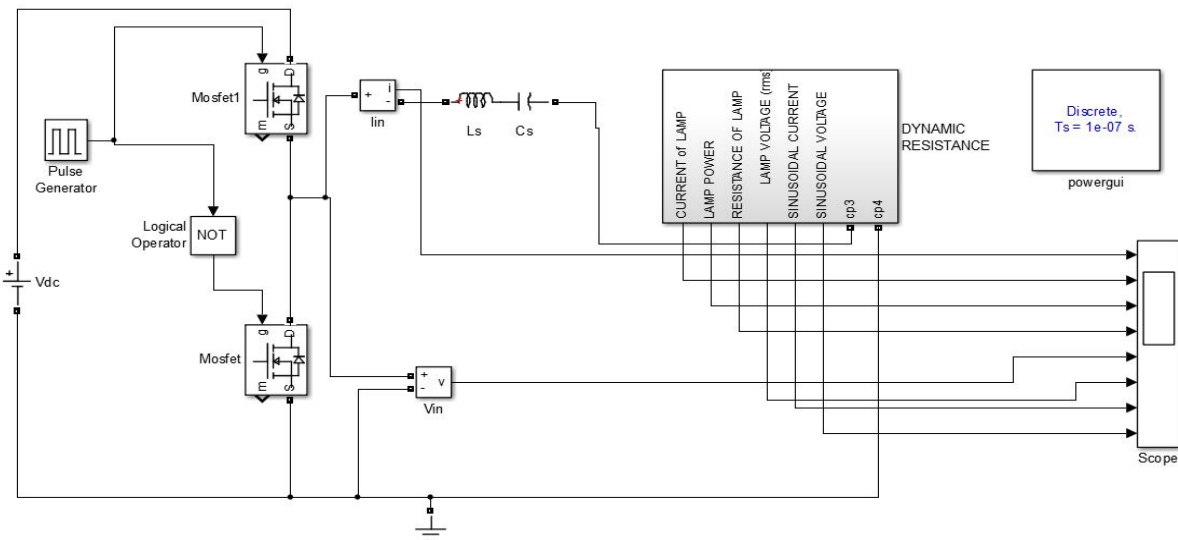


Fig. 4. A high frequency electronic ballast circuit with a dynamic resistant fluorescent lamp model

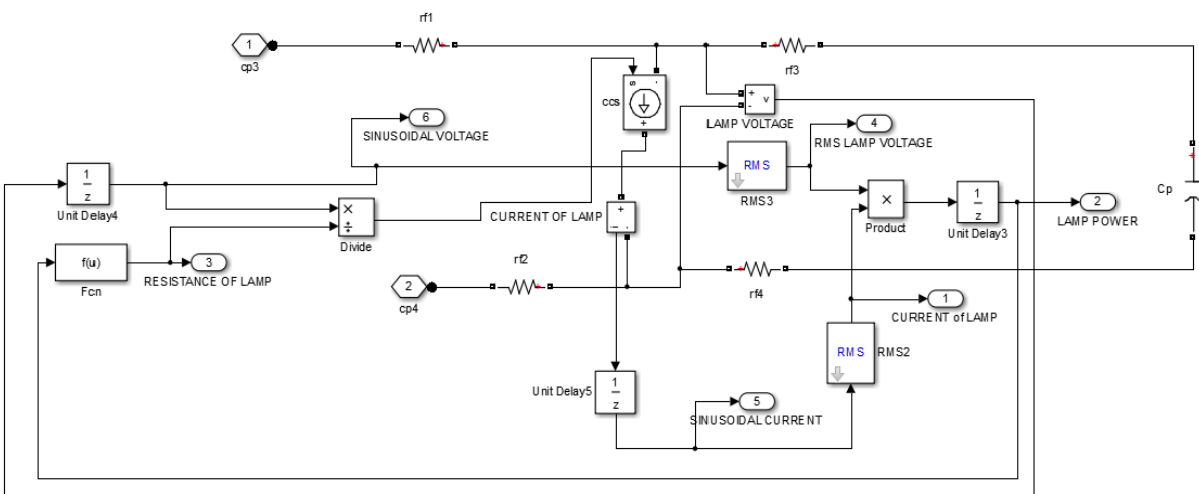


Fig. 5. Demonstration of dynamic resistant and the fluorescent lamp model

5. Results

High frequency electronic ballast with dynamic resistance fluorescent lamp model, presented in Fig.4, whose subsystem is shown in Fig.5, is run. The results are presented in following figures. To design the circuit Matlab/Simulink is used.

Lamp voltage and current are presented with general overview in Fig.6, with root mean square forms. It is seen clearly that Lamp voltage is high at transient response because of the reason mentioned in section 1. This means that, the lamp can be run and the resistance model is successful. In addition, before ignition, the lamp pretends open circuit because its resistant equals to roughly infinite value. Then in the ignition the current increases sharply due to decreasing of the resistant. This can be comprehended by means of reviewing to Eq .1. Finally, the current is suitable value in steady state operation.

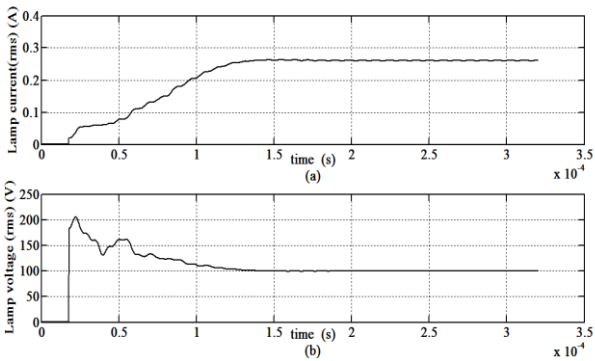


Fig. 6. Lamp Voltage and current versus time (a) Lamp current vs time (b) Lamp voltage vs time

Figure 7 is presented to better understand the relationship of lamp voltage and current at ignition. On the other hand, there is a lamp dynamic resistance variation ($r_{lamp} = \Delta V_{lamp} / \Delta I_{lamp}$).

Voltage and current waveforms of the lamp in lamp running is presented in Fig.8, with sinusoidal waveforms. It can be seen that phase difference between them nearly equal to zero. Thus ensuring that the lamp represents a pure resistive load with high linearity at high operating frequency. Also they have no fluctuations.

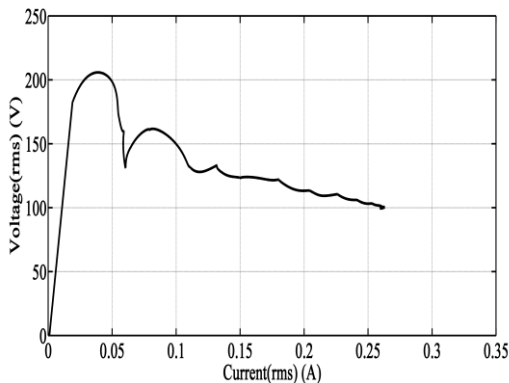


Fig. 7. Lamp voltage versus lamp current

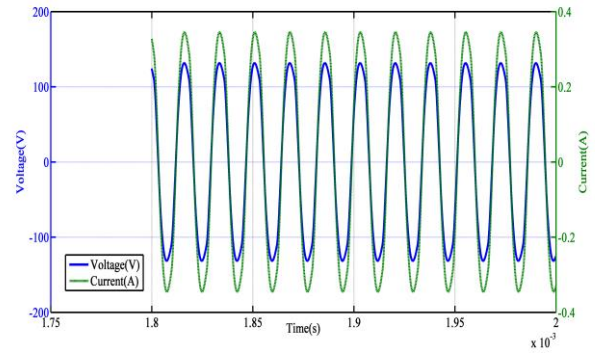


Fig. 8. Voltage-current of the lamp versus time at steady state operation

Figure 9 is represented to behave of the lamp at ignition. Especially the voltage signal has become sinusoidal signals varying its amplitude due to variable lamp resistant in 0.12 sec implemented the ignition. Sinusoidal the current and the voltage signals are obtained 0.12 sec after lamp operating as to have constant amplitude in steady state. The high voltage at ignition able to be seen in that figure as well. This voltage is sufficient to ignite the lamp.

The Voltage, V_s , with square form, and Current, I_s , with sinusoidal form, waveforms are presented in Fig.10. To expect from the resonant circuit is to minimize the phase difference between voltage and current of series branch. This expectancy is satisfied thanks to the given ballast circuit, designed in frequency domain.

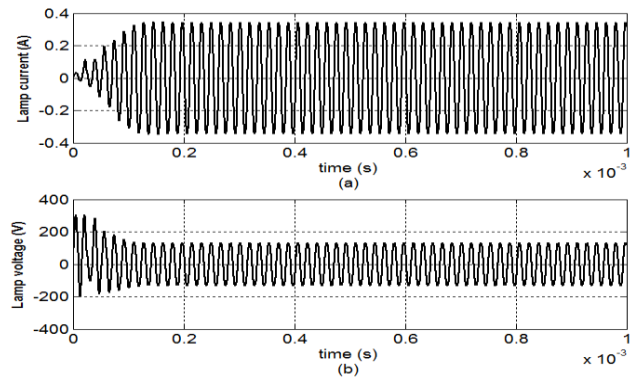


Fig. 9. The signals of the lamp versus time at ignition (a) Current of lamp vs time (b) Voltage of lamp vs time

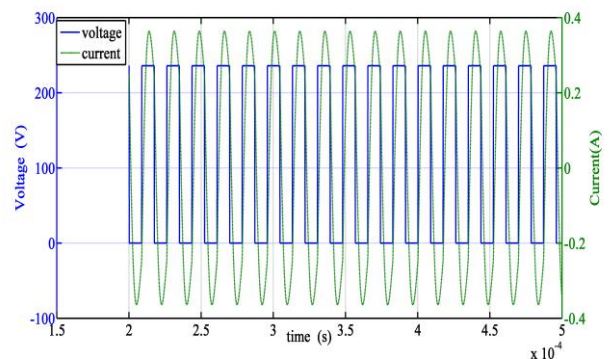


Fig. 10. Input Current and voltage waveforms after just switching process

6. Conclusion

This paper presented that root placement method about to calculate the electronic ballast parameters through roots of the transfer function. Resonance tank circuit has been developed to base on operating point resistant of the fluorescent lamp through roots of frequency domain. Modelling of a dynamic resistance in software environment depends on the view of researchers. It can be seen that success of this in Fig.5. The method has simple mathematic calculations and is capable to provide accurate values, which can be employed in new types to ballasts. Whereas, previous studies about this topic were based on one of the circuit parameters or a function which is complex. This study is different to them from this aspect. In other words, this is innovator side of the method.

A critical issue that has been validated in this study is the starting voltage needed by fluorescent lamps is supplied. This can be seen from Fig. 6, 9. The phase difference between lamp voltage and current could be seen in Fig.8. It is nearly zero value. Simulation studies are made to observe success in virtual environment putting in process of integrated structure. To perform simulations of the integrated structure, comprising a component to have a dynamic resistance, and reaching the instantaneous value of the electrical signal is one of the success of this paper. The mathematical value of equation (1) and the dynamic resistance value obtained on the simulation environment is equal. This is another success of the simulation.

References

- [1] U.S. Lighting Market Characterization, Building Technologies Program: 2010 U.S. Lighting Market Characterization, U.S. Department of Energy, 2012.
- [2] I. Galkin, O. Teteryonok, I. Milashevski, "Weight and Size Estimation of Energy Efficient LED Ballasts" *Elektronika Ir Elektrotechnika*, vol. 120, No. 4, 2012.
- [3] Mader U., Horn P., "A Dynamic Model for the Electrical Characteristics Lamp Model of Fluorescent Lamps" *Industry Applications Society Annual Meeting, Conference Record of the 1992 IEEE*, vol. 2, pp. 1928-1934, 04-09 October 1992.
- [4] R. Verderber, "Electronic Ballast Improves Efficiency" *Elec. Consultant*, vol. 60, pp. 22-26, November 1980.
- [5] J. R. Coaton, A. M. Marsden, *Lamps and Lighting 4th Edition*, 4th ed. Routledge; November 1, 1996.
- [6] J. Choi, "LED Driver Compatible with Electronic Ballast", Ph. D. Dissertation, Dept. Elect. Eng. KAIST, 2013.
- [7] Cheng C. A., Liang T. J., Chuang C. M., Chen J. F. "A Novel Method of Using Second-Order Lamp Model to Design Dimmable Fluorescent Lamps Electronic Ballast" *Industrial Electronics Society, The 27th Annual Conference of the IEEE*, pp. 1033-1037, 29-02 November/December 2001.
- [8] Yu T. H., Wu L. M., Wu T. F., "Comparisons among Self-Excited Parallel Resonant, Series Resonant and Current-Fed Push-Pull Electronic Ballasts", *Applied Power Electronics Conference and Exposition, IEEE*, vol. 1, pp. 421-426, February 1994.
- [9] Istok R., "High Frequency Emissions of Electromagnetic and Electronic Fluorescent Lamps", *IEEE International Symposium on Applied Computational Intelligence and Informatics*, Romania, pp. 21-23, 21-23 May 2015.
- [10] Sheeraz A.; Faizan A.; S. Riaz-ul-Hasnain; Duri S.; Sagib J. "Electronic Ballast Circuit Configurations for Fluorescent Lamps" *Power Generation System and Renewable Energy Technologies (PGSRET), IEEE Conference Publications*, pp. 1-8, 2015.
- [11] A. Vitanza, R. Scollo, A. Hayes "Electronic Fluorescent Lamp Ballast", *Application Note, Microelectronics*, 1999.
- [12] Y. Ji, R. Davis, "Starting Performance of High-Frequency Electronic Ballast for Four-Foot Fluorescent Lamps" *IEEE Transactions on Industry Applications*, vol. 33, pp. 234-238, January/February 1997.
- [13] R. A. Gupta, R. Agarwal, H. Soni, M. Ajay, "Design and Simulation of Single Stage High PF Electronic Ballast with Boost Topology for Multiple Fluorescent Lamp" vol. 2, pp. 323-331, November 2009.
- [14] A. A. Mansour, O. A. Arafa, "Comparative study of 250 W high pressure sodium lamp operating from both conventional and electronic ballast", *Journal of Electrical Systems and Information Technology*, vol.1, pp: 234-254, December 2014.
- [15] Wakabayashi F. T., Dantas F. D., Pinto J. O. P., Canesin C. A. "Fluorescent Lamp Model based on Equivalent Resistances, Considering the Effects of Dimming Operation" *2005 IEEE 36th Power Electronics Specialists Conference*, pp. 1136-1141, 2005.
- [16] Ribarich T. J., Ribarich J. J., "A new High-Frequency Fluorescent Lamp Model" *IEEE Industry Applications Society Annual Meeting, St. Louis, Missouri, October*, pp. 12-16, 1998.
- [17] Moo C. S., Chuang Y. C., Huang Y. H., Chen H. N. "Modeling of Fluorescent Lamps for Dimmable Electronic Ballasts" *Industry Applications Conference, San Diego, CA*, vol. 4, pp. 2231 - 2236, 06-10 October 1996.
- [18] J. David Irwin, R. Mark Nelms, *Basic Engineering Circuit Analysis*, 9. edition Wiley; (January 2, 2008)
- [19] Shao J., Stamm T., "Cost Effective High Performance LED Driver Powered by Electronic Ballasts", *IEEE Applied Power Electronics Conference and Exposition (APEC), Long Beach, CA*, pp. 3659-3662, 20-24 March 2016.
- [20] Moo C. S., Cheng H. L., Lin T. F., Yen H. C. "Designing a Dimmable Electronic Ballast with Voltage Control for Fluorescent Lamp" *Industrial Electronics, 1999. ISIE '99. Proceedings of the IEEE International, Bled*, pp. 786 - 791, 12-16 July 1999.
- [21] Perdigão M., Saraiva E. S., "Electronic Ballast with Wide Dimming Range: Matlab-Simulink Implementation of a Double Exponential Fluorescent Lamp Model" *Spanish Portuguese Congress on Electrical Engineering, Spain*, pp. 1-6, 02-30 June 2005.

Dynamic Spectrum Access: A New Paradigm of Converting Radio Spectrum Wastage to Wealth

Jide J. Popoola[‡], Oluwaseun A. Ogunlana, Ferdinand O. Ajie, Olaleye Olakunle, Olufemi A. Akiogbe, Saint M. Ani-Initi, Sunday K. Omotola

Department of Electrical and Electronics Engineering, Federal University of Technology, P.M.B. 704, Akure, Ondo State, Nigeria

(jidejulius2001@gmail.com, ayolana2002@yahoo.com, odefyeddy@yahoo.com, kunvicleye2011@yahoo.com, ayodejiakiogbe@gmail.com, saintzoba@gmail.com, omotolasunday@yahoo.com)

[‡]Corresponding Author: Jide J. Popoola, Department of Electrical and Electronics Engineering, Federal University of Technology, Akure, Ondo State, Nigeria. Tel: +23 4803413/1860, jidejulius2001@gmail.com

Received: 16.08.2016 Accepted: 31.08.2016

Abstract-The study presented in this paper reveals the limitations of the current fixed radio spectrum allocation policy as a major bottleneck for availability of radio spectrum for emerging wireless services, devices and applications as a result of its contributions to current radio spectrum artificial scarcity and underutilization problems. In investigating these problems scientifically, series of radio spectrum occupancy studies were carried out in developed nations of the world with little or none in most under-developed nation like Nigeria. In order to ascertain the usage profile of radio spectrum in under-developed nation like Nigeria, actual radio spectrum usage in three different locations in South-West Geo-political zone of Nigeria was carried out. The study was conducted using Aaronia AG HF-6065 V4 spectrum analyzer. The results obtained like other similar studies conducted in other parts of the world show that the usage of radio spectrum varies with time, space and frequency. The results also show that the actual radio spectrum usages in the three locations for the frequency range of 80-2200 MHz vary from 0.08% to 64.4%. In addition, the paper enumerates various ways of converting the current wasting spectrum holes to wealth as well as some economic advantages of dynamic spectrum access as a flexible radio access policy that can replace the current fixed radio spectrum allocation policy without compromising the performance of the existing radio being governed by the fixed spectrum allocation policy.

Keywords Spectrum holes, spectrum occupancy measurements, dynamic spectrum access, cognitive radio, spectrum trading.

1. Introduction

Over the past two decades, the exponential growth in demand for radio or wireless communication services, devices and applications has brought with it the need for a change in the way radio spectrum is being regulated. Currently, the radio spectrum regulatory bodies worldwide are of the opinion that the rigid spectrum management policy granting exclusive right to use licensed spectrum is still efficient. However, observations have shown that the idea of statically apportioning of radio spectrum into blocks and allocated for specific purposes as well as licensed to specific user or operator on either short or long term is long overdue and inefficient. This is because majority of the available radio spectral resources have already been licensed to users indicating that there is little or no room to add any new

wireless services, devices and applications unless some of the existing licenses are discontinued [1]. In addition, according to Buddhikot and Ryan [2], current spectrum management also has another serious operational problem as several licensed bands are not efficiently utilized with utilization varying dramatically over frequency, space and time. Furthermore, it was discovered through actual spectral occupancy measurements that vast portions of the licensed radio spectrum are randomly or rarely used by the licensed users [3-10]. For instance, a study conducted by the Federal Communications Commission (FCC) reported by Popoola and Van Olst [11], showed that usage of the licensed radio spectrum varied from 15% to 85% in the United State of America (USA).

Also, as reported by [11], similar actual spectral occupancy measurements showed that as little as 22% of allocated spectrum is utilized in urban areas and less than 3% is being utilized in rural areas buttressing the fact that usage of radio spectrum varies with space. Similarly, as reported by [11], observation from actual radio spectrum occupancy measurements conducted in downtown Berkeley showed that allocated frequency bands to licensed users are underutilized especially in the 3-6 MHz, while some other frequency bands are rarely occupied and the remaining frequency bands are heavily occupied showing that radio spectrum usage also vary with frequency. A typical result of these measurements presented in [9] is shown in Fig.1. From these observations, according to [11], the concept of spectrum holes was introduced, which was defined in [10, 12] as bands of frequencies assigned to primary users (PUs) also known as licensed users but at a particular time and in specific geographical location the bands are not being utilized by the licensed users.

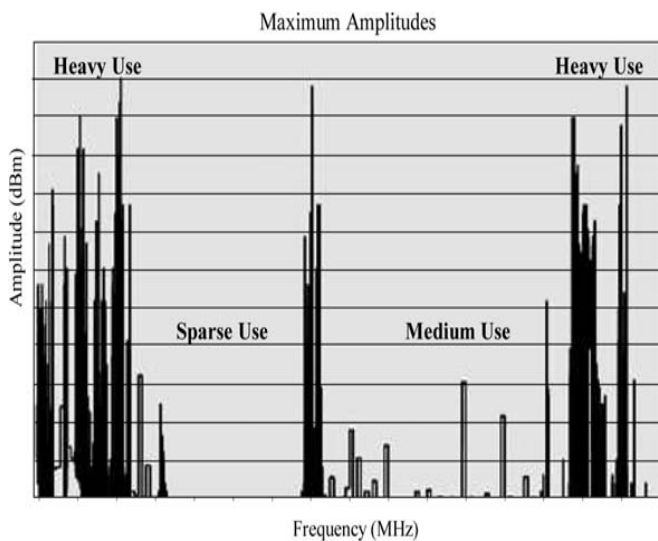


Fig. 1. Typical spectrum under-utilization profile [9]

Generally, according to Najashi and Feng [13], spectrum occupancy measurements have been used to ascertain the level of spectrum utilization by licensed users. The essence of spectrum occupancy measurements is to prove the need for deployment of another radio spectrum access technology for both effective and efficient radio spectrum management. However, out of the several spectrum occupancy measurements conducted all over the world, it was discovered that most were done in USA and Europe with few in Asia and Africa [14]. For instance in South Africa, the spectrum occupancy measurements carried out in the Hatfield area of Pretoria for ultra-high frequency (UHF) band, global system for mobile communications (GSM) 900 MHz and GSM 1800 MHz bands by [15] show variations in usage of the three bands. The UHF band for instance has an approximately occupancy of 20% while those of GSM 900 MHz and GSM 1800 MHz bands are at approximately 92% and 40% respectively. Similar study carried out in Kampala, Uganda capital recently using GSM900, GSM1800, the universal mobile telecommunications system 2100 (UMTS2100) and long term evolution 2600 (LTE2600) bands presented in [16] shows variations in those frequency

bands considered. The result of the study, gave an average occupancy rates of 8.8% and 52.4% respectively for both the uplink and downlink in GSM900 band. The corresponding results for the uplink and downlink occupancy rates for GSM1800 band obtained in [16] are 0.6% and 13.6% respectively. Also, the obtained uplink and downlink occupancy results in the study are 0.56% and 48.7% respectively for the UMTS2100 band while the corresponding results for the LTE2600 band are 0% and 0.6% respectively.

Similarly, in Nigeria, one of the studies on spectrum occupancy measurements in searched literature was conducted and published by [14]. The study presented in [14] was conducted at Gwarinpa District in Abuja. The results obtained by [14] showed that the variation of usage of licensed spectrum in Abuja, the Nigeria Federal Capital Territory, ranges from 17% to 26% at 700 – 2400 MHz frequency bands considered. Furthermore, the results of another recent study on spectrum occupancy measurements [17], which were conducted in Abuja and Katsina both in Nigeria show variations in spectrum usage in the two locations with occupancies variations from 0.45% to 26%. Thus, in order to ascertain the level of licensed spectrum usage in other parts of the country, the study reported in this paper was embarked upon. It was embarked upon to ascertain whether or not dynamic spectrum access also known as opportunistic spectrum access (OSA) can be proposed in Nigeria as in other nations of the world. The study was conducted in three state capitals (Ado-Ekiti, Akure and Ikeja) in the South-West Geopolitical zone of Nigeria. The full details on how the occupancy measurements were conducted are presented in Section 3 of this paper.

The rest of the paper is organized as follows: In Section 2, a brief background on dynamic spectrum access (DSA) and cognitive radio technology as an enabler of DSA is presented. The details on the field measurements conducted to evaluate the spectrum occupancy in the study areas are presented in Section 3. The results obtained in Section 3 were analyzed and discussed in Section 4. The economic advantages of DSA in converting spectrum holes to wealth by the regulatory bodies and/or licensed users are also presented in this section. Section 5, which is the last section, concludes the paper.

2. Brief on DSA and Cognitive Radio Technology

Dynamic spectrum access also known as OSA is defined as a new spectrum sharing paradigm that allows unlicensed or secondary user (SU) to access the idle or unused spectrum otherwise called spectrum holes or white spaces in the licensed spectrum band. It is a flexible radio spectrum access policy to alleviate the current problems of spectrum scarcity and spectrum underutilization in order to increase spectrum utilization [18]. The concept of DSA is to find a means of accessing the unused portion of already assigned licensed spectrum without interfering with the transmission of the PU as illustrated in Fig.2. The type of radio that enables SU to operate in idle portion of the licensed spectrum in this opportunistic manner is known as cognitive radio.

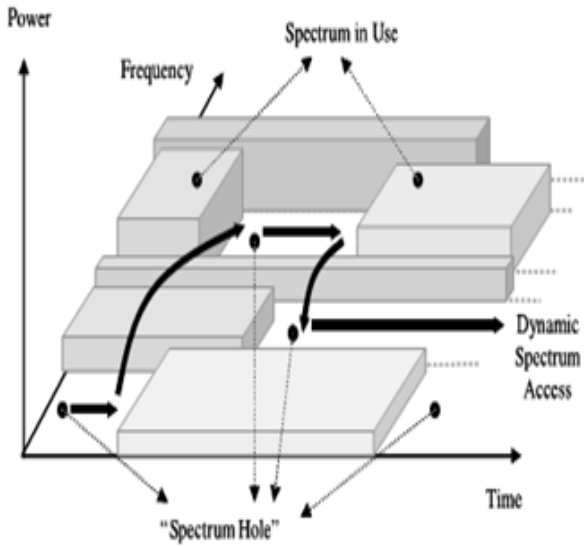


Fig. 2. Spectrum hole concept [9]

Cognitive radio (CR) technology is the main technology that enables already assigned spectrum to be used in a dynamic manner. It is defined as a radio that can change its transmitter parameters based on interaction with the environment in which it operates [9]. The cognitive capability of CR enables its real time interaction with its environment to determine appropriate communications parameters and adapt to the dynamic radio environment. According to [9], the tasks required for CR to perform this adaptive operation and ensuring interference free communication with the PU of the spectrum is referred to as the cognitive cycle. The three main steps in cognitive cycle as shown in Fig.3 are spectrum sensing, spectrum analysis and spectrum decision.

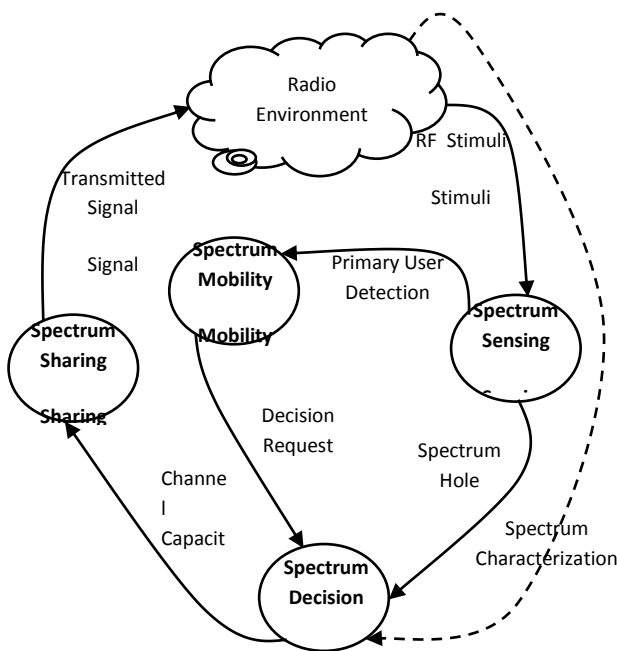


Fig. 3. Cognitive cycle [19]

The process of monitoring the available spectrum band in order to detect the presence of unused spectrum is known as spectrum sensing. Spectrum analysis on the other hand is a means of estimating the characteristics of the detected spectrum holes while spectrum decision is a means of determining the data rates and the transmission mode as well as the bandwidth of transmission with a view to choosing appropriate spectrum band according to spectrum characteristics and user requirements. As availability of spectrum hole is essential for adoption of DSA, the method employed to ascertain the availability of spectrum holes and the level of radio spectrum usage in this study are presented in the next section.

3. Methodology

In carrying out the study presented in this paper to ascertain the availability of spectrum holes in Nigeria for proposing adoption of DSA in the country, actual spectrum occupancy measurements were carried out in three states out of the six states that made up of the South-West Geo-Political zone in Nigeria. The actual spectrum occupancy measurements were conducted in Ado-Ekiti, Akure and Ikeja, which are respectively the state capitals for Ekiti, Ondo and Lagos states respectively. The three locations were chosen as the good representation of the geo-political zone due to their socio-economic developments, industrial activities, and population size.

In Lagos state, the actual spectrum occupancy measurement was conducted in Ikeja, longitude $3^{\circ} 20' 28'' E$ and latitude $6^{\circ} 38' 13'' N$. This study location is a densely populated residential and business area of the state, which is predominantly characterized by schools, banks, office blocks, shopping complex and residential buildings. The location is strategic and ideal for the study because of its proximity to radio and television broadcasting stations, mobile phone base stations, military headquarter, harbour and airport among others radio spectrum users in that vicinity. Likewise, in Akure, the study location lies at longitude $5^{\circ} 11' 42'' E$ and latitude $7^{\circ} 15' 0'' N$ while the study location in Ado-Ekiti lies at longitude $5^{\circ} 13' 47'' E$ and latitude $7^{\circ} 35' 16'' N$. These study locations are equally strategic locations with proximity to different radio spectrum licensed users. In the three locations, the same measurement setup was employed, which consists of an Aaronia AG HF-6065 V4 spectrum analyzer with a range of 10 MHz - 6 GHz, an Aaronia AG HyperLOG antenna, a laptop system that is connected to the spectrum analyzer via a USB cable, and an MCS software specially designed to run on Aaronia AG spectrum analyzers as shown in Fig.4.

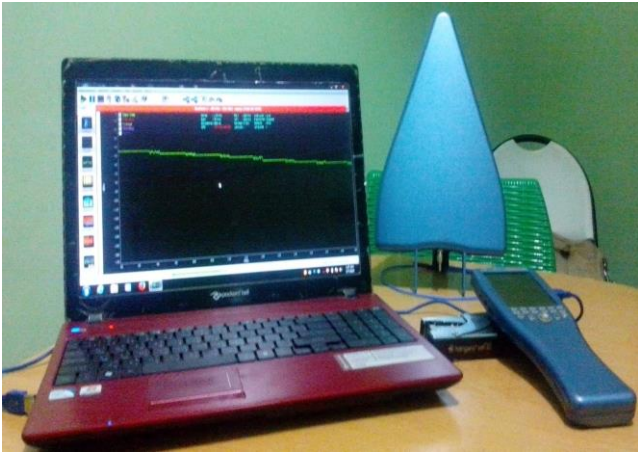


Fig. 4. Measurement set-up

The block diagram representation of the measurement set-up is shown in Fig.5. The arrows in Fig.5 show the direction of flow of signal in the set-up. The antenna receives the signal, the meter quantifies it, and the values of the quantified signals are stored in the laptop which also serves as the display unit for the set-up.

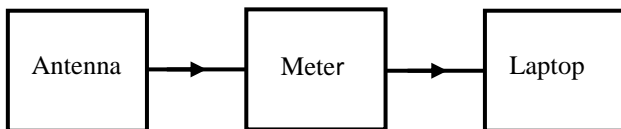


Fig. 5. Block representation of the measurement set-up

In determining the availability of the spectrum hole in any channel, energy detection method was employed, which necessitate the determination of threshold value for each frequency band considered in the three locations. This is because when energy detection method is employed in radio spectrum occupancy measurements, correct determination of the decision threshold upon which a particular channel can be either deemed free or busy is essential since there is no prior-knowledge about the channel. Hence, according to [16], correct setting of the threshold metric is important because high value will lead to under estimation of the

channel. On the other hand, if the threshold metric is low it will lead to over estimation of the channel under consideration.

Thus in determining the decision threshold values for each band at each location for this study, the average noise level was first determined by connecting a 50 Ω resistor to the spectrum analyzer [16]. The decision threshold was set by adding 3 dB to measured thermal noise. The decision threshold obtained varies from one location to another as well as the frequency band since the noise level varies with locations and frequencies. The decision threshold values employed are presented in Table 1. The threshold values were used in determining the actual spectrum occupancy for each frequency band by finding the ratio between the points above the threshold to the total number of points during the measurement period. The actual spectrum occupancy (SO) is defined using the relation;

$$SO = \frac{N_0}{N} \tag{1}$$

where N_0 is the total number of points above the threshold value and N is the total number of points during the measurement period. The results obtained from the measurements conducted are presented and discussed in the next section.

4. Results and Discussions

Four actual spectral usage profiles for the three locations for 80 – 150 MHz, 400 – 960 MHz, 900 – 1300 MHz and 1900 – 2200 MHz bands out of the eight frequency bands considered are presented graphically in Figs.6-9. The Figures show variations in the spectral usage in those frequency bands in the three locations. Also, the results of the actual spectral usage in the three locations show variations in the spectral usage in time as the occupancy measurements in the three locations were conducted on different days though the same time and days of the week in the same month. The overall results of the study show that the usage of the radio spectrum in the study locations varies with time, location and frequency.

Table 1. Decision threshold for each frequency band

Frequency band (MHz)	Band Designation	Applications	Threshold value (dBm)		
			Ado-Ekiti	Akure	Ikeja
80 – 150	A	Radio broadcasting band	-65.73	-55.63	-54.58
150 – 400	B	Television and Land Mobile	-53.82	-72.25	-72.24
400 - 960	C	Television broadcasting band	-69.32	-73.34	-79.12
700 - 1000	D	Trunk radio services and GSM band	-70.18	-72.46	-78.32
900 - 1300	E	GSM band	-73.11	-71.22	-75.55
1300- 1700	F	Rural Telecoms and GSM bands	-65.66	-93.43	-93.13
1700- 1900	G	GSM, Oil coy and Satellite broadcast	-80.27	-84.63	-86.99
1900- 2200	H	3G band	-86.44	-86.26	-94.69

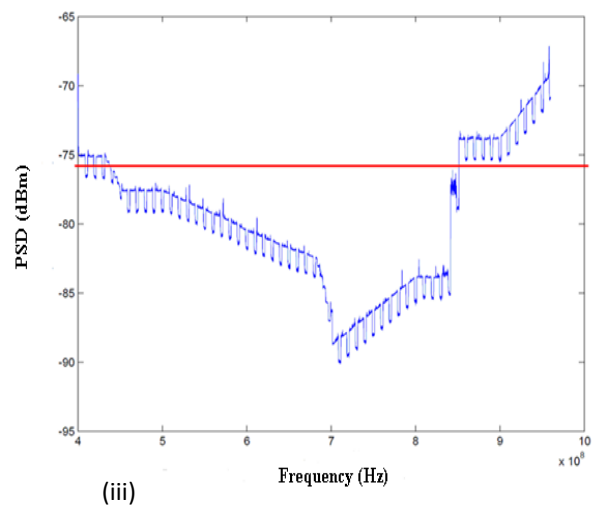
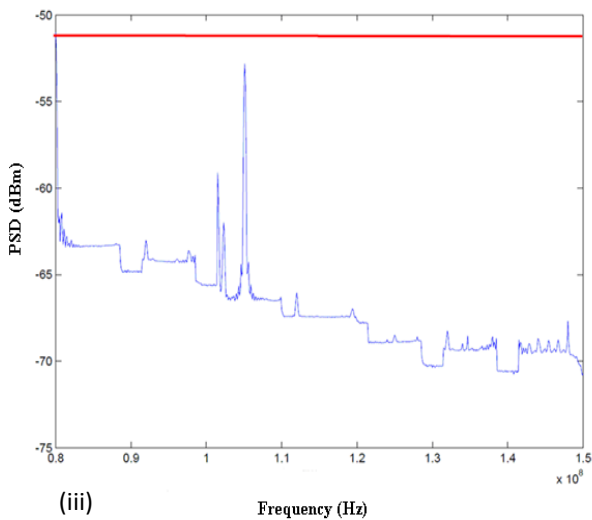
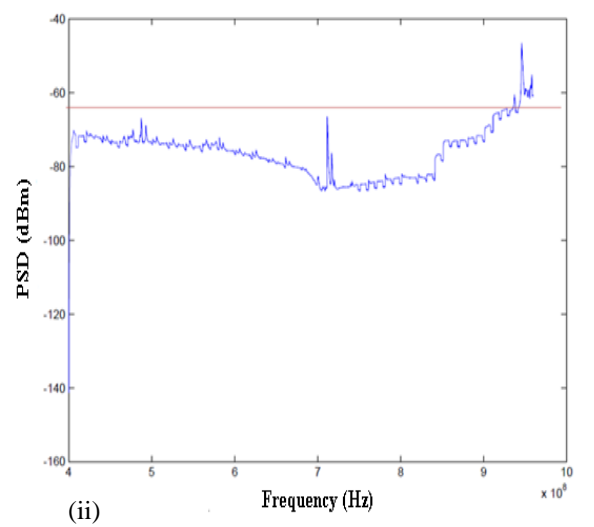
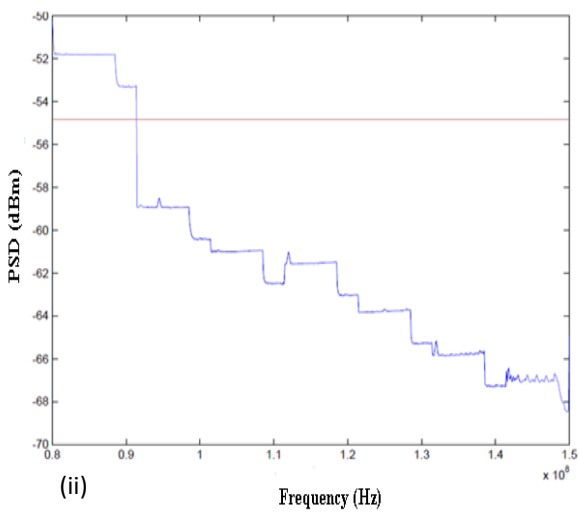
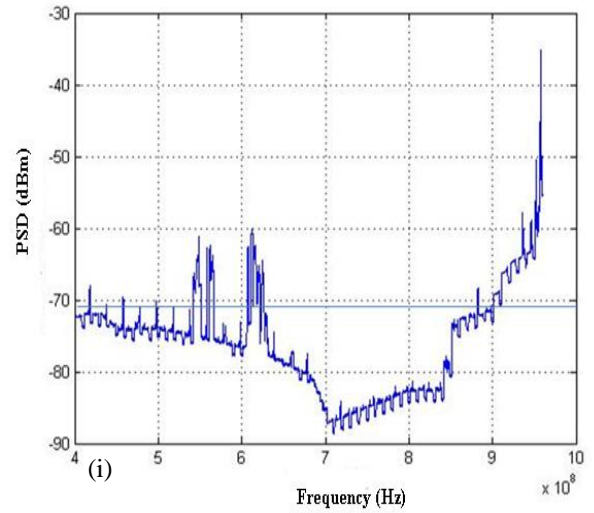
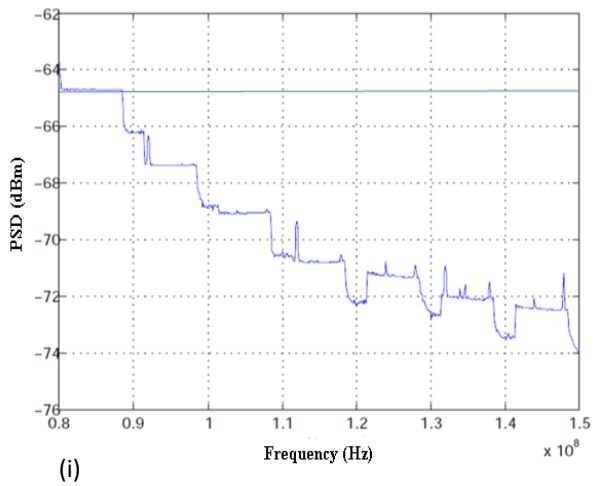


Fig. 6. Spectrum occupancy at 80-150 MHz for (i) Ado-Ekiti, (ii) Akure and (iii) Ikeja respectively

Fig. 7. Spectrum occupancy at 400-960 MHz for (i) Ado-Ekiti, (ii) Akure and (iii) Ikeja respectively

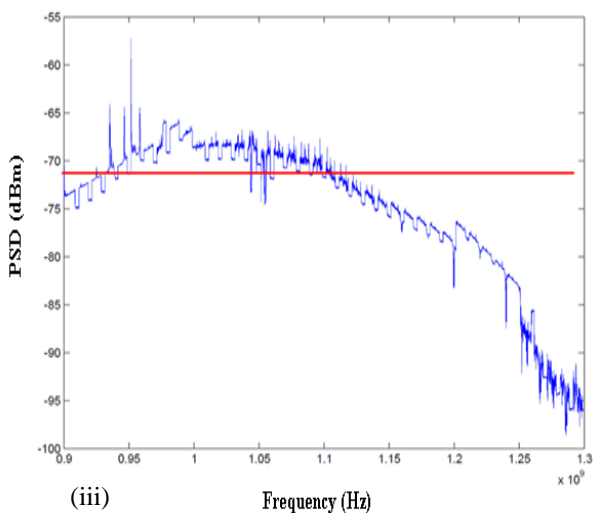
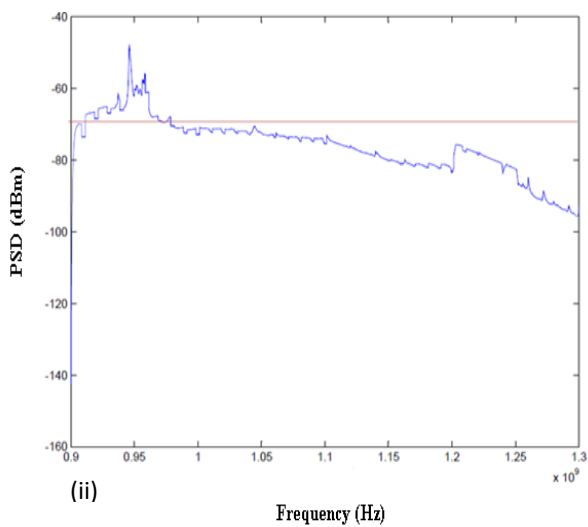
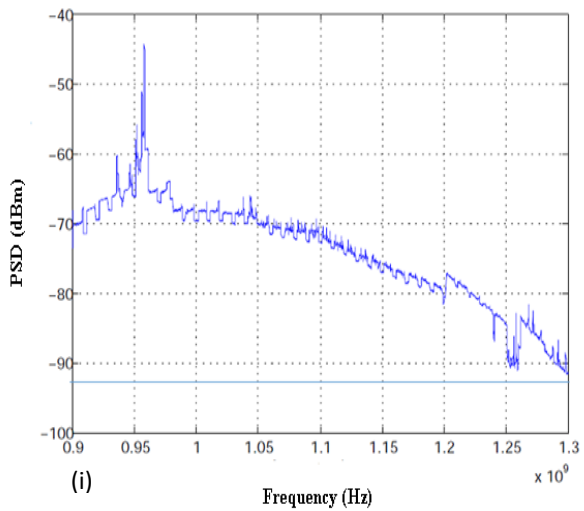


Fig. 8. Spectrum occupancy at 900-1300 MHz for (i) Ado-Ekiti, (ii) Akure and (iii) Ikeja respectively

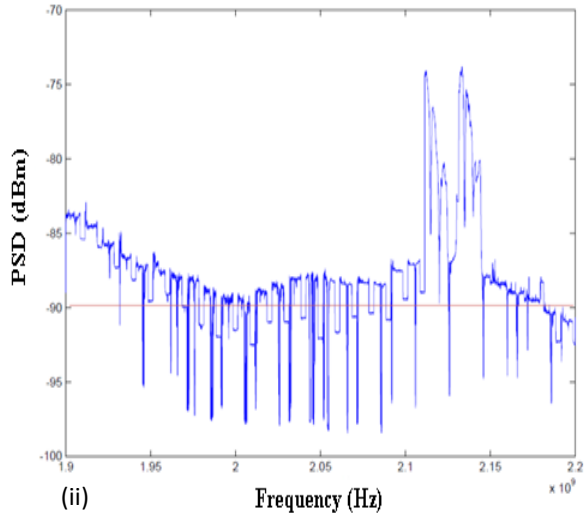
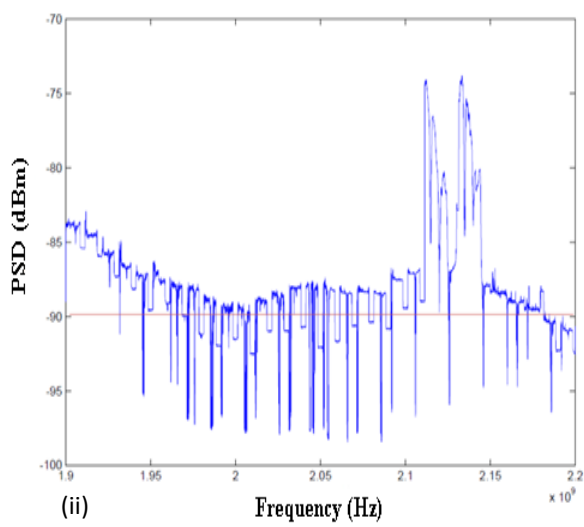
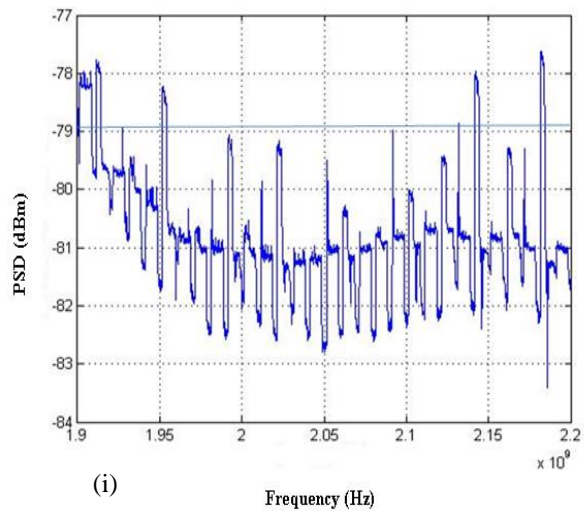


Fig. 9. Spectrum occupancy at 1900-2200 MHz for (i) Ado-Ekiti, (ii) Akure and (iii) Ikeja respectively

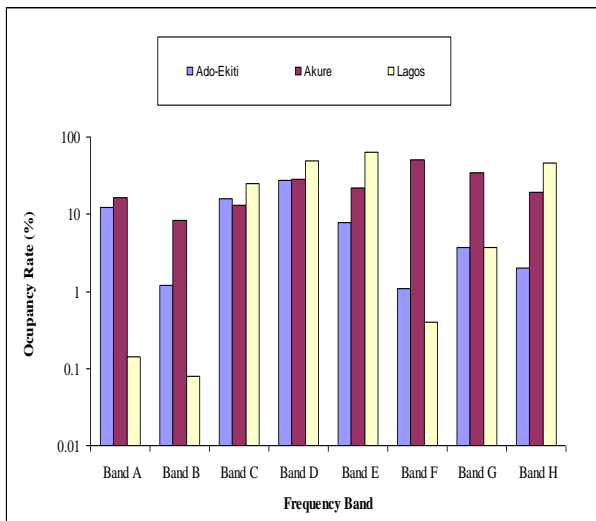


Fig. 10. Overall radio spectrum occupancy for each band

Fig.10 shows the overall radio spectral occupancy for each band using the band designation used in Table 1. The logarithm scale of the actual occupancy rate obtained was plotted against the frequency band. The logarithm scale was used on the vertical axis in Fig.10 in order to normalise the occupancy rate. The results show variation in the usage of each frequency band with location. The results also show that while a particular frequency was being heavily utilized in a particular location the same frequency was being sparingly utilized in another location. For example, the 80 – 150 MHz frequency band has utilization level of 12.41% in Ado-Ekiti while the corresponding values for the frequency band in Akure and Lagos are 16.3% and 0.14% respectively. This shows that Band A is sparingly utilised in Ikeja while the band has medium utilization in Akure and Ado-Ekiti. On the other hand, the overall result as shown in Fig.10 shows that Bands D, E and H which are GSM bands are heavily utilized in Ikeja while the bands are fairly utilised in Akure and sparingly utilised in Ado-Ekiti. Generally, Fig.10 shows that the overall spectrum occupancy in the three locations range from 0.08% - 64.4%. This shows that there is availability of spectrum holes that can be converted from waste to wealth if DSA is deployed in the country’s radio spectrum management. Recently, according to [20], the radio spectrum regulators in the United States and the United Kingdom have given conditional endorsement to DSA mode of spectrum access based on its economic advantages. This implies that adoption of DSA in radio spectrum management policy in underdeveloped nation like Nigeria and generally all over the world has some economic advantages.

One of the economic benefits of DSA is that it enables secondary users of the radio spectrum to utilize the spectrum holes in an opportunistic manner. It thus enhances the efficiency of spectrum usage as well as helping in eradicating the current problem of radio spectrum scarcity and underutilization. Also, the deployment of the DSA technology will enhance the availability of spectral resources for future emerging wireless services, devices and applications [19]. Apart from the fact that DSA can enhance spectral utilization efficiency, another economic advantage of DSA is that it also provides extra revenue for the PU or

licensed owner of the spectrum via spectrum trading [19], which according to [21] is the act of selling and buying radio spectrum in a cognitive radio environment. This economic advantage is feasible under DSA because the flexibility involved permits dynamic spectrum market where PUs or licensed owners lease out their spectrum holes or unused channels to generate revenue whenever their channels are not used. Thus the capability of DSA in converting the unused channel that is currently a waste under the current rigid radio spectrum management to wealth for the PUs or licensed owners is a major economic benefit.

In addition, another economic advantage of DSA is that it enhances cost effective access. This enables secondary users to use free and leased spectrum as well as usage of existing radio towers and other infrastructures. According to [19], this act enables smaller scale and lower entry costs become feasible to drive down the service prices. These lower entry costs according to Reference [19] brings about increase in the introduction of new wireless products and services in the marketplace. This cost effective access provides by DSA does not only improve broadband communication system but also promote job opportunity as well as contributing to the nation’s economy. Similarly, according to [22], another economic advantage of DSA is that its cost effective access methodology increases faster entry and exist in the market place as well as driving down wireless service prices. This also enhances job creation and socio-economic advancement of the nation.

5. Conclusion

Obviously, radio spectrum is a major enabler of wireless communication systems. As a result of its indispensability in wireless communication systems, radio spectrum is being regulated by both the international and national bodies worldwide. However, recent observations have shown that radio spectrum is not effectively and efficiently utilized by licensed owners under the current fixed radio spectrum allocation policy. Specifically, the overall spectrum occupancy or utilization efficiency obtained in this study that ranges from 0.08% to 64.4% shows that the current fixed radio spectrum management policy is far overdue and needs to be replaced with flexible management policy that will improve the utilization of radio spectrum. With the rapid progress in DSA technology and economic advantages of DSA, this paper is recommending the replacement of the current fixed spectrum allocation policy with DSA so that the current radio spectrum wastage can be converted to wealth.

Another significant contribution of this study is that it shows the practical relationship of spectrum occupancy with locations. Unlike most similar studies in surveyed literature that consider one or two location(s) with few frequency bands, the study presented in this paper was conducted in three different locations using eight different frequency bands. The results of the study show that spectrum occupancy varies from one location to another. Finally, as a way of concluding this paper, it is obvious that the replacement of the current fixed or rigid radio spectrum management policy with DSA will not only convert the current radio spectrum wastage to wealth and enhancing

radio spectrum management and its utilization, but will also not compromise the performance of the existing radio being governed by the fixed spectrum allocation policy.

Acknowledgements

Authors thank Akinlolu Ponnle of Department of Electrical and Electronics Engineering, School of Engineering and Engineering Technology of the Federal University of Technology, Akure, Nigeria for proofreading the manuscript.

References

- [1] I. Budiarjo, H. Nikookar, L.P. Ligthart, (2008) "Cognitive radio modulation techniques", *IEEE Signal Pro. Mag.*, vol. 25, no. 6, pp. 24-34.
- [2] M.M. Buddhikot, K. Ryan, (2005) "Spectrum management in coordinated dynamic spectrum access based cellular networks", *Proc. of 1st IEEE Int. Conf. on Dynamic Spectrum Access Networks*, Baltimore, USA, November 8-11, pp. 299-307.
- [3] G. Ding, Q. Wu, Y. Zou, J. Wang, Z. Gao, (2014) "Joint spectrum sensing and transmit power adaptation in interference-aware cognitive radio networks", *Trans. on Emerg. Telcomm. Techn.*, vol. 25, no. 2, pp. 231-238.
- [4] J. Wang, G. Diang, Q. Shen, F. Song, (2014) "Spatial-temporal spectrum hole discovery: A hybrid spectrum sensing and geolocation database framework", *Chinese Sci. Bulletin*, vol. 59, no. 16, pp. 1896-1902.
- [5] R. Shukla, D. Sharma, (2013) "Estimation of spectrum holes in cognitive radio using PSD", *Int. J. Inf. and Comp Techn.*, vol. 3, no. 7, pp. 663-670.
- [6] A.S. Kadhim, H.M. AISabbagh, (2012) "Detection the spectrum holes in the primary bandwidth of the cognitive radio systems in presence noise and attenuation", *Int. J. Comm. Networks and Sys. Sci.*, vol. 5, no. 10, pp. 685-690.
- [7] S. Haykin, D.J. Ehomson, J.H. Reed, (2009) "Spectrum sensing for cognitive radio", *Proc. of the IEEE*, vol.97, no. 5, pp. 849-977.
- [8] G. Zhao, J. Ma, G.Y. Li. T. Wu, Y. Kwon, A. Song, C. Yang, (2009) "Spatial spectrum holes for cognitive radio with relay-assisted directional transmission", *IEEE Trans. on Wireless Comm.*, vol. 8, no. 10, pp. 5270-5279.
- [9] I.F. Akyildiz, W.Y. Lee, M.C. Vuran, S. Mohanty, (2006) "Next generation/dynamic spectrum access/cognitive radio wireless networks: A survey", *Comp. Networks*, vol. 50, no. 13, pp. 2127-2159.
- [10] S. Haykin, (2005) "Cognitive radio: Brain-empowering wireless communications", *IEEE J. on Selected Areas in Comm.*, vol. 23, no. 2, pp. 201-220.
- [11] J.J. Popoola, R. Van Olst, (2011) "Application of neural network for sensing primary radio signals in a cognitive radio environment", *Proc. of IEEE AFRICON*, Livingstone, Zambia, September 13 – 15, pp. 1-6.
- [12] M. Chiani, A. Giorgetti, G. Liva, (2005) "Ultra wide bandwidth communications towards cognitive radio", *Proc. Electromag. Comp. EU. Workshop*, Rome, Italy, September 19 – 21, pp. 114-117.
- [13] B.G. Najashi, W. Feng, (2014) "Cooperative spectrum occupancy based spectrum prediction modelling", *J. Comp. Infor. Syst.*, vol. 10, no. 10, pp. 4083-4100.
- [14] B.G. Najashi, W. Feng, C. Kadri, (2013) "An insight into spectrum occupancy in Nigeria", *Inter. J. Comp. Sci. Issues*, vol. 10, no. 1, pp. 394-399.
- [15] S.D. Barnes, P.A.J. van Vuuren, B.T. Maharaj (2013) "Spectrum occupancy investigation: Measurements in South Africa", *Measurement*, vol. 46, no. 9, pp. 3098-3112.
- [16] G. Ayugi, A. Kisolo, T.W. Ireeta, (2015) "Telecommunication frequency band spectrum occupancy in Kampala Uganda", *Inter. J. Research in Eng. and Techn.*, vol. 4, no. 9, pp. 390-396.
- [17] B.G. Najashi, M.D. Almstapha, A.S. Abdi, S.A. Ashurah, (2015) "Spectrum occupancy measurements in Nigeria: Results and analysis.", *Int. J. of Comp. Sci. Issues*, vol. 12, no. 4, pp. 156-165.
- [18] M. Song, C. Xin, Y. Zhao, X. Cheng, (2012) "Dynamic spectrum access: From cognitive radio to network radio", *IEEE Wireless Comm.*, vol. 19, no. 1, pp. 23-29.
- [19] J.J. Popoola, R. Van Olst, (2014) "A survey on dynamic spectrum access via cognitive radio: Taxonomy, requirements, and benefits", *Universal J. Comm. and Network*, vol. 2, no. 4, pp. 70-85.
- [20] M. Nekovee, (2010) "A survey of cognitive radio access to TV white spaces", *Inter. J. Digital Broadcasting*, vol. 2010, pp. 1-11. Online [Available] http://www.hindawi.com/journals/ijdmb/2010_236568. Accessed on May 17, 2016.
- [21] K.G. Shin, H. Kitn, A.W. Min, A. Kumar, (2010) "Cognitive radios for dynamic spectrum access: From concepts to reality", *IEEE Wireless Comm.*, vol. 17, no. 6, pp. 64-74.
- [22] J.M. Chapin, W.H. Lehr, (2007) "Cognitive radios for dynamic spectrum access- the path to market success for dynamic spectrum access technology", *IEEE Comm. Mag.*, vol. 45, no. 5, pp. 96-102.

Guide for Authors

The *International Journal of Engineering Technologies (IJET)* seeks to promote and disseminate knowledge of the various topics of engineering technologies. The journal aims to present to the international community important results of work in the fields of engineering such as imagining, researching, planning, creating, testing, improving, implementing, using and asking. The journal also aims to help researchers, scientists, manufacturers, institutions, world agencies, societies, etc. to keep up with new developments in theory and applications and to provide alternative engineering solutions to current.

The *International Journal of Engineering Technologies* is a quarterly published journal and operates an online submission and peer review system allowing authors to submit articles online and track their progress via its web interface. The journal aims for a publication speed of **60 days** from submission until final publication.

The coverage of IJET includes the following engineering areas, but not limited to:

All filed of engineering such as;

Chemical engineering

- Biomolecular engineering
- Materials engineering
- Molecular engineering
- Process engineering

Civil engineering

- Environmental engineering
- Geotechnical engineering
- Structural engineering
- Transport engineering
- Water resources engineering

Electrical engineering

- Computer engineering
- Electronic engineering
- Optical engineering
- Power engineering

Mechanical engineering

- Acoustical engineering

- Manufacturing engineering
- Thermal engineering
- Vehicle engineering

Systems (interdisciplinary) engineering

- Aerospace engineering
- Agricultural engineering
- Applied engineering
- Biological engineering
- Building services engineering
- Energy engineering
- Railway engineering
- Industrial engineering
- Mechatronics
- Military engineering
- Nano engineering
- Nuclear engineering
- Petroleum engineering

Types of Articles submitted should be original research papers, not previously published, in one of the following categories,

- Applicational and design studies.
- Technology development,
- Comparative case studies.
- Reviews of special topics.
- Reviews of work in progress and facilities development.
- Survey articles.
- Guest editorials for special issues.

Editorial Board

Editor-in-Chief:

Professor ILHAMI COLAK

Associate Editors:

Dr. Selin ÖZCIRA

Dr. Mehmet YESILBUDAK

Ethic Responsibilities

The publication of an article in peer-reviewed “*International Journal of Engineering Technologies*” is an essential building block in the development of a coherent and respected network of knowledge. It is a direct reflection of the quality of the work. Peer-reviewed articles support and embody the scientific method. It is therefore important to agree upon standards of expected ethical behavior for all parties involved in the act of publishing: the author, the journal editor, the peer reviewer, the publisher and the society of society-owned or sponsored journals.

All authors are requested to disclose any actual or potential conflict of interest including any financial, personal or other relationships with other people or organizations within three years of beginning the submitted work that could inappropriately influence, or be perceived to influence, their work.

Submission of an article implies that the work described has not been published previously that it is not under consideration for publication elsewhere. The submission should be approved by all authors and tacitly or explicitly by the responsible authorities where the work was carried out, and that, if accepted, it will not be published elsewhere in the same form, in English or in any other language, including electronically without the written consent of the copyright-holder.

Upon acceptance of an article, authors will be asked to complete a “Copyright Form”. Acceptance of the agreement will ensure the widest possible dissemination of information. An e-mail will be sent to the corresponding author confirming receipt of the manuscript together with a “Copyright Form” form or a link to the online version of this agreement.

Author Rights

As a journal author, you retain rights for a large number of author uses, including use by your employing institute or company. These rights are retained and permitted without the need to obtain specific permission from *IJET*. These include:

- ❖ The right to make copies (print or electronic) of the journal article for your own personal use, including for your own classroom teaching use;
- ❖ The right to make copies and distribute copies (including via e-mail) of the journal article to research colleagues, for personal use by such colleagues for scholarly purposes;
- ❖ The right to post a pre-print version of the journal article on internet web sites including electronic pre-print servers, and to retain indefinitely such version on such servers or sites for scholarly purposes

- ❖ the right to post a revised personal version of the text of the final journal article on your personal or institutional web site or server for scholarly purposes
- ❖ The right to use the journal article or any part thereof in a printed compilation of your works, such as collected writings or lecture notes.

Article Style

Authors must strictly follow the guide for authors, or their articles may be rejected without review. Editors reserve the right to adjust the style to certain standards of uniformity. Follow Title, Authors, Affiliations, Abstract, Keywords, Introduction, Materials and Methods, Theory/Calculation, Conclusions, Acknowledgements, References order when typing articles. The corresponding author should be identified with an asterisk and footnote. Collate acknowledgements in a separate section at the end of the article and do not include them on the title page, as a footnote to the title or otherwise.

Abstract and Keywords:

Enter an abstract of up to 250 words for all articles. This is a concise summary of the whole paper, not just the conclusions, and is understandable without reference to the rest of the paper. It should contain no citation to other published work. Include up to six keywords that describe your paper for indexing purposes.

Abbreviations and Acronyms:

Define abbreviations and acronyms the first time they are used in the text, even if they have been defined in the abstract. Abbreviations such as IEEE, SI, MKS, CGS, sc, dc, and rms do not have to be defined. Do not use abbreviations in the title unless they are unavoidable.

Text Layout for Peer Review:

Use single column layout, double spacing and wide (3 cm) margins on white paper at the peer review stage. Ensure that each new paragraph is clearly indicated. Present tables and figure legends in the text where they are related and cited. Number all pages consecutively; use 12 pt font size and standard fonts; Times New Roman, Helvetica, or Courier is preferred.

Research Papers should not exceed 12 printed pages in two-column publishing format, including figures and tables.

Technical Notes and Letters should not exceed 2,000 words.

Reviews should not exceed 20 printed pages in two-column publishing format, including figures and tables.

Equations:

Number equations consecutively with equation numbers in parentheses flush with the right margin, as in (1). To make equations more compact, you may use the solidus (/), the exp function, or appropriate exponents. Italicize Roman symbols for quantities and variables, but not Greek symbols. Use an dash (–) rather than a hyphen for a minus sign. Use parentheses to avoid ambiguities in denominators. Punctuate equations with commas or periods when they are part of a sentence, as in

$$C = a + b \tag{1}$$

Symbols in your equation should be defined before the equation appears or immediately following. Use “Eq. (1)” or “equation (1),” while citing.

Figures and Tables:

All illustrations must be supplied at the correct resolution:

- * Black and white and colour photos - 300 dpi
- * Graphs, drawings, etc - 800 dpi preferred; 600 dpi minimum
- * Combinations of photos and drawings (black and white and color) - 500 dpi

In addition to using figures in the text, upload each figure as a separate file in either .tiff or .eps format during submission, with the figure number.

Table captions should be written in the same format as figure captions; for example, “Table 1. Appearance styles.”. Tables should be referenced in the text unabbreviated as “Table 1.”

References:

Please ensure that every reference cited in the text is also present in the reference list (and viceversa). Any references cited in the abstract must be given in full. Unpublished results and personal communications are not recommended in the reference list, but may be mentioned in the text. Citation of a reference as “in press” implies that the item has been accepted for publication. Number citations consecutively in square brackets [1]. Punctuation follows the bracket [2]. Refer simply to the reference number, as in [3]. Use “Ref. [3]” or Reference [3]” at the beginning of a sentence: “Reference [3] was ...”. Give all authors’ names; use “et al.” if there are six authors or more. For papers published in translated journals, first give the English citation, then the original foreign-language citation.

Books

- [1] J. Clerk Maxwell, *A Treatise on Electricity and Magnetism*, 3rd ed., vol. 2. Oxford:Clarendon Press, 1892, pp.68-73.

Journals

- [2] Y. Yorozu, M. Hirano, K. Oka, and Y. Tagawa, “Electron spectroscopy studies on magneto-optical media and plastic substrate interface”, *IEEE Transl. J. Magn. Japan*, vol. 2, pp. 740-741, August 1987.

Conferences

- [3] Çolak I., Kabalci E., Bayindir R., and Sagiroglu S, “The design and analysis of a 5-level cascaded voltage source inverter with low THD”, *2nd PowerEng Conference*, Lisbon, pp. 575-580, 18-20 March 2009.

Reports

- [4] IEEE Standard 519-1992, Recommended practices and requirements for harmonic control in electrical power systems, *The Institute of Electrical and Electronics Engineers*, 1993.

Text Layout for Accepted Papers:

A4 page margins should be margins: top = 24 mm, bottom = 24 mm, side = 15 mm. Main text should be given in two column. The column width is 87mm (3.425 in). The space between the two columns is 6 mm (0.236 in). Paragraph indentation is 3.5 mm (0.137 in). Follow the type sizes specified in Table. Position figures and tables at the tops and bottoms of columns. Avoid placing them in the middle of columns. Large figures and tables may span across both columns. Figure captions should be centred below the figures; table captions should be centred above. Avoid placing figures and tables before their first mention in the text. Use the abbreviation “Fig. 1,” even at the beginning of a sentence.

Type size (pts.)	Appearance		
	Regular	Bold	<i>Italic</i>
10	Authors’ affiliations, Section titles, references, tables, table names, first letters in table captions, figure captions, footnotes, text subscripts, and superscripts	Abstract	
12	Main text, equations, Authors’ names, ^a		<i>Subheading (1.1.)</i>
24	Paper title		

Submission checklist:

It is hoped that this list will be useful during the final checking of an article prior to sending it to the journal's Editor for review. Please consult this Guide for Authors for further details of any item. Ensure that the following items are present:

- ❖ One Author designated as corresponding Author:
 - E-mail address
 - Full postal address
 - Telephone and fax numbers
- ❖ All necessary files have been uploaded
- Keywords: a minimum of 4
- All figure captions (supplied in a separate document)
- All tables (including title, description, footnotes, supplied in a separate document)
- ❖ Further considerations
 - Manuscript has been "spellchecked" and "grammar-checked"
 - References are in the correct format for this journal
 - All references mentioned in the Reference list are cited in the text, and vice versa

- Permission has been obtained for use of copyrighted material from other sources (including the Web)
- Color figures are clearly marked as being intended for color reproduction on the Web (free of charge) and in print or to be reproduced in color on the Web (free of charge) and in black-and-white in print.

Article Template Containing Author Guidelines for Peer-Review

First Author*, Second Author**‡, Third Author***

*Department of First Author, Faculty of First Author, Affiliation of First Author, Postal address

**Department of Second Author, Faculty of First Author, Affiliation of First Author, Postal address

***Department of Third Author, Faculty of First Author, Affiliation of First Author, Postal address

(First Author Mail Address, Second Author Mail Address, Third Author Mail Address)

‡Corresponding Author; Second Author, Postal address, Tel: +90 312 123 4567, Fax: +90 312 123 4567, corresponding@affl.edu

Received: xx.xx.xxxx Accepted:xx.xx.xxxx

Abstract- Enter an abstract of up to 250 words for all articles. This is a concise summary of the whole paper, not just the conclusions, and is understandable without reference to the rest of the paper. It should contain no citation to other published work. Include up to six keywords that describe your paper for indexing purposes. Define abbreviations and acronyms the first time they are used in the text, even if they have been defined in the abstract. Abbreviations such as IEEE, SI, MKS, CGS, sc, dc, and rms do not have to be defined. Do not use abbreviations in the title unless they are unavoidable.

Keywords- Keyword1; keyword2; keyword3; keyword4; keyword5.

2. Introduction

Authors should any word processing software that is capable to make corrections on misspelled words and grammar structure according to American or Native English. Authors may get help by from word

processor by making appeared the paragraph marks and other hidden formatting symbols. This sample article is prepared to assist authors preparing their articles to IJET.

Indent level of paragraphs should be 0.63 cm (0.24 in) in the text of article. Use single column layout, double-spacing and wide (3 cm) margins on white paper at the peer review stage. Ensure that each new paragraph is clearly indicated. Present tables and figure legends in the text where they are related and cited. Number all pages consecutively; use 12 pt font size and standard fonts; Times New Roman, Helvetica, or Courier is preferred. Indicate references by number(s) in square brackets in line with the text. The actual authors can be referred to, but the reference number(s) must always be given. Example: "..... as demonstrated [3, 6]. Barnaby and Jones [8] obtained a different result"

IJET accepts submissions in three styles that are defined as Research Papers, Technical Notes and Letter, and Review paper. The requirements of paper are as listed below:

- Research Papers should not exceed 12 printed pages in two-column publishing format, including figures and tables.
- Technical Notes and Letters should not exceed 2,000 words.
- Reviews should not exceed 20 printed pages in two-column publishing format, including figures and tables.

Authors are requested write equations using either any mathematical equation object inserted to word processor or using independent equation software. Symbols in your equation should be defined before the equation appears or immediately following. Use "Eq. (1)" or "equation (1)," while citing. Number equations consecutively with equation numbers in parentheses flush with the right margin, as in Eq. (1). To make equations more compact, you may use the solidus (/), the exp function, or appropriate exponents. Italicize Roman symbols for quantities and variables, but not Greek symbols. Use an dash (–) rather than a hyphen for a minus sign. Use parentheses to avoid ambiguities in denominators. Punctuate equations with commas or periods when they are part of a sentence, as in

$$C = a + b \tag{1}$$

Section titles should be written in bold style while sub section titles are italic.

3. Figures and Tables

3.1. *Figure Properties*

All illustrations must be supplied at the correct resolution:

- Black and white and colour photos - 300 dpi
- Graphs, drawings, etc - 800 dpi preferred; 600 dpi minimum
- Combinations of photos and drawings (black and white and colour) - 500 dpi

In addition to using figures in the text, Authors are requested to upload each figure as a separate file in either .tiff or .eps format during submission, with the figure number as Fig.1., Fig.2a and so on. Figures are cited as “Fig.1” in sentences or as “Figure 1” at the beginning of sentence and paragraphs. Explanations related to figures should be given before figure. Figures and tables should be located at the top or bottom side of paper as done in accepted article format.



Figure 1. Engineering technologies.

Table captions should be written in the same format as figure captions; for example, “Table 1. Appearance styles.”. Tables should be referenced in the text unabbreviated as “Table 1.”

Table 1. Appearance properties of accepted manuscripts

Type size (pts.)	Appearance		
	Regular	Bold	<i>Italic</i>
10	Authors’ affiliations, Abstract, keywords, references, tables, table names, figure captions, footnotes, text subscripts, and superscripts	Abstract	
12	Main text, equations, Authors’ names, Section titles		<i>Subheading (1.1.)</i>
24	Paper title		

4. Submission Process

The *International Journal of Engineering Technologies* operates an online submission and peer review system that allows authors to submit articles online and track their progress via a web interface. Articles that are prepared referring to this template should be controlled according to submission checklist given in “Guide f Authors”. Editor handles submitted articles to IJET primarily in order to control in terms of compatibility to aims and scope of Journal.

Articles passed this control are checked for grammatical and template structures. If article passes this control too, then reviewers are assigned to article and Editor gives a reference number to paper. Authors registered to online submission system can track all these phases.

Editor also informs authors about processes of submitted article by e-mail. Each author may also apply to Editor via online submission system to review papers related to their study areas. Peer review is a critical element of publication, and one of the major cornerstones of the scientific process. Peer Review serves two key functions:

- Acts as a filter: Ensures research is properly verified before being published
- Improves the quality of the research

5. Conclusion

The conclusion section should emphasize the main contribution of the article to literature. Authors may also explain why the work is important, what are the novelties or possible applications and extensions. Do not replicate the abstract or sentences given in main text as the conclusion.

Acknowledgements

Authors may acknowledge to any person, institution or department that supported to any part of study.

References

- [1] J. Clerk Maxwell, *A Treatise on Electricity and Magnetism*, 3rd ed., vol. 2. Oxford:Clarendon Press, 1892, pp.68-73. (Book)
- [2] H. Poor, *An Introduction to Signal Detection and Estimation*, New York: Springer-Verlag, 1985, ch. 4. (Book Chapter)
- [3] Y. Yorozu, M. Hirano, K. Oka, and Y. Tagawa, "Electron spectroscopy studies on magneto-optical media and plastic substrate interface", *IEEE Transl. J. Magn. Japan*, vol. 2, pp. 740-741, August 1987. (Article)
- [4] E. Kabalci, E. Irmak, I. Çolak, "Design of an AC-DC-AC converter for wind turbines", *International Journal of Energy Research*, Wiley Interscience, DOI: 10.1002/er.1770, Vol. 36, No. 2, pp. 169-175. (Article)
- [5] I. Çolak, E. Kabalci, R. Bayindir R., and S. Sagiroglu, "The design and analysis of a 5-level cascaded voltage source inverter with low THD", *2nd PowerEng Conference*, Lisbon, pp. 575-580, 18-20 March 2009. (Conference Paper)
- [6] IEEE Standard 519-1992, Recommended practices and requirements for harmonic control in electrical power systems, *The Institute of Electrical and Electronics Engineers*, 1993. (Standards and Reports)

Article Template Containing Author Guidelines for Accepted Papers

First Author*, Second Author**[‡], Third Author***

*Department of First Author, Faculty of First Author, Affiliation of First Author, Postal address

**Department of Second Author, Faculty of First Author, Affiliation of First Author, Postal address

***Department of Third Author, Faculty of First Author, Affiliation of First Author, Postal address

(First Author Mail Address, Second Author Mail Address, Third Author Mail Address)

[‡]Corresponding Author; Second Author, Postal address, Tel: +90 312 123 4567,

Fax: +90 312 123 4567, corresponding@affl.edu

Received: xx.xx.xxxx Accepted:xx.xx.xxxx

Abstract- Enter an abstract of up to 250 words for all articles. This is a concise summary of the whole paper, not just the conclusions, and is understandable without reference to the rest of the paper. It should contain no citation to other published work. Include up to six keywords that describe your paper for indexing purposes. Define abbreviations and acronyms the first time they are used in the text, even if they have been defined in the abstract. Abbreviations such as IEEE, SI, MKS, CGS, sc, dc, and rms do not have to be defined. Do not use abbreviations in the title unless they are unavoidable.

Keywords Keyword1, keyword2, keyword3, keyword4, keyword5.

1. Introduction

Authors should use any word processing software that is capable to make corrections on misspelled words and grammar structure according to American or Native English. Authors may get help by using word processor by making sure the paragraph marks and other hidden formatting symbols are visible. This sample article is prepared to assist authors preparing their articles to IJET.

Indent level of paragraphs should be 0.63 cm (0.24 in) in the text of article. Use single column layout, double-spacing and wide (3 cm) margins on white paper at the peer review stage. Ensure that each new paragraph is clearly indicated. Present tables and figure legends in the text where they are related and cited. Number all pages consecutively; use 12 pt font size and standard fonts; Times New Roman, Helvetica, or Courier is preferred. Indicate references by number(s) in square brackets in line with the text. The actual authors can be referred to, but the reference number(s) must always be given. Example: "... as demonstrated [3,6]. Barnaby and Jones [8] obtained a different result"

IJET accepts submissions in three styles that are defined as Research Papers, Technical Notes and Letter, and Review paper. The requirements of paper are as listed below:

➤ Research Papers should not exceed 12 printed pages in two-column publishing format, including figures and tables.

➤ Technical Notes and Letters should not exceed 2,000 words.

➤ Reviews should not exceed 20 printed pages in two-column publishing format, including figures and tables.

Authors are requested to write equations using either any mathematical equation object inserted to word processor or using independent equation software. Symbols in your equation should be defined before the equation appears or immediately following. Use "Eq. (1)" or "equation (1)," while citing. Number equations consecutively with equation numbers in parentheses flush with the right margin, as in Eq. (1). To make equations more compact, you may use the solidus (/), the exp function, or appropriate exponents. Italicize Roman symbols for quantities and variables, but not Greek symbols. Use an dash (-) rather than a hyphen for a minus sign. Use parentheses to avoid ambiguities in denominators. Punctuate equations with commas or periods when they are part of a sentence, as in

$$C = a + b \quad (1)$$

Section titles should be written in bold style while sub section titles are italic.

6. Figures and Tables

6.1. Figure Properties

All illustrations must be supplied at the correct resolution:

- Black and white and colour photos - 300 dpi
- Graphs, drawings, etc - 800 dpi preferred; 600 dpi minimum
- Combinations of photos and drawings (black and white and colour) - 500 dpi

In addition to using figures in the text, Authors are requested to upload each figure as a separate file in either .tiff or .eps format during submission, with the figure number as Fig.1., Fig.2a and so on. Figures are cited as “Fig.1” in sentences or as “Figure 1” at the beginning of sentence and paragraphs. Explanations related to figures should be given before figure.



Fig. 1. Engineering technologies.

Figures and tables should be located at the top or bottom side of paper as done in accepted article format. Table captions should be written in the same format as figure captions; for example, “Table 1. Appearance styles.”. Tables should be referenced in the text unabbreviated as “Table 1.”

Table 1. Appearance properties of accepted manuscripts

Type size (pts.)	Appearance		
	Regular	Bold	<i>Italic</i>
10	Main text, section titles, authors’ affiliations, abstract, keywords, references, tables, table names, figure captions, equations, footnotes, text subscripts, and superscripts	Abstract-	<i>Subheading (1.1.)</i>
12	Authors’ names,		
24	Paper title		

6.2. Text Layout for Accepted Papers

A4 page margins should be margins: top = 24 mm, bottom = 24 mm, side = 15 mm. The column width is 87mm (3.425 in). The space between the two columns is 6 mm (0.236 in). Paragraph indentation is 3.5 mm (0.137 in). Follow the type sizes specified in Table. Position figures and tables at the tops and bottoms of columns. Avoid placing them in the middle of columns. Large figures and tables may span across both columns. Figure captions should be centred below the figures; table captions should be centred above. Avoid placing figures and tables before their first mention in the text. Use the abbreviation “Fig. 1,” even at the beginning of a sentence.

7. Submission Process

The International Journal of Engineering Technologies operates an online submission and peer review system that allows authors to submit articles online and track their

progress via a web interface. Articles that are prepared referring to this template should be controlled according to submission checklist given in “Guide f Authors”. Editor handles submitted articles to IJET primarily in order to control in terms of compatibility to aims and scope of Journal. Articles passed this control are checked for grammatical and template structures. If article passes this control too, then reviewers are assigned to article and Editor gives a reference number to paper. Authors registered to online submission system can track all these phases. Editor also informs authors about processes of submitted article by e-mail. Each author may also apply to Editor via online submission system to review papers related to their study areas. Peer review is a critical element of publication, and one of the major cornerstones of the scientific process. Peer Review serves two key functions:

- Acts as a filter: Ensures research is properly verified before being published
- Improves the quality of the research

8. Conclusion

The conclusion section should emphasize the main contribution of the article to literature. Authors may also explain why the work is important, what are the novelties or possible applications and extensions. Do not replicate the abstract or sentences given in main text as the conclusion.

Acknowledgements

Authors may acknowledge to any person, institution or department that supported to any part of study.

References

- [7] J. Clerk Maxwell, A Treatise on Electricity and Magnetism, 3rd ed., vol. 2. Oxford:Clarendon Press, 1892, pp.68-73. (Book)
- [8] H. Poor, An Introduction to Signal Detection and Estimation, New York: Springer-Verlag, 1985, ch. 4. (Book Chapter)
- [9] Y. Yorozu, M. Hirano, K. Oka, and Y. Tagawa, "Electron spectroscopy studies on magneto-optical media and plastic substrate interface", IEEE Transl. J. Magn. Japan, vol. 2, pp. 740-741, August 1987. (Article)
- [10] E. Kabalcı, E. Irmak, I. Çolak, "Design of an AC-DC-AC converter for wind turbines", International Journal of Energy Research, Wiley Interscience, DOI: 10.1002/er.1770, Vol. 36, No. 2, pp. 169-175. (Article)
- [11] I. Çolak, E. Kabalcı, R. Bayindir R., and S. Sagioglu, "The design and analysis of a 5-level cascaded voltage source inverter with low THD", 2nd PowerEng Conference, Lisbon, pp. 575-580, 18-20 March 2009. (Conference Paper)
- [12] IEEE Standard 519-1992, Recommended practices and requirements for harmonic control in electrical power systems, The Institute of Electrical and Electronics Engineers, 1993. (Standards and Reports)

**INTERNATIONAL JOURNAL OF ENGINEERING TECHNOLOGIES (IJET)
COPYRIGHT AND CONSENT FORM**

This form is used for article accepted to be published by the IJET. Please read the form carefully and keep a copy for your files.

TITLE OF ARTICLE (hereinafter, "The Article"):

.....
.....
.....

LIST OF AUTHORS:

.....
.....
.....

CORRESPONDING AUTHOR'S ("The Author") NAME, ADDRESS, INSTITUTE AND EMAIL:

.....
.....
.....

COPYRIGHT TRANSFER

The undersigned hereby transfers the copyright of the submitted article to International Journal of Engineering Technologies (the "IJET"). The Author declares that the contribution and work is original, and he/she is authorized by all authors and/or grant-funding agency to sign the copyright form. Author hereby assigns all including but not limited to the rights to publish, distribute, reprints, translates, electronic and published derivatives in various arrangements or any other versions in full or abridged forms to IJET. IJET holds the copyright of Article in its own name.

Author(s) retain all rights to use author copy in his/her educational activities, own websites, institutional and/or funder's web sites by providing full citation to final version published in IJET. The full citation is provided including Authors list, title of the article, volume and issue number, and page number or using a link to the article in IJET web site. Author(s) have the right to transmit, print and share the first submitted copies with colleagues. Author(s) can use the final published article for his/her own professional positions, career or qualifications by citing to the IJET publication.

Once the copyright form is signed, any changes about the author names or order of the authors listed above are not accepted by IJET.

Authorized/Corresponding Author

Date/ Signature